ANL-7349

ANL-7349

Argonne National Laboratory

REACTOR DEVELOPMENT PROGRAM PROGRESS REPORT

June 1967

The facilities of Argonne National Laboratory are owned by the United States Government. Under the terms of a contract (W-31-109-Eng-38) between the U. S. Atomic Energy Commission, Argonne Universities Association and The University of Chicago, the University employs the staff and operates the Laboratory in accordance with policies and programs formulated, approved and reviewed by the Association.

MEMBERS OF ARGONNE UNIVERSITIES ASSOCIATION

The University of Arizona
Carnegie Institute of Technology
Case Institute of Technology
The University of Chicago
University of Cincinnati
Illinois Institute of Technology
University of Illinois
Indiana University
Iowa State University
The University of Iowa
Kansas State University
The University of Kansas
Loyola University
Marquette University
Michigan State University
The University of Michigan
University of Minnesota
University of Missouri
Northwestern University
University of Notre Dame
The Ohio State University
Purdue University
Saint Louis University
Washington University
Wayne State University
The University of Wisconsin

Printed in the United States of America
Available from
Clearinghouse for Federal Scientific and Technical Information
National Bureau of Standards, U. S. Department of Commerce
Springfield, Virginia 22151
Price: Printed Copy $3.00; Microfiche $0.65

ANL-7349
Reactor Technology
(TID-4500)
AEC Research and
Development Report

ARGONNE NATIONAL LABORATORY
9700 South Cass Avenue
Argonne, Illinois 60439

REACTOR DEVELOPMENT PROGRAM PROGRESS REPORT

June 1967

Winston M. Manning, Acting Laboratory Director
Stephen Lawroski, Associate Laboratory Director

Division	Director
Chemical Engineering	R. C. Vogel
Idaho	M. Novick
Metallurgy	M. V. Nevitt
Reactor Engineering	L. J. Koch
Reactor Physics	R. Avery
Remote Control	D. P. Mingesz (Acting)

Report coordinated by
C. L. Chernick and A. Glassner

Issued July 31, 1967

FOREWORD

The Reactor Development Program Progress Report, issued monthly, is intended to be a means of reporting those items of significant technical progress which have occurred in both the specific reactor projects and the general engineering research and development programs. The report is organized in a way which, it is hoped, gives the clearest, most logical overall view of progress. The budget classification is followed only in broad outline, and no attempt is made to report separately on each sub-activity number. Further, since the intent is to report only items of significant progress, not all activities are reported each month. In order to issue this report as soon as possible after the end of the month editorial work must necessarily be limited. Also, since this is an informal progress report, the results and data presented should be understood to be preliminary and subject to change unless otherwise stated.

The issuance of these reports is not intended to constitute publication in any sense of the word. Final results either will be submitted for publication in regular professional journals or will be published in the form of ANL topical reports.

The last six reports issued
in this series are:

December 1966	ANL-7286
January 1967	ANL-7302
February 1967	ANL-7308
March 1967	ANL-7317
April 1967	ANL-7329
May 1967	ANL-7342

REACTOR DEVELOPMENT PROGRAM

Highlights of Project Activities for June 1967

EBWR Plutonium Recycle Program

Operation at 60 MW of power was resumed in early June after a shutdown had been made to remove sample fuel pins and to make repairs in the turbine plant. Because the program is being terminated, power operation will end on June 29. During the month of July, it is planned to activate foils, determine boric acid worth, and the unpoisoned, unrodded critical loading.

EBR-II

The plan of action to locate the source of the fission gas release as discussed in the May Report was approved on June 3. Operation of the reactor in accordance with this plan was begun immediately. A fission gas release was obtained at 30 MW on June 11, and the reactor was shut down and a program of analyses of the specific components of the released fission products was again started. In a subsequent repeat of a fission gas release test, a release was obtained at 10 MW on June 19.

The three most suspect experimental irradiation subassemblies, XG05, XA08, and XO11, were then removed from the reactor and operation restarted on June 21. After 150 MW-days of operation with no evidence of fission gas release, the reactor was shut down and Subassembly XO11 reinserted. After startup and at 7.5-MW power level, a fission gas release occurred. XO11 was removed from the core, and XA08 and XG05 were reinserted. The reactor was then started up on June 29 for a scheduled 150 MW-days of operation at 30 MW or until a fission gas release occurred. No release had been observed by month's end.

Normal EBR-II driver fuel production activities at the Fuel Cycle Facility were continued. Thirteen alloy preparation runs were made with unirradiated material to supplement the irradiated fuel inventory. A total of 18 subassemblies were fabricated during the month. Work on the cold line for the fabrication of supplemental driver fuel is proceeding on schedule.

The vertical assembly and disassembly machine (VAD) designed for installation in the Air Cell was received in Idaho, set up and tested in the mockup area, and used for training of its future operators during this month. Installation of the VAD in the Air Cell is scheduled for July.

ZPR-3

Experiments with Assembly 49 were completed and the approach to critical of Assembly 50 was in progress this month. The aim of the experimental program with each assembly is to provide an integral set of data with which the accuracy of existing cross-section sets and analytical techniques can be checked. Some of the results of the analyses of data taken on Assembly 48B, which was described in the March Report (ANL-7317), are reported this month. Sodium removal coefficients and central fission ratios for various isotopes are given.

ZPPR

The earth fill has been completed up to the bottom of the cell ring beam. The ring beam forms are complete and installation of cable sleeves is in progress. Completion of the support wing roof awaits only the final patching and gravel coat. The support wing is estimated to be about 70% complete.

Grading of roof filter sand is underway. Approximately 50 cu yd have been processed. A check sample indicates that with some further processing the sand should be acceptable for this application.

The Final Safety Analysis Report was reviewed within the Laboratory. Following minor revisions it will be submitted to the AEC.

The status of reactor and facility components is also reported.

AARR

The contract has been awarded for Construction Package No. 1, Site Grading and Excavation. Groundbreaking ceremonies were held on June 12, 1967.

Proposals were received for the primary heat exchangers and for fabrication of the permanent beryllium.

TABLE OF CONTENTS

TABLE OF CONTENTS

TABLE OF CONTENTS

I. PLUTONIUM UTILIZATION--EBWR

A. Operations

In the early part of June EBWR operated at a reduced power level of 35 MW due to flux and pressure variations. Examination showed that a small metal plate from the steam duct within the reactor vessel was lodged in the reboiler pressure control valve. Removing the plate from the valve eliminated the gross variations; however, variations of a lesser degree were still exhibited. By selective control-rod movement, it was found that with the center rod (No. 9) below the No. 1 through No. 8 rod bank, the fluctuation became more intense. Moving the No. 9 rod above the bank eliminated the fluctuations. After discovery of the above, the power level was raised to 65 MW with the No. 9 rod in the full "out" position.

These flux and pressure variations are believed to be due to the burnup of the fuel in the center of the core. This resulted in a reduction of the power density in the core center, producing an unbalanced hydraulic situation and caused a "chugging" within the core center. Raising the No. 9 rod increases the power density and eliminates the variations. Verification of the above will not be obtained due to the limited duration of the program.

The EBWR facility continued operation through the end of June, thus completing the third irradiation step and the final power operations for the Plutonium Recycle Program.

Gathering of the final critical data, core unloading, and plant layup will begin July 1, 1967.

The power generated by the plant was as follows:

	Thermal Power	Electrical Power
During June 1967	40,341.0 MWh	-
Total since start of Plutonium Recycle Program	212,534.6 MWh	16,671.0 MWh

II. LIQUID-METAL FAST BREEDER REACTORS

A. EBR-II

1. Operations

a. Studies of Fission Gas Release. Authorization to proceed with modified Phase-II operations for the location of the source of the fission gas release (see Progress Report for May 1967, ANL-7342, pp. 4-5) was received on June 3. In this plan the reactor will be operated at a minimum level which would provide a fission gas release. The magnitude of the signals accompanying the release would then be used as the basis of comparison in subsequent operation with removal of one or more of the suspect subassemblies. Power was increased in steps of 2.5 MW, holding each step up to and including 17.5 MW for 8 hr. No activity in the blanket gas above normal background was observed in signals from either the charged-wire fission gas monitor (FGM) or the fuel-element-rupture detector (FERD). Cover gas samples being monitored for Xe^{133} and Xe^{135} activity showed only a normal increase in the Xe^{135} activity.

On June 7, power was increased from 17.5 to 20 MW. Operation at this power until 0150 hr, June 9 gave no indication of fission gas release.

Authorization was then received to begin a 2.5-MW stepwise increase to still higher reactor power. A power of 30 MW was reached at 1555 hr. Primary cover gas samples were taken at each power step. There was no detectable increase in gas activity.

On June 11, at 0223 hr (2754 MWh accumulated) the fission gas monitor showed an increase in fission gas activity (fission gas release No. 2), and reactor shutdown was started as required. The FGM signal increased to a maximum of about 17 times the background count rate.

The reactor remained shut down after the June 11 fission gas release until June 19, at which time it was restarted to obtain further information on the source of gas release. During this time, the cover gas was purged to lower its activity. Power was increased to 10 MW at 2120 hr and was scheduled to be maintained at this level for 1.5 hr to obtain power coefficient data and a primary-tank gas sample. However, at 2229 hr (16 MWh accumulated), the fission gas monitor (FGM) began to increase (gas release No. 3). By 2231 hr, the FGM signal had increased from a background reading of 2 to 23 cps, and reactor shutdown was initiated. The FGM signal continued to increase to a maximum of 580 cps at 2315 hr. Gas samples were taken frequently until 0200 hr, June 20, at which time the sampling interval was increased to one hour.

Fission gas samples before and after the shutdown were counted by gamma spectrometry. Table I lists the counts per minute in the channel of maximum activity corresponding to the listed isotope. The sampling time is also given, but the counts given are those observed approximately 10-15 min after sampling in each case.

TABLE I. Activities (cpm) in Fission Gas Samples

Sampling Time	Xe^{133}	Xe^{135}	Kr^{85}	Kr^{87}	Cs^{138}
1615	383	8	13	3	4
1945	370	6	10	5	5
2220	910	60	149	78	53
2231	Reactor shutdown started				
2240	90015	5376	19317	11659	3657
2305	98111	3727	18252	9516	2570
2327	92339	2948	16192	7373	2126
2347	104301	2854	16819	6881	1772
0005	117150	2490	16209	5756	1221
0035	120690	2317	15642	4674	963
0058	115196	2163	14267	3574	694
0125	116595	2005	13855	3017	570
0150	117329	2063	12813	2460	449
0300	119838	1880	11097	1402	285
0402	123865	1691	9685	821	231
0510	122639	1463	8463	527	156

The FGM indicated the count rates given in Table II before and after the shutdown.

TABLE II. Fission Gas Monitor

Time	Count Rate (cps)	Time	Count Rate (cps)
2220	2 (background)	0100	270
		0200	180
2229	10	0300	135
2231[a]	23	0400	100
2257	460	0500	75
2315	580 (maximum)	0600	62
		0700	46
0000	480		

[a]Reactor shutdown started.

The FERD system did not indicate any activity other than the normal background during this period.

A plan of action was prepared which called for removal of the three experimental irradiation subassemblies XG05, XA08, and XO11 followed by reactor operation at 30 MW. Approval was received and operations begun on June 20.

As a preparatory operation to fuel handling, the force-limit trips of the main fuel-handling gripper were checked and calibrated.

In fuel-handling operations, two fuel subassemblies in Row 6 were first removed and replaced with two stainless steel subassemblies for reactivity adjustment.

Subassemblies XG05, XA08, and XO11 (maximum burnup 5.8, 4.4, and 3.5 a/o, respectively) were removed, with substitution, from the reactor core and placed in the primary-tank storage basket. Each subassembly was lifted and held in the raised position several minutes on the main fuel-handling gripper. This lift and hold operation was to allow and detect any incipient gas release from the assembly before placement in the storage basket. After placement of each subassembly in the basket, the storage basket was left in the "Up" position for 30 min and a primary-tank blanket gas sample was obtained at the end of this period.

The gas samples were counted by gamma spectrometry. No increase in count rate was noted. The results are given in Table III.

TABLE III. Activities (cpm) of Primary-tank Blanket Gas Samples

Date	Time	Xe^{133}	Xe^{135}	Kr^{85}	Kr^{87}	Cs^{138}
6/20/67	2140	119786	443	1380	20	6
	2300	XG05 to storage basket				
	2330	118012	357	1022	16	5
6/21/67	0120	XO11 to storage basket				
	0150	112789	357	1022	16	5
	0235	XA08 to storage basket				
	0310	109183	327	937	21	5

The fuel-handling operations were normal and no evidence of sticking or binding were observed during any of the transfers.

The reactor was returned to operation on June 21. Reactor power was increased in 2.5-MW steps, 1 hr at each level, to 30 MW. Operation continued for 150 MWd with no evidence of fission gas release or any other

anomaly. The reactor was again shut down at 0910 hr on June 27 and preparations made for fuel-handling operations. Experimental irradiation subassembly XO11, previously removed, was reinserted in grid position 2-F-1 and the reactor restarted at 1000 hr, June 28.

Power was again increased in 2.5-MWt power increments, holding at each increment to obtain primary-tank gas samples. The 7.5-MWt increment was reached at 1416 hr and at 1430 hr the fission gas monitor began to increase (gas release No. 4). The reactor was shut down (integrated power 11.0 MWh) and again the three FERD loop channels showed no delayed-neutron activity. The fission gas signal increased from 3 to 295 cps at 1510 hr. The reactor cover was raised for fuel handling at 1945 hr. The central subassembly was raised first on the main fueling gripper and then returned to establish that no binding or interference existed with the adjacent suspect subassembly XO11, which was then raised and held in the elevated position for 30 min. Three cover gas samples revealed no increase in cover gas activity. During subsequent fuel handling, experimental subassemblies XA08 and XG05 were returned to the core and appropriate reactivity adjustments were made.

The reactor was restarted on June 29 for a scheduled 150-MWd run at 30 MW or until another fission gas release is observed.

Table IV is a summary of the four fission gas releases, tabulating the maximum FGM signals and maximum gas activities noted.

TABLE IV. Summary of Fission Gas Release in EBR-II

Fission Gas Release No.	Date	Differential (MWd)	Count Rate before Release (cps)	Maximum Count Rate after Release (cps)	Gas-sample Activity Just Prior to and Maximum after Fission Gas Release	
					Xe^{133} (cpm)	Xe^{135} (cpm)
1	5/24	525[a]	12.5	35,000[e]	2.4×10^3 to[d]	1.8×10^3 to[d]
2	6/11	115	5	85	7.0×10^3 to 8.3×10^3	8.5 to 10^2 to 5×10^3
3	6/19	0.66	0.5	580	4.0×10^2[c] to 1.4×10^5	8[c] to 5.5×10^3
4	6/28	0.46[b]	1.5	295	2×10^4 to 1.5×10^5	1.1×10^3 to 3.0×10^3

(a)From the start of Run No. 25.
(b)A 150-MWd run with experimental irradiation subassemblies XG05, XA08, and XO11 removed, with no gas release preceding this run.
(c)Primary-tank cover gas purged with fresh argon to reduce residual activity prior to this run.
(d)Samples too hot to count under standard geometry. Approximately 450-fold increase in activity.
(e)Extrapolated value.

b. New Gripper. The gripper of the fuel-unloading machine (FUM) was replaced by a new unit designated "Mark III." Operational tests with the new gripper were satisfactory (see Sect. II.A.3.p). The gripper was removed, inspected, cleaned, and reinstalled. Internal approval was given to its use in normal full transfer operations. Twenty-one transfers have been successfully completed utilizing the new gripper.

c. Operational Support and Maintenance. Purchase orders for procuring major spare parts were initiated for a generator rotor for the main secondary-pump motor-generator and for a generator rotor and exciter for the main primary-pump motor-generators. In addition, the necessary information for purchase of the materials for fabrication of a spare subassembly-hold-down lower shaft assembly was started.

A spare 2400-V breaker was received from the Hallam Nuclear Power Facility and satisfactorily tested.

Work has been performed on the following equipment during this report period:

The alignment of the (new) No. 2 interbuilding coffin to the fuel unloading machine was completed.

The replacement of the cam rollers in the Ferguson rotational drive for the storage basket was completed. The vertical alignment has also been completed, although further adjustment will probably be required.

The installation and initial checkout of the new Mark-III FUM gripper have been satisfactorily completed.

The large rotating plug seal trough was cleaned by the manual "brush-clean" method to remove the oxides which had built up in the trough since the last cleaning operation.

The annual leak-rate test of the personnel-air-lock doors and the purge exhaust dampers was satisfactorily completed. The leakage rates (normalized to 36.2 psia and 32°F) were as follows:

1)	Inner door	2 standard ft^3/day
2)	Outer door and lock	12 standard ft^3/day
3)	Purge exhaust damper	1.8 standard ft^3/day

(i) Instrument Thimble Cooling System. Because the reliable operation of the instrument thimble cooling system is absolutely essential to the safe operation of the reactor, an extensive survey and evaluation of this system was undertaken. A compendium of the system-performance parameters was compiled and is tabulated in Tables V and VI. The reactor was at zero power. These tables provide a readily available reference for future use.

The necessary manufacturers' data, such as drawings, parts list, repair and maintenance procedures, are being systematically accumulated. To date this has been accomplished for the turbo compressor, air pistons, hydrochecks, and solenoids for flow branches A and B. Once all information has been accumulated, it will be placed in a central file.

TABLE V. Thimble Cooling System: Operating Data for Turbo Blowers.

	Turbo #1 (R8-F 709)	Turbo #2 (R8-F 710)
Capacity	94.5%	0
Amperes	69	0
Branch	B	A
Air Flow, Branch A (Control Room) Air Flow, Branch A (Corridor Pnl.) [FT-521-A]		940 cfm 960 cfm
Air Flow, Branch B (Control Room) Air Flow, Branch B (Corridor Pnl.) [FT-521-B]		900 cfm 900 cfm
Pressure, Inlet to Absolute Filters, Branch A [PIA-642B] Pressure, Inlet to Absolute Filters, Branch B [PIA-642A]		5.6 in. Hg 5.6 in. Hg
Δp Across Absolute Filters [DPIA-648]		0.85 in. H_2O
Inlet Pressure to Turbo #1, Branch B [PIA-643A] Inlet Pressure to Turbo #2, Branch A [PIA-643B]		5.7 in. Hg Vac 5.6 in. Hg Vac
Δp Across Turbo #1 [DPT-1563A] Δp Across Turbo #2 [DPT-1563B]		7.2 in. Hg 5.9 in. Hg
Ambient Temperature Reactor Floor		72°F
Inlet Temperature, Turbo #1 Inlet Temperature, Turbo #2		115°F 78°F
Common Turbo Outlet Temperature		206°F
Turbo #1 Outboard Bearing Temperature		152°F
Outlet Temperature, Branch A (Corridor Pnl.) Outlet Temperature, Branch B (Corridor Pnl.)		135°F 147°F

TABLE VI. Thimble Cooling System: Temperature Data.

PT No.	Temperature	Thimble No.	TC Designation	PT No.	Temperature	Thimble No.	TC Designation
1	0		R4-TC-511	11	136	Outlet air duct from J-2, 3 and O-1, 2.	R4-TC-511-BE
2	90	J-1	-A				
3	90	J-2	-B	12	90	J-1	-V
4	101	J-4	-C	13	90	J-2	-W
5	95	J-3	-D	14	93	J-3	-Y
6	98	O-3	-E	15	101	J-4	-X
7	98	O-1	-F	16	100	O-1	-AA
8	92	O-4	-G	17	97	O-2	-BH
9	95	O-2	-H	18	98	O-3	-BG
10	130	Outlet air duct from J-1, 4 and O-3, 4.	-BF	19	94	O-4	-Z

Note: Reference drawing Number RE-2-36573-D for thermocouple location. Readout is through recorder P4-TRA-511-96 located in the control room.

d. Operator Training. Training activities for the past month have involved reorganization and rewriting of the electrical, power-plant, and coolant-systems training material. The reorganization and rewriting of the reactor control-console training material has been completed. Three revised training units were completed for the electrical operations, two for the sodium coolant systems, and one for power-plant operations. A training unit consists of a study guide, open-book assignment, and closed-book test.

Two operators were qualified, one for fuel handling and one for the power plant. In addition, one operator who had qualified in all training areas, was designated a Reactor Plant Operator.

e. Operating Manual. Review and revision of the facility Operating Manuals continued to reflect plant modifications and changes brought to light through operating experience and a system-evaluating program. Revision Bulletins Nos. 51 and 52 were issued and contained revised procedures for the following sections:

Division VIII E	"Fuel Handling System - Special Procedures"
Division X A	"Plant and Instrument Air"
Division X B	"Radiation Monitoring"
Division X C	"Reactor Building Isolation"
Division X E	"Seal Heating"
Division X F	"Plant Suspect Exhaust"
Division VIII D	"Fuel Handling - Abnormal Conditions"

The Master Startup Check Sheets and System Data Sheets are currently being revised. Review of Divisions II B, "Normal Procedures" and II C, "Special Procedures" has begun.

The following Special Operating and Administrative Procedures were issued:

1. Primary Sodium Sampling
2. Backshift Procurement of Materials and Services from Central Facilities
3. Selected Parameter Data Processing System
4. Storage Basket Packing Gland Argon Supply
5. Emergency Procedure for Fuel Element Rupture

f. Planning and Scheduling. Specific activities for this report period are as follows:

1. Preparation of schedules for routine maintenance activities.
2. Preparation of yearly schedule continued.
3. Preparation of a Five-Year Milestone Chart.
4. Preparation of long-range plan continued.
5. Processing of applicants to fill the vacancy in the Scheduling Group continued.
6. Preparation of schedule for secondary em pump replacement began.

2. Fuel Procurement

Contract negotiations were completed with the Nuclear Products and Services Group of Aerojet-General Corporation. The contract provides for fabrication of 34,000 fuel elements for a fixed price of $2,545,907, with delivery to be completed by February 15, 1969. Initial production is anticipated to start April 1968, following preproduction activities. An option for the procurement of 17,000 additional elements, immediately following completion of the first contract, is also contained in the

Frequent contacts with the vendor have been effected to discuss process technology and his procurement and production plans. He is actively engaged in making plant changes for this work, completing equipment designs, and initiating procurement of materials and equipment.

3. Reactor Improvements

a. Irradiated-fuel Monitor. Fabrication was completed. All components are ready for final assembly and testing. A short delay was caused by misalignment difficulties during welding of the lower part of the thimble to the adjacent section; proper alignment was achieved by stress-relieving procedures. The assembly will be tested for proper mechanical operation before shipment to the reactor.

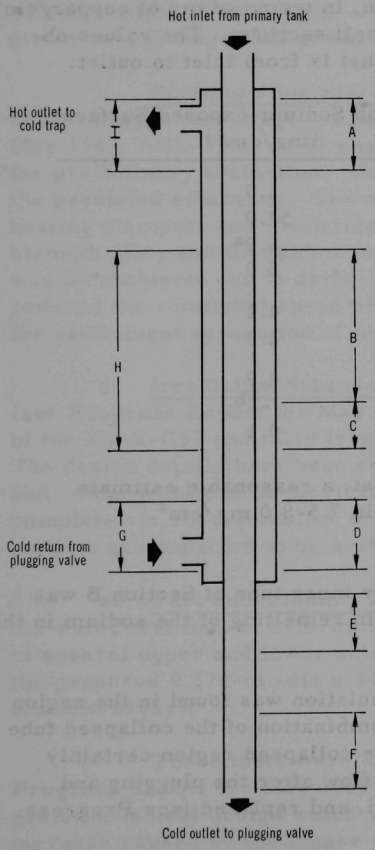

Fig. 1. Schematic Diagram of EBR-II PI-A Loop Economizer, Showing Locations of Samples.

b. Sodium Chemistry Technology. In connection with analyses of possible causes of and problems from copper contamination in the primary-system sodium (see Progress Report for March 1967, ANL-7317, pp. 4-7), the original plugging-loop (PI-A) economizer is being examined destructively, and plans are being made for a new plugging loop and sampling station.

(i) Examination of Plugging-loop Economizer. Soon after copper deposits were found in the EBR-II primary-system plugging valve, the economizer from the PI-A loop was frozen and cut out of the loop. The economizer is being cut into several longitudinal sections so that the nature and extent of any copper deposits can be determined (see Progress Report for May 1967, ANL-7342, p. 8).

The component being examined consists of the economizer, or heat-exchange section, plus about 14 in. of attached 1/2-in. line that led to the plugging valve. The heat-exchange section consists of a 36-in. length of 1/2-in. 20-gauge tube surrounded by 3/4-in. Schedule-40 pipe; 1/2-in. sodium inlet and outlet ports are located in the shell about 1.5 in. from the bottom and the top (see Fig. 1). The entire unit is of Type 304 stainless steel. The economizer was mounted vertically. Inlet flow was from a 2-in. line upstream from the crystallizer tank. The sodium enters

the 1/2-in. tube at the top of the economizer and flows downward; return flow enters the shell side of the economizer at the bottom and exits at the top.

Five separate sections were cut out of the economizer for examination and analysis. Their relative locations are shown in Fig. 1. Each section was carefully slit lengthwise and laid open. The sodium was removed by dissolution in ethyl alcohol. Photographs were taken of all surfaces that had been exposed to sodium. These clearly show varying amounts of copper remaining on the surfaces of the tubes. The copper was removed from each surface by several rinsings with 6N HNO_3. The acid rinse solutions and alcohol solutions containing the reacted sodium were analyzed separately for copper by atomic absorption. From the data collected, a copper inventory was generated, in terms of mg of copper/cm^2 of exposed surface, for both the tube and shell sections. The values obtained are listed below according to flow, that is from inlet to outlet:

	Sample Section	Copper on Sodium-exposed Surface (mg/cm^2)
Tubeside	A	1.9
	B	54.0
	C	6.9[a]
	D	5.0
	E	4.1
	F	4.3
Shellside	G	4.9
	H	- [b]
	I	0.1

[a] A small portion of this sample was lost; a reasonable estimate would be that this value might be within 7.5-8.0 mg/cm^2.

[b] Analysis not completed.

A portion of the economizer inner tube at Section B was found collapsed. This was due to nonuniform remelting of the sodium in the economizer following a period of shutdown.

The greatest copper accumulation was found in the region of the collapsed portion of the tube. The combination of the collapsed tube plus the heavy accumulation of copper in the collapsed region certainly explains the failure to re-establish normal flow after the plugging and throttling valves had been removed, cleaned, and replaced (see Progress Report for March 1967, ANL-7317, p. 3).

The presence of some copper (0.1 mg/cm^2) in Section J indicates that at some time sodium leaving the economizer was above saturation with respect to copper. It also appears obvious from these data that cold trapping would be an effective method for removing copper from sodium.

Sections of the economizer not used for the study reported here are being examined metallographically to determine whether any copper had intergranularly penetrated the stainless steel.

All solutions on which copper determinations were made will be analyzed carefully for several other trace impurities known to be present in the as-received EBR-II sodium. Then the present concentrations will be compared with the as-received concentrations to determine the direction and magnitude of changes.

c. Rotating-Plug Seal Cleaning System. The laboratory mockup of a prototype centrifugal-separator (see Monthly Progress Report for May 1967, ANL-7342, p. 8) was tested with a homogenized oil-water fluid for preliminary evaluation. The results were satisfactory and verified the predicted efficiency. The mockup was modified by the addition of heating elements and insulation to enable a test to be made using tin-bismuth alloy and its oxides as the working fluid. A preliminary test run was inconclusive due to drive-motor problems. The higher-density alloy reduced the rotational speed of the small air-motor below that necessary for centrifugal separation of the oxide.

d. Irradiation Subassemblies Mark C. As reported previously (see Progress Report for May 1967, ANL-7342, pp. 8-9), the final tests of the Mark-C37 and -C19 irradiation subassemblies were performed. The design details have been completed; thus materials can be procured and components can be fabricated. Sufficient hardware will be acquired to complete six subassemblies of the Mark-C37 and -C19 types. The components are expected to be available by November 1, 1967.

e. Fuel Subassembly Mark II. Flow studies were conducted in the water test loop to determine the pressure-drop (Δp) characteristics of several upper and lower shield-piece designs as well as the Δp through the proposed 0.174-in.-dia x 34-in.-long fuel-element tube bundle (91-element array).

These tests were a continuation of the program (see Monthly Progress Report for May 1967, ANL-7342, p. 9) to provide a suitable radiation-shield design which will have a lower Δp to compensate for the increase caused by the longer fuel elements.

Two new shield-piece designs were fabricated and delivered for testing. One, Model-SCPS (Stainless Central Plug Shield), was found to have a Δp of 7 psi through the lower section and 6 psi through the upper section. The total Δp of 13 psi is 1.2 psi less than that of the standard STB (Stainless Triflute Blanket) model, but not enough less to be acceptable.

The inherent difficulties of calculating accurately the hydraulic behavior of these complex flow passages make it necessary to test, modify, and retest in order to optimize the design. Through this process of modification, the Δp of Model-SCPS was further reduced by 1.4 to 11.6 psi. Additional adjustments are planned for further testing.

Initial flow tests with the second design, Model-SSS (Stainless Sextuple-flute Shield), showed a total Δp of 13.3 psi through this model. Slight modification resulted in only 0.8 psi reduction; further modification is planned.

Dummy elements of the proposed Mark-II fuel element were flow tested in a partial mockup of the subassembly. The Δp of the 91-element array was found to be 19.2 psi, which is very close to the anticipated value. Further tests will be performed with these dummy fuel elements installed with the shield designs to determine if there are any changes in hydraulic flow characteristic or interaction due to the various shield configurations.

f. Instrumented-subassembly System. System concepts and equipment requirements for placing instrumented subassemblies in the reactor core are being developed.

(i) Subassembly Attachment and Lead Severance. Design and evaluation continues on various concepts for coupling and decoupling the top of the instrumented subassembly and the extension tube and for severing the instrument leads so the extension tube can be lifted from the reactor and the subassembly can be removed from the core. The internal-bayonet coupling (see Progress Report for March 1967, ANL-7317, pp. 17-18) has been redesigned so that the subassembly will be supported axially as well as restrained radially by the extension tube while the leads are being cut (see Fig. 2). This modified coupling concept, called the internal-bayonet-latch coupling, employs a spider with a central ring built into the transition piece at the lower end of the extension tube. A tubular latch is captive in the spider ring by means of a collar. The lower part of the latch consists of three bayonet hooks which engage three radial arms in the base of the top end fixture. To disconnect, a long tool is inserted through the extension tube. This tool engages castellations in the collar at the top of the latch. Decoupling is achieved by rotation through 45°. The entire coupling is recessed below the lead cutting surface so that the leads can be severed while the coupling is still connected. There are no holding and tensioning

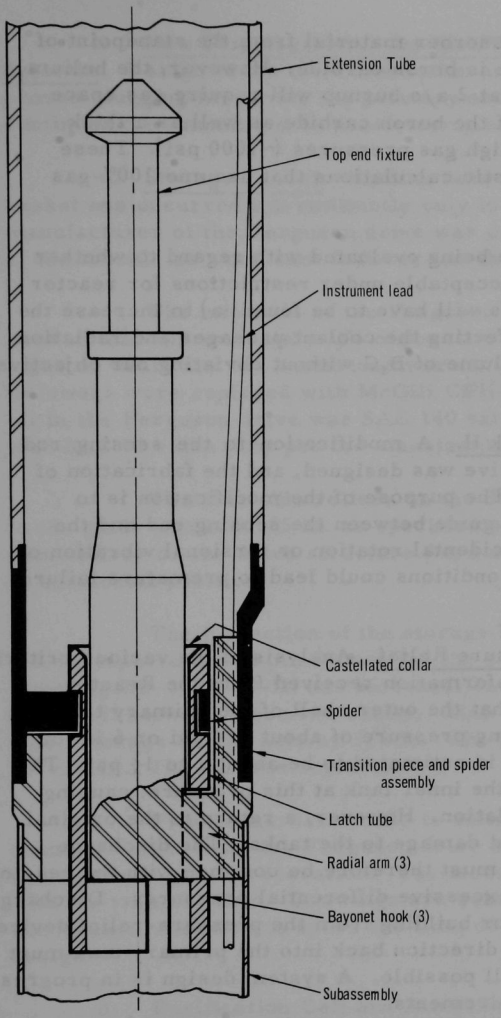

Fig. 2. Internal-bayonet-latch Coupling

devices at the top end of the extension tube. A model has been fabricated for further study.

It has been planned to subject the fabricated test specimens of the various coupling schemes to axial, bending, and torsional loadings for further evaluation. Thus far, the top-end-fixture, the hexagonal-support coupling (see Progress Report for March 1967, ANL-7317, pp. 15-18), and the internal-bayonet-latch coupling have been subjected to tensile axial loads up to the reference design load of 3000 lb. Elongation and tensile loads were recorded. The couplings returned to original configuration upon removal of the load. Thus, it is concluded that these couplings were stressed within the elastic limit of Type 304 stainless steel.

g. System Design Descriptions. The assembly of input data is continuing; major effort is for organizing components construction drawings. A complete set of "as-built" architect-engineer drawings has been assembled. A 92-page detailed working outline was completed and forwarded to the Commission.

h. Greater-worth Control Rod. A feasibility study is being made of an all-absorber-type (boron carbide) control rod which could be used to replace the present fuel-type control rods when instrumented subassemblies are installed in some of the present control-rod locations. An all-absorber rod, because of its greater reactivity worth, might free four of the present 12 rod locations for experimental-subassembly use.

The most suitable absorber material from the standpoint of maximum worth per unit volume is boron carbide. However, the helium generated in the B_4C (~65% B^{10}) at 2 a/o burnup will require gas space greater than twice the volume of the boron carbide as well as a thick (~0.109 in.) wall to contain the high gas pressures (~1000 psi). These estimates are based on pessimistic calculations that assume 100% gas release from the B_4C.

The calculations are being evaluated with regard to whether a gas pressure of ~1000 psi is acceptable under restrictions for reactor operation safety. If not, methods will have to be found (a) to increase the gas space without drastically affecting the coolant passages and radiation shielding or (b) to reduce the volume of B_4C without obviating our objective of sufficiently high rod worth.

i. Oscillator Rod Mark II. A modification to the sensing rod on the Mark-II oscillator-rod drive was designed, and the fabrication of the new pieces is in progress. The purpose of the modification is to install a hex-shaped mechanical guide between the sensing rod and the jaw-actuator shaft to prevent accidental rotation or torsional vibration of the sense rod. Either of these conditions could lead to premature failure of the sensing rod bellows.

j. Primary Tank Pressure Relief. Analysis of the various criteria for this system is continuing. Information received from the Reactor Engineering Division indicates that the outer shell of the primary tank can take an allowable external working pressure of about 1/4 psi or 6 in. of water. The collapsing pressure is estimated to be about 1 to $1\frac{1}{4}$ psi. The outer tank would buckle against the inner tank at this pressure, causing considerable damage to the insulation. However, a return to the original shape would lead to no permanent damage to the tanks. The discharge from the pressure-relief device must therefore be common with the reactor building atmosphere to prevent excessive differential pressures. Discharge of radioactive gas into the reactor building from the pressure-relief device or passage of air in the reverse direction back into the primary tank must also be protected against, if at all possible. A system design is in progress which will satisfy the above requirements.

k. FERD Loop Plugging Meter and Sampler. A proof-test of the FERD loop plugging meter has been completed. The cold trap in the secondary purification system is normally operated at an outlet temperature of 250°F, which is the practical lower limit without the possibility of freezing of the sodium in the system. In order to test the performance of the FERD plugging meter at more than one point, it will be necessary to raise the temperature of the cold trap somewhat to provide higher plugging temperatures for this test. The results of the first test at the lowest temperature indicated that all components of the plugging loop are functioning properly.

l. New Plugging Meter for the Primary and Secondary Purification Systems. Design of the instrumentation and electrical system for an improved plugging meter for the primary and secondary purification systems continued this month and is nearly complete.

m. Storage Basket. Binding between the subassembly and storage basket has occurred intermittently only in select storage holes. The manufacturer of the Ferguson drive was contacted. He diagnosed the source of the trouble as worn cam followers in the Ferguson drive.

The internals of the Ferguson drive were inspected. This showed that approximately 1/4 of the cam followers were worn, 1/2 showed signs of wear, and the remainder were in good condition. All 30 of the cam followers were replaced with McGill CFH-1$\frac{1}{4}$ cam followers. The original oil in the Ferguson drive was SAE 140 extra duty. This has been replaced with SAE 90 extra duty per the manufacturer's recommended procedure.

The four side rollers on the drive structure were aligned parallel to the guide within 0.005 in. as specified on drawing EB-1-26875-E. The cam rollers on the drive structure were adjusted to hold the Ferguson drive in horizontal position.

The inspection of the storage basket also revealed that the 0.5-in. tapered dowel pin connecting the basket shaft to connecting shaft (drawing EB-1-27370-D) has loosened, causing a relative motion of approximately 1° between these two shafts. This could cause a misplacement of an outer storage basket hole by 3/8 in. The pin was removed and the hole rereamed. The pin was replaced.

Provisions were made to relieve the weight of the 5000-lb counter-weight from the Ferguson drive at the circle-2 and -3 elevations during the alignment operation. The storage basket was then aligned with the transfer arm. Drawings are being changed to indicate the new conditions. A device to speed the time of alignment is in the process of design.

n. Purification Cell and Sampling Cell Ventilation. The ventilation systems for the purification cell and sampling cell are being reviewed to determine if these systems can be improved to confine combustion products in case of fire and to offer better protection to personnel from activated combustion products. It is desirable to balance the supply and exhaust ventilation systems to establish a slight negative pressure in the cells. This would minimize the spreading of smoke to surrounding spaces in case of fire.

The ventilation supply system for the sampling cell is a temporary arrangement, with a duct routed through the doorway into the cell. This

prevents shutting the door to help isolate the sampling cell from the upper basement space during sampling operations.

Tests of the ventilation systems were conducted to determine flow rates with the following results:

Purification Cell

Supply = 256 cfm (Pitot Tube)
Exhaust = 240 cfm (Pitot Tube)
Exhaust = 230 cfm (Anemometer)

Sampling Cell

Supply = 1050 cfm (Anemometer)
Exhaust = 890 cfm (Pitot Tube)

The cell supply ducts have a common air source, which is from the upper basement heating and cooling unit. Each exhaust duct has a blower rated as follows:

Cell	Speed (rpm)	Flow (cfm)	Pressure (in. of water)
Purification	1930	300	3.5
Sampling	1750	210	3.0

Since the exhaust flow from the purification cell is below rated flow, the speed of the blower was checked. This fan, which is belt driven, is operating at 1825 rpm, less than rated speed (1930 rpm). However, this does not account for all of the less-than-rated flow experienced. It is therefore suspected that the exhaust filter may be partially plugged and needs replacing. However, pressure gauges do not indicate a pressure differential across the filter.

o. Relief Valve for Main Steam Header. The relief valve on the main steam header in the Power Plant is lacking in dependability. Although this valve is not necessary for plant safety, it is nevertheless unsatisfactory. It has never popped or reset at consistently constant pressures and has been a high maintenance item. It was decided to obtain a suitable replacement, one that would overcome the shortcomings of the existing valve. Initiation of this work is awaiting a planned reactor shutdown of sufficient length to permit completion of the installation during the shutdown period.

p. Fuel Unloading Machine (FUM) Revisions. Operating experience with the FUM dictates that although operation has been adequate to date, modification is required for long-term reliability. A large maintenance effort has been necessary to date. With the emphasis on increasing plant

factor, the operating reliability of the FUM must be substantially improved to insure its availability for the increased usage which will accompany higher plant factor.

The modification work planned for the FUM consists of two phases: (i) the argon gas system and (ii) the mechanical system. Work on the mechanical system will include design of a new gripper, a redesign of the entire position-indication system, elevation drive system, and jaw-actuating mechanism.

Two basic problems associated with the FUM argon system are in-leakage of air, and entrained sodium and sodium vapor in the gas stream. As a result of air in-leakage, sodium oxide deposits built up in the area of the gripper as well as in other parts of the system. These deposits have critically affected the operation of the FUM during past operating periods.

The procedure to eliminate these problems will be to detect all leakage and eliminate its source, to devise a more effective method of separating entrained sodium from the gas stream before its entry into the main system, and to improve filtration.

(i) Argonne Gas System. The fabrication of horizontal sieves of an improved design to prevent channeling of the gas over the top of the bed has been completed. These will be installed at the earliest convenience.

An investigation has shown that the incorporation of a micrometallic filter to remove particulate matter from the FUM argon gas system is feasible. The design of such a filter is in progress.

(ii) Mechanical System. Operation of the FUM with the prototype Mark-III gripper started this month. A test of the new gripper system was performed before normal fuel transfers were initiated. The test consisted of twenty-five simulated transfers between a subassembly on the transfer arm and another in the IBC. Upon completion of the test, the gripper was removed, cleaned, and inspected. Inspection showed all parts were operating properly and smoothly, so the gripper was reassembled and reinstalled into the FUM. All new operating and maintenance procedures were completed, and each operating shift crew received instruction in the operation of the new system. Normal fuel transfers between the IBC and the primary tank were then initiated. Approximately twenty-five subassembly transfers have now been completed without difficulty.

Fuel handling with the prototype gripper will continue until sufficient operations have been completed to verify the design criteria and materials selection. Design of the permanent Mark-III gripper has been initiated, and it is planned to modify the prototype as necessary to make an identical standby gripper available for the FUM.

q. Nuclear Instrumentation Improvements. Improvements will be made in the nuclear instrumentation in order to reduce the maintenance caused by radiation damage of components placed in the thimbles, and to improve reliability, accuracy, safety, and plant factor.

Circuit design work necessary to incorporate the new nuclear instrumentation into the existing circuits is in the final stage.

A solid-state unit has been developed which checks for welded relay contacts of the relays in the shutdown circuit (IBM No. 766046 and Clark). The unit has been tested and operates properly. The unit will not allow the relay to be picked up if a welded contact is detected. The material necessary for the safety review of the nuclear channels has been prepared and submitted for review.

r. Reactor Systems Instrumentation Improvements

(i) Temperature-monitoring Devices. Temperature-monitoring switches (shutdown-initiating components) which load the primary sensors are being replaced. The new units replace existing units that monitor thimble-cooling and blanket-gas temperature. The new units will provide improved accuracy and reliability.

Panel fabrication has been completed, and wire interconnections are being made. The millivolt converters have been checked and calibrated, and are ready for installation in the panels.

(ii) Multipoint Recorders. These units, for which there are no existing standbys, are required for operation of the reactor. This program provides for scheduled replacement of these units to permit factory rebuilding and upgrading. The extra units will then serve as standbys when the program is completed.

The equipment has been delivered, is being unpacked, inspected, and checked out. One unit has been installed for readout of bulk sodium temperatures.

(iii) Miniature Recorders. Equipment delivery has been delayed by Leeds and Northrup Company until the second week in July 1967. No further work is possible until this equipment is received.

(iv) Selected-parameter Data-processing System

(1) Operational checkout and debugging of a 50-point system for alarm and surveillance of selected parameters, such as the subassembly thermocouples for reactor protection, have been completed. The system has been calibrated and is now undergoing long-term-stability tests.

(2) A 100-point system for routine surveillance of plant parameters and for nonroutine analysis of system dynamics will provide improved data acquisition for reporting plant performance. Factory checkout of the equipment has been completed. Our engineer has acceptance tested the unit at the factory and reports only minor problems with the equipment. These will be corrected prior to shipment.

(v) Pressure and Temperature Sensors. Two pressure sensors and eight thermocouples will be incorporated into a thimble assembly to be introduced into the reactor outlet plenum by way of the unused auxiliary gripper hole. These new sensors will replace units which have previously failed.

The design of the thimble assembly is complete.

The pressure-sensor vendor must be provided with the completed upper portion of the thimble assembly before he can thread the capillary tube through the top flange and complete the final filling and sealing operation. The fabrication of this upper flange assembly is under way in the EBR-II machine shop.

4. Reactor Analysis and Testing

a. Power-coefficient Measurements. In three startups to power during this month, detailed power coefficients were measured. The results of all three were in agreement with each other and with the initial power-coefficient curve.

In addition there were three scrams from power. Upon restart, the reactor returned to the same reactivity condition within one or two Ih. These results indicate that within this range of reproducibility, the reactor parameters characterizing the power coefficient are not changing. The amplitude of the 10-cps oscillator was carefully measured during one startup, and confirmed the fact that the percent amplitude of 10-cps oscillation decreases with increasing power and is nearly gone at 25-30 MW.

b. Calculations. A series of problems have been run using regional and energy-dependent bucklings in order to better characterize the flux shapes measured in Run 25D with the stainless steel blanket. The regional and energy-dependent bucklings were obtained from CANDID r, z geometry. The first results have been very encouraging, giving a good fit to the experimental data, even through the first row of the uranium blanket. The results appear to be adequate for use in estimating the power distribution for the increase to 50-MW power. This study requires the investigation of effects of moving experiments to new positions which match their required power generation rate at the higher power.

In addition, a few preliminary calculations have been made relating to fuel enrichment of Mark-II fuel, and reactivity effects of a nickel blanket.

A revised burnup code, which will follow the burnup limits on core, experimental and blanket subassemblies, has been completed for the 1604 computer.

As part of the power coefficient study for (88-subassembly core) Run 25, a series of two-dimensional transport calculations were performed to investigate some of the separate components. The computation concerned only dimensional and density changes of the materials in the reactor with temperature. The reactivity feedbacks resulting from the mechanical movement of the core, "bowling effect," and the Doppler effect have not been included in this phase of the study. A brief description of the results of the computations appears in Table VII.

TABLE VII. Calculated Values of k_{eff} for Various Conditions of EBR-II Run 25

Problem No.	Problem Description	$-\Delta k/k_{eff}$	$-\Delta k/k/MW$ ($\times 10^{+5}$)	Comment
1	Uniform Core Temperature: 700°F	-	-	Basic configuration at zero power
2	45-MW Operation	0.002276	5.058	
3	Fuel Temperature: 960°F	0.000573	1.273	Fuel expansion
4	Steel	0.000780	1.636	Structural expansion
5	Sodium--Core	0.000426	0.947	Sodium-density change
6	--Core and Upper Reflector	0.000866	1.924	
7	--Overall	0.000932	2.071	Core blanket and reflector
8	Uniform Core Temperature: 900°F	0.005356	-	Isothermal change at zero power

In order to estimate the effect of the loading changes in EBR-II, temperature effects were computed for a reactor identical to Run 25 except that the stainless steel radial reflector was replaced with a depleted uranium blanket. Some results of this study are listed in Table VIII; included are the values associated with the 67-subassembly core using the Mark-I design and depleted uranium axial and radial blanket. The measured and/or computed coefficients are presented in ANL-5719 (Addendum).

The overall change in reactivity obtained in this investigation appears to be not very much different from the 67-assembly EBR-II core. The individual components may vary significantly in the two loadings; for example, the coefficient for sodium is less in the core but greater in the upper reflector regions for Run 25 as compared to the 67-assembly core. It also appears that the density and dimension changes due to temperature produces about the same reactivity changes for EBR-II with a steel reflector and with a depleted uranium blanket in Rows 7 and 8. This similarity is not found to be the case for the bowing effect.

TABLE VIII. Comparison of Calculations with Results Shown in ANL-5719 (Add.)

Component of Coefficient	67-subassembly Core with Depleted Radial and Axial Blanket -Coef. x Temp at 45 MW ($\times 10^5$)	Run No. 25 (88 Subassemblies) (with Depleted U Blanket) Calculated, Δk ($\times 10^5$)
Core--Fuel	56.3	56.3
--Axial Growth	3.2	-
--Coolant	48.3	42.6
--Radial Growth	80.8	-
Total	188.7	-
Upper Gap	20.2	-
Upper Blanket--Coolant	10.2	
--Fuel and Structure	2.5	
Total	12.7	
Outer Blanket--Coolant	0.9	
--Fuel	1.4	-
--Structure	2.4	-
Total	4.7	
Overall Total	226.4	227.6

The computed axial fuel expansion coefficient has been found to be in good agreement with the preliminary values obtained from the two-power-level, variable-coolant-flow experiment. Essentially, with coolant flow proportioned directly to power, the thermal conditions of the bulk sodium, subassembly stainless steel and all other components except for the fuel remain constant. The difference in the reactivity as measured by control rods is then that due to the change in the fuel temperature effects. The preliminary agreement between the experiment and the computed value will allow the further analysis of the components of the power coefficient to proceed with a higher degree of confidence.

5. Surveillance

a. Effect of Recycling Types 304 and 304L Stainless Steel Tubes. Data were obtained to show the effect of recycling a stainless steel tube, such as a clad fuel element, back into the reactor sodium after a nondestructive examination. In the Phase-I tests (see Progress Report for May 1967, ANL-7342, pp. 20-22), the samples were exposed to 1100°F sodium for 7 days. For the Phase-II tests just completed, similarly exposed specimens were stored in normal or in dry air for 10 days and re-exposed in an 1100°F sodium loop for another 7 days. After the Phase-II samples were removed from the loop and cleaned in the same manner as the Phase-I samples, they

were examined and tested for sensitization by means of Strauss-reagent accelerated-corrosion tests and electrical-resistivity measurements that indicated the rates of attack.

After the initially sodium-exposed 304L specimens were stored for 10 days in normal or dry air at room temperature, their average electrical resistivities decreases ≲2% and ~5%, respectively. Metallographic inspection of the microstructure showed slight sensitization near the tube surface. Then the specimens were exposed to Strauss reagent in a corrosion test with the results shown in Fig. 3. No differences were visually detected in the microstructures. During immersion in reagent, the normal-air-stored specimens corroded at about the same average rate as did the specimens tested before storage; however, the data spread became more pronounced. But the specimens that had been stored in dry air corroded faster in the reagent; in explanation, it might be speculated that, because the intergranular sodium in these specimens had less moisture to react with during storage, the sodium reacts more vigorously with the Strauss reagent.

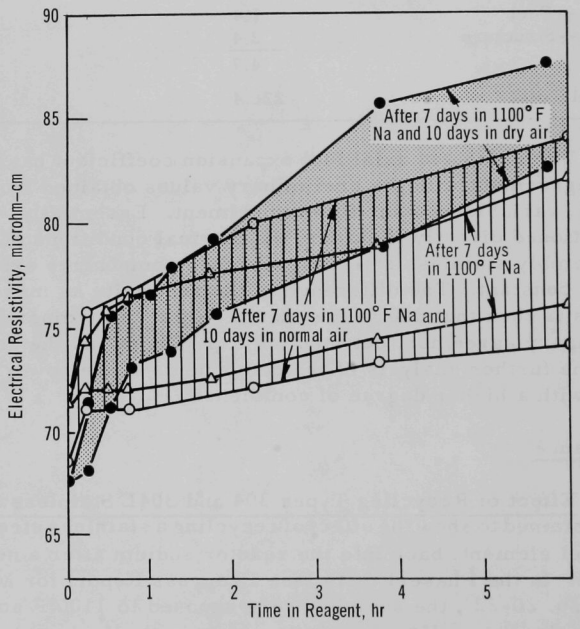

Fig. 3. Corrosive Attack of Type 304L Stainless Steel Tubes after Exposure to 1100°F Sodium for 7 days and Storage in Normal or Dry Air for 10 days, as Indicated by Changes in Electrical Resistivity during Subsequent Exposure to Strauss Reagent.

Specimens of Type 304L stainless steel that had been exposed to sodium and stored were again exposed to 1100°F sodium for another 7 days, after which they were cleaned. Some were examined metallographically and others were corrosion-tested in Strauss reagent. Photomicrographs show that the second sodium exposure highly sensitized the grain boundaries. Most of the 0.004-in.-deep intergranular attack occurred in the first 45 min in the reagent. As shown in Fig. 4, the Strauss

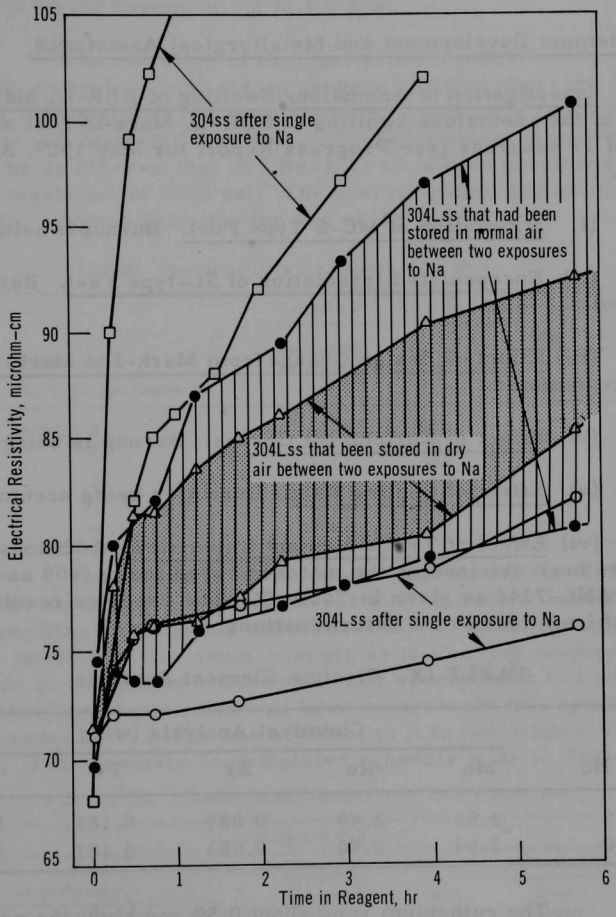

Fig. 4. Corrosive Attack of Type 304L Stainless Steel Tubes That Had Been Stored in Normal or Dry Air for 10 days between Two 7-day Exposures to 1100°F Sodium, as Indicated by Changes in Electrical Resistivity during Subsequent Exposure to Strauss Reagent. Data for Types 304 and 304L tubes that had only single exposure to sodium are shown for comparison.

accelerated-corrosion test caused a significant increase of the resistivity of the specimen that had been stored in air (between sodium exposures). The resistivity changes confirm that the grain structure was highly sensitized. After a few hours in the Strauss solution, the air-stored specimens showed signs of brittleness, and the highly resistive specimens began to blister and lose metallic "ring." The spread in the data is at least partly due to the faster corrosion of the tube wall area relative to the welded-seam area.

6. Fuel-element Development and Metallurgical Assistance

a. Investigation of Anomalous Swelling of EBR-II, Mark-IA Fuel. The study of the anomalous swelling of EBR-II, Mark-IA fuel was considered in terms of 11 subareas (see Progress Report for May 1967, ANL-7342, pp. 23-28).

(i) Irradiation of MC-S Type Fuel. Burnup is being accumulated.

(ii) Encapsulated Irradiation of SL-type Fuel. Burnup is being accumulated.

(iii) Effect of Design Change from Mark-I to Mark-IA. Burnup is being accumulated.

(iv) Effect of Enrichment Change. Burnup is being accumulated.

(v) Effect of Cooling Rate. Burnup is being accumulated.

(vi) Effect of Trace-element Impurities. Additional analytical results have been obtained on the matched set of melts (409 and 410) described in ANL-7342 as given in Table IX. The reported results are the averages of from four to six determinations.

TABLE IX. Fissium Element Analysis

	Chemical Analysis (w/o)				
Melt No.	Mo	Ru	Zr	Pd	Rh
409	2.52	2.49	0.089	0.185	0.280
410	2.54	2.50	0.083	0.187	0.291

The ruthenium runs about 0.5% too high; the contents of the other alloying elements are within specifications. The isotopic analyses are within the specified limits as shown in Table X.

TABLE X. Isotopic Analysis

Melt No.	Chemical Analysis (w/o) U^{235}	U^{238}	U^{234}	U^{236}
409	52.167	47.132	0.538	0.163
410	52.327	46.875	0.532	0.268

(vii) Effect of Pressure upon Swelling. Specimens for pressure studies are U-5 w/o Fs (52% enriched) alloy jacketed in Inconel 625 with 15-mil wall, and are sodium bonded. Each has an ~3-in. pressurized plenum. The individually jacketed specimens are inserted in groups of six in two tiers, enclosed in Zircaloy irradiation capsules, and placed in CP-5 for a target burnup of 1.2 to 1.5 a/o.

The objective of the first capsule test (P-1) is, as explained in ANL-7342, to seek a relationship between ambient pressure and rate of swelling. A material that has been shown by experience to have a high swelling rate (SL Material) was selected. The ambient temperature was adjusted to be as close to that of EBR-II at 45 MW as possible (603°C) for a pressure maximum of 2000 psi. The operating data are as in Table XI. Specimen No. 1 comes from the top end of the cast pin.

TABLE XI. Operating Data for Capsule Test (P-1)

Identification Melt/Cast Pin/1-in. Specimen No.	Capsule P-1 [(in-pile 5/22/67)(burnup - 0.15%)] Operating Pressure (psi)	Temp (°C) Max Fuel	Max Jacket	Avg Plenum
409/53-5	43	595	495	188
-11	85	595	495	188
-1	213	595	495	188
-7	426	595	495	188
-3	853	595	495	188
-9	1706	595	495	188

The objective of the second capsule test (P-2) is twofold: (1) to provide statistical confirmation for P-1, and (2) to cancel out of the pressure-swelling relationship differences due to metallographic factors insofar as possible. The same cast pin as in P-1 was employed, but use will be made of the alternate sections. The specimen in P-1 which was exposed to the lowest pressure will have a corresponding specimen at the highest pressure in P-2 that was adjacent to it in the original cast pin, and vice versa. The presently contemplated schedule is as in Table XII.

TABLE XII. Contemplated Schedule for Capsule Test (P-2)

Identification Melt/Cast Pin/1-in. Specimen No.	Capsule P-2 Operating Pressure (psi)	Temp (°C) Max Fuel	Max Jacket	Avg Plenum
409/53-4	2000	603	515	200
-10	1000	603	515	200
-6	500	603	515	200
-12	250	603	515	200
-2	100	603	515	200
-8	50	603	515	200

(viii) Effect of Heat Treatment. The specimens that have been introduced into Capsules No. 1 and 2 were, after injection casting, heat treated in a manner simulating the thermal treatment that EBR-II fuel pins undergo during sodium bonding. The treatment involved aging the as-cast specimens for one hr at 500°C, followed by slow cooling to room temperature. The aging is seen from metallographic, hardness, and density studies to affect (1) transformation of metastable gamma to alpha uranium, (2) a precipitation of very fine particles of U_2Ru and other secondary phases, and (3) a partial coalescence of U_2Ru particles that are segregated in large amounts in the as-cast structures at parent gamma grain boundaries. The latter boundaries are clearly evident in the aged structures, and parent gamma grain diameters range from 0.01 to 0.12 mm, with the larger grain diameters occurring in specimens taken from the botton end of the cast pin. As a result of the transformation to alpha and the precipitation of secondary phases, the hardness is increased to VHN = 498 to 579 from VHN = 266 to 366 in the as-cast condition. The room-temperature density of the aged pins range from 17.99 to 18.05 g/cc, which is closely consistent with that determined previously for sodium-bonded EBR-II Mark-IA (SL series) pins, 17.99 to 18.03 g/cc.

Preliminary studies have been made to determine the effects of heat treatment upon the chemical homogeneity and the distribution and size of precipitates in U-5 w/o Fs alloy. The work is being done with pin sections from Melt No. 410, which contained 2000 ppm Al, 800 ppm Si, and 250 ppm C, as well as with pin sections from a normal reactor grade U-5 w/o Fs alloy, Melt No. 409. Homogenization of the grossly heterogeneous structures produced on injection casting has been determined to be readily affected upon annealing at temperatures above 725°C in the gamma-phase region. With increasing annealing temperature, above 725°C, increased solution of extraneous phases formed from impurity elements appears to occur. With, however, 800 ppm of Si in the alloy Melt No. 410, a phase based on U_3Si_2 and containing molybdenum occurs as a stable phase in equilibrium with the gamma at temperatures as high as 950°C. The modified alloy containing the Al, Si, and C additions is also seen to undergo a eutectic reaction at approximately 940°C. On quenching from above 725°C the gamma is retained in a metastable condition in both the normal and modified alloys. Subsequent aging at temperatures below 552°C effects uniform distribution of precipitate in alpha uranium. Studies are in progress to determine the effects of aging time and temperature upon the particle size of the precipitated phases. To determine the influence upon swelling behavior of (1) retained metastable gamma, (2) heterogeneity, and (3) the amount of precipitate, six specimens from each of the two melts and having the following thermal histories are to be encapsulated and irradiated:

(a) as injection cast;
(b) as injection cast + aged one hr at 500°C;

(c) heat treated two hr at 980°C;[1] water quenched;
(d) heat treated two hr at 980°C;[1] + one hr at 500°C;
(e) heat treated 16 hr at 740°C; water quenched;
(f) heat treated 16 hr at 740°C; water quenched + one hr at 500°C.

(ix) Hot Lab Examination of Irradiated Fuel. Fifty-eight Mark-IA fuel elements were returned to Illinois for detailed hot lab examination. The sampling includes the three types of fuel: (1) SL-type, cast at Argonne, Illinois, in Building 350 (this type swells 14 to 16% at an average burnup of 1 a/o); (2) MR-type, the regular recycle of fuel pin in FCF at Idaho, and (3) MR-C-type, the consolidation melts of scrap generated in FCF. Except for chemical analysis, thermal conductivity measurements, and microstructural examination, all scheduled tests have been completed and the data are being analyzed. The status of each test or examination is summarized below:

(a) Fuel-element Radiography--58 completed.
(b) Fuel-element Gamma Scan--55 completed, three not scheduled.
(c) Fuel-pin Diameter and Length--56 completed, two not scheduled.
(d) Fuel-pin Weight, Volume, and Density--56 completed, two not scheduled.
(e) Fuel-pin Incremental Density--31 completed, 27 not scheduled.
(f) Furnace Heating Tests--two completed, 56 not scheduled.
(g) Gas Analysis--two completed, 56 not scheduled.
(h) Thermal Conductivity--four in process.
(i) Metallography--four in process.
(j) Chemical Analysis: carbon--20 completed, 36 scheduled, two not scheduled; silicon--25 completed, 31 scheduled, two not scheduled; aluminum--none completed, 56 scheduled, two not scheduled; iron--20 completed, 36 scheduled, two not scheduled.

The major unfinished work are the chemical analyses for trace-element impurities. The available analyses are tabulated in Table XIII. Pins 4002(9) and 4003(92) appear to have been interchanged prior to sampling for chemical analysis. It is not yet possible to establish an unequivocal correlation between swelling, fuel type, and content of trace-element impurity. A preliminary correlation should be possible by the end of next month. In general, however, it appears that the rapidly swelling SL-type fuel is low in total impurities, the MR-type material is low in carbon and silicon but not necessarily in iron (see 4001 and 4004), and that the low-swelling MR-C type

[1] The specimens from Melt No. 410 are to be heat treated at 900°C instead of 980°C to avoid liquid phase formation.

material is high in silicon but not necessarily in iron (see 4022 and 4025). Aluminum analyses, which will be available next month, may be helpful in clarifying these relationships.

TABLE XIII. Chemical Analyses of Irradiated Fuel Pins

Casting Batch and Pin No.		Melt Refining No.	Subassembly Element No.		Chemical Analysis (ppm) Carbon	Silicon	Iron
4001	1	22	C-184	87	107	88	470
4002	9[a]	23	C-180	60	189	226	440
4002	14	23	C-180	57	121	88	
4002	24	23	C-184	32	139	57	190
4002	82	23	C-184	60	146	89	155
4003	3	24[b]	C-186	53	200	162	425
4003	5	24[b]	C-186	52	199	165	
4003	19	24[b]	C-186	46	198	290	
4003	48	24[b]	C-184	57	192	217	520
4003	71	24[b]	C-180	32	193	203	
4003	86	24[b]	C-179	82	214	181	420
4003	90	24[b]	C-179	81	211	216	455
4003	92[a]	24[b]	C-179	79	132	94	
4004	9	25	C-184	7	108	140	435
4008	19	30	C-196	31		71	160
4022	33	C-30	C-217	3		175	340
4025	24	C-33	C-218	1		207	240
4025	44	C-33	C-217	78		213	280
4026	21	C-32	C-217	57		221	430
SL-20	40	-	C-185	2	149	85	150
SL-20	52	-	C-184	36	143	90	145
SL-21	20	-	C-186	60	153	87	155
SL-29	51	-	C-184	43	157	102	200
SL-29	68	-	C-179	52	138	116	105
SL-30	8	-	C-184	37	217	108	255

[a]4002(9) and 4003(92) appear to have been interchanged.
[b]MR-24 was a C-type melt.

(x) Analysis of Fuel-pin Swelling. Another 500 data sets of fuel-pin swelling versus maximum and average fuel-pin burnup have been transmitted to the Applied Mathematics Division (AMD) for programming. AMD now has nearly all of the available swelling burnup data. A preliminary analysis of the data should be completed next month.

b. Mark-II Driver-fuel Development

(i) Fabrication of EBR-II, Mark-II Fuel Elements. During the reporting period, 67 experimental EBR-II, Mark-II fuel elements were assembled and inspected for use in studies of irradiation performance. Element jacket hardware was of Type 304 stainless steel. The jacket tubes were 24 and 26 in. in length. Tube inside diameter was 0.150 in. and wall thickness was 0.012 in. The fuel pins were of U-5 w/o Fs alloy. Uranium enrichments were 93 and 80%. Pin length was 14.22 in. and pin diameter was 0.130 in. The fuel column in two elements was composed of segmented pins.

The fuel pins were sodium bonded to the jacket. A vacuum-pressure cycle of sodium filling and bonding was used in addition to the standard method of low-frequency impact bonding. Three types of restrainers were installed in the elements. Among these was a recently developed "triple-indented tube" restrainer. Restrainer positions and sodium levels were nominally 0.2 and 0.7 in. above the fuel pin. The sodium bond was inspected by means of point probe and encircling-coil eddy-current test equipment. Sodium levels were determined at 150°C by X radiography. The elements were shipped to the Engineering Irradiation Group for secondary encapsulation and irradiation testing in EBR-II.

Hardware Preparation: Jacket tubing from a commercial source was eddy-current inspected and was of the quality specified for EBR-II. Tubes and end plugs were machined as a part of fuel-element fabrication. The internal volume of each tube was determined by filling with liquid, and calculating the tube volume from the weight and density of the liquid. Tubes and end plugs were cleaned in acetone and alcohol, and were oven dried. Bottom end plugs were girth welded to the tubes by the TIG method. An identification number was electroetched on each jacket near the top. This number was also stamped on the tab attached to the corresponding end plug.

Fuel-pin Fabrication: Seventy U-5 w/o Fs alloy fuel pins were produced by injection casting in four melts. The castings were inspected for porosity by gamma radiography. Pins that contained defects larger than the maximum allowed for EBR-II production elements were rejected. The castings were sheared to length, length and diameter were measured, and pin surfaces were wire brushed. Pin weights were determined, and pin volumes were calculated by use of a nominal pin density, which was determined by liquid immersion of pin ends and reject pins.

Twelve density measurements were made with as-cast pin sections. The average density was 17.84 g/cc with a standard deviation of 0.044 g/cc. Four density determinations were made with pins that had been subjected to a bonding treatment at 500°C for 2 hr. The average

density of treated pins was 18.02 g/cc. These results show that retained gamma phase was present in the uranium cast structure, but that the metastable material transformed back to the higher density alpha phase during the bonding cycle.

Fuel-element Assembly: Each fuel pin was inserted through a metal funnel into a jacket subassembly. A length of 0.135-in.-dia sodium wire of predetermined weight was inserted above the pin. The amount of sodium addition was calculated to provide (0.2- and 0.7-in.) overfill above the pin.

A variation of previous assembly techniques was used in an attempt to improve the sodium bond and to simplify the sodium-bonding procedure. Bonding parameters were varied to derive information of use in future studies of the nature of the sodium bond.

Loaded elements were placed in a vacuum furnace and evacuated to 0.1 Torr; the furnace was then heated to 150°C to melt the sodium. A 60-Hz vibration was applied for 10 sec to seal the molten sodium to the jacket wall. The furnace was pressurized to 15 psig to drive the molten sodium down into the element annulus. The elements were heated to 500°C and held at temperature for 2 hr. This soak cycle allowed the sodium to dissolve foreign materials from pin and jacket surfaces to promote wetting. A 30-sec 60-Hz vibration cycle was applied to the element, after 1 hr of soaking time, to turn the pin in the jacket. When bonding was completed the elements were furnace-cooled to room temperature.

An approximate measurement of sodium level was made by inserting a calibrated metal rod into each element. Twenty-three slotted ferrule restrainers and 16 cylindrical ferrule restrainers were inserted into designated elements. The ferrules were pushed lightly into the sodium to prevent restrainer dislocation during subsequent handling. Top end plugs were TIG girth welded to the jackets to seal the elements. The elements were removed from the glovebox and were tested for leaks by helium mass spectrometry.

The elements were placed upon a reference gauge and an X radiograph was taken to show the position of the ferrule restrainer. The restrainers were fixed in place by making three radially spaced indentations in the jacket wall, both above and below the ferrule. A maximum axial movement of 1/32 in. was allowed for the ferrules. Tube indentations were made to sufficient depth to prevent movement of the ferrule restrainer past the indents. Triple-indent restrainers were installed in 28 elements at 0.2 and 0.7 in. above the fuel pin.

Development of Triple-indent Restrainer: A triple-indented tube type of restrainer was developed and installed in several fuel elements. Figure 5 is a composite view of a pin seated against the restrainer. The fuel pin is restrained by three radially oriented indentations in the tube wall as shown in Fig. 6. The indents are spaced 120° apart, are 0.050/0.040 in. long, and of sufficient depth, 0.017 in., to prevent passage of the fuel pin. The gaps between indents allow passage of sodium from the element annulus even when the fuel pin is seated tightly against the restrainer. The three indents are made simultaneously by a handwheel chuck and six-jawed rubber collet with floating steel inserts. Alternate jaws are ground down to achieve contact with the tube wall when the three indentor jaws are fully extended. The indentor jaws are radiused to insure smooth-edged indentations. The element is held firmly in a 2-in. die cavity during the operation to prevent excessive element bowing.

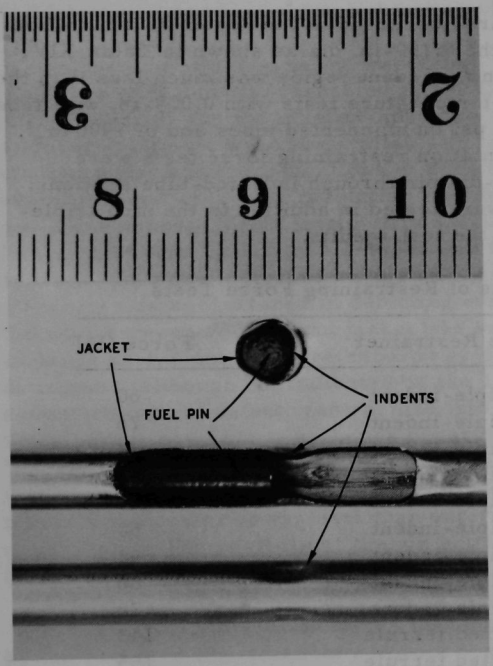

Fig. 5. Triple-indent Restrainer

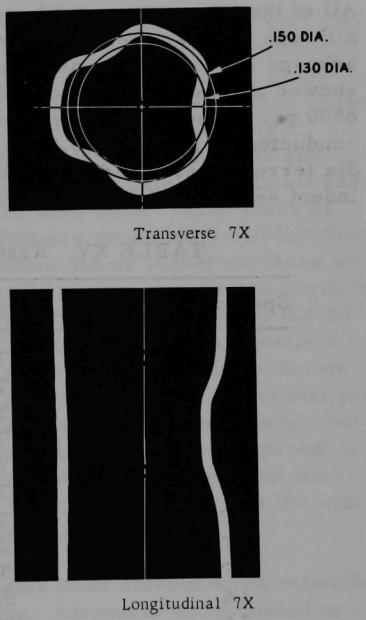

Fig. 6. Tube Sections through a Triple-indent Restrainer

Mechanical tests and metallographic examination were conducted with triple-indent restrainer samples to determine whether indentation caused tube wall damage. Nine indented tube sections were subjected to a tube burst test. Table XIV shows the test data.

TABLE XIV. Results of Tube Burst Tests (Triple-indent Restrainer)

Specimen	Temp (°C)	Burst Pressure (psi)	Average Diameter (in.)
1-350S	25	10,250	0.199
2-350S	25	9,950	0.182
3-350S	25	10,300	0.197
4-350F	25	9,825	0.200
5-350S	500	7,275	0.195
6-350S	500	7,100	0.195
7-350S	500	7,050	0.193
8-350F	550	6,550	0.192
9-350F	650	5,550	0.193

None of the failures occurred in the region of indentation. All of the tubes increased from the 0.150-in. dia as shown in Table XIV, although the diameter increase in the indent region was much less than the average shown. Previous room-temperature tests with 0.009-in. wall tubes showed a burst pressure of 8200 psi on unindented tubes and of 7900 to 8500 psi on indented tubes. Indentation restraining force tests were conducted by pushing a 0.127-in.-dia pin through indented-tube sections. Six ferrule restrained sections were tested in addition to the nine triple-indent sections; Table XV shows the test results.

TABLE XV. Results of Restraining Force Tests

Specimen	Type Restrainer	Force (lb)
1S	Triple-indent	60
2S	Triple-indent	76
3S	Triple-indent	74
5S	Triple-indent	60
6S	Triple-indent	86
7S	Triple-indent	50
1F	Triple-indent	92
2F	Triple-indent	86
3F	Triple-indent	76
1A	Slotted ferrule	143
2A	Slotted ferrule	155
3A	Slotted ferrule	229
1B	Cylindrical ferrule	178
2B	Cylindrical ferrule	112
3B	Cylindrical ferrule	222

Triple-indent restrainer tests resulted in an average restraining force of 73 lb when a 0.127-in.-dia pin was used. Because the fuel pins are 0.130 in. in diameter, a much higher restraining force is expected in the actual fuel-element indents. Similar tests were made with ferrule restrainers that were held in place by indents 0.006 in. deep. The restraining force averaged 173 lb and was much higher than the minimum required for the fuel elements.

Test indents were made in empty tubes as well as tubes filled with solid sodium. Six triple-indent restrainers were sectioned, both transversely and longitudinally, and inspected metallographically for tube wall thinning. No measurable wall thinning was seen on any sections. The indents of sodium-filled tubes were slightly more uniform. Some advantages accrue from deferring installation of the triple-indent restrainer until after fuel-element bond inspection and sodium-level measurements are completed.

Fuel-element Inspection: The sodium bond of the fuel element was eddy-current inspected at 150°C. Both the pulsed, differential, encircling-coil and the masked-aperture point probe were used. Fuel-element standards were not available to calibrate the eddy-test coils. Five elements that showed indications of bond defects were destructively examined, and eddy-test resolution was determined. Annular voids and sodium-shrinkage voids larger than 3/32-in. dia were detectable in all cases. Nearly all voids larger than 1/16-in. dia were also seen. Many voids of 1/32-in. dia were indicated when annulus thickness exceeded 0.010 in. Some difficulty was encountered in detecting nonwetted pin or jacket surfaces when the void between sodium and jacket was very thin. Some nonwetted surfaces as large as 1/4-in. dia were exposed by destructive examination of the sodium bond, although not indicated by the 150°C eddy test. Occasionally a nonwetted type of defect transformed into a detectable defect after two or three reheatings. Some nonbonds occurred at the bottom end of the fuel pin. The end effects of the bottom end plug masked the defect indication on the traces and made detection difficult. Pin-end indications on point-probe traces were easier to evaluate than encircling-coil traces. In some elements the nonbond defects at the pin bottom were seen to rise into the annulus on reheating cycles and appeared as bond voids.

All fuel elements that indicated bond defects were rebonded by the standard low-frequency impact bonding. Elements were heated to 500°C for 2 hr and were impacted for 1000 cycles. Bond reinspection was done to determine whether bond defects were removed. A total of 26 elements were passed by initial bond inspection, and rebonding was required on 41 elements.

The height of sodium overfill in the fuel elements was measured at 150°C by X radiography. Determination of the sodium level in the molten state eliminated spurious results caused by shrinkage voids

that are usually present in the sodium at room temperature. The sodium level in elements with a ferrule restrainer was not usually measurable because of lack of definition in the restrainer area. In these rods the level was determined with the assumption that the restrainer was one-half filled with sodium. Levels in elements with triple-indent restrainers were clearly defined. Sodium level at 150°C was calculated to be 0.19 in. higher than at 25°C. Sodium levels in the fuel elements were from 0.31 to 1.03 in. above the fuel pin. Measurements from 28 clearly defined levels showed an average level deviation of +0.04 in. from the expected value and level deviation range of +0.16 in. to -0.08 in. from the expected value.

(ii) Preirradiation Testing. Forty-five Mark-II elements were reported in ANL-7342 as being characterized by a series of measurements and tests. Sixty-seven Mark-II driver fuel elements have now been fabricated and preirradiation tested. The sodium annuli in the elements were without bond defects and the elements were acceptable. The entire group has been encapsulated and processed through sodium loading of the capsules, sealing the latter by welding, and impact bonding with the sodium at 500°C.

These 67 elements are among those contained in 42 capsules. Twenty of the latter proved to be sodium bonded, i.e., a liquid-metal bond between the outer surfaces of the fuel elements and the inner surfaces of the capsules has been confirmed by radiographic and eddy-current testing. Eleven capsules that had been initially rejected were again impact bonded and are ready for retesting. Eleven other capsules are being tested. Seventeen more capsules are required to complete the initial loading and should be available early in July.

7. Quality Monitoring and Control of Sodium Coolant

a. Sampling of Primary Sodium. The sampling system described in the Progress Report for March 1967 (ANL-7317, p. 5) was utilized for taking the samples listed in Table XVI. The table indicates the type of sampling vessel, the analysis for which the sample is intended, and other pertinent information. The "Al (aluminum) Tube" is the relatively large-volume (approximately 100 ml) tube currently used for taking bulk samples to be analyzed in the Chemistry Division at ANL-Illinois for hydrogen and oxygen. This type of vessel is also used for taking historical samples of primary sodium and for samples set aside for future "carburization potential" measurements.

The "beaker" sample is taken in a 10-ml Pyrex glass beaker. The entire sample is used for analysis to avoid the effects of impurity segregation or other inhomogeneity of the sample.

TABLE XVI. Samples of Primary Sodium Taken June 1967

Date	Container	Analysis	Remarks
5/29/67	Al Tube	Hydrogen, Oxygen	To Chem. Div., ANL-Ill.
6/1/67	Beaker	Activity	
6/1/67	Beaker	Cu	
6/2/67	Extrusion Vessel	Activity	
6/4/67	Beaker	Activity	Reactor at 2.5 MW
6/4/67	Beaker	Cu	Reactor at 5.0 MW
6/4/67	Beaker	Activity	Reactor at 5.0 MW
6/4/67	Beaker	Cu	Reactor at 7.5 MW
6/5/67	Beaker	Activity	Reactor at 7.5 MW
6/5/67	Beaker	Cu	Reactor at 10.0 MW
6/5/67	Beaker	Activity	Reactor at 10.0 MW
6/5/67	Beaker	Cu	Reactor at 12.5 MW
6/5/67	Beaker	Activity	Reactor at 12.5 MW
6/6/67	Beaker	Cu	Reactor at 15.0 MW
6/6/67	Beaker	Activity	Reactor at 15.0 MW
6/7/67	Beaker	Activity	Reactor at 17.5 MW
6/7/67	Extrusion Vessel	Activity	Reactor at 20.0 MW
6/7/67	Beaker	Cu	Reactor at 20.0 MW
6/8/67	Beaker	Activity	Reactor at 20.0 MW
6/9/67	Beaker	Activity	Reactor at 22.5 MW
6/9/67	Beaker	Activity	Reactor at 30.0 MW
6/11/67	Beaker	Activity	Reactor at 0 MW
6/19/67	Beaker	Cu	
6/21/67	Al Tube	Hydrogen, Oxygen	To Chem. Div., ANL-Ill.
6/21/67	Al Tube	Carb. Potential	Stored for future analysis
6/28/67	Beaker	Cu	
6/28/67	Beaker	Activity	

The samples designated for "activity" were dissolved and aliquots of the solution were analyzed by gamma-ray spectrometry in the ID Chemistry Laboratory. The purpose was to follow the Cs^{137} activity and to look for the appearance of other fission products as reactor power level was varied incrementally for investigative work related to the EBR-II fission product release incidents (see Sect. II.A.1.a).

A sample for copper analysis was not obtained during the week of June 12-18 because access to the sodium sampling room was restricted pending decay of Na^{24} activity following the small radioactive sodium fire of June 10 (see below).

A small radioactive sodium fire occurred in the primary sodium sampling room on June 10. This occurred after failure of the bellows in a valve in the waste sodium line from the primary sodium sampling station. It appeared that about 2 g of sodium had leaked to the atmosphere.

The failed valve was replaced on June 11, and a sodium sample was taken for fission product analysis, following the second fission product release incident early on June 11. Thereafter, access to the sampling room was restricted until the Na^{24} activity had decayed.

Some Na^{24} activity was carried out of the sampling room by the flow of ventilating air, causing minor air and surface contamination in the reactor building. Accordingly, the ventilating system for the sampling room is being redesigned to provide for exhausting air from the room through absolute filters at a rate sufficient to prevent escape of sodium smoke from the room.

b. Analysis for Carbon in Primary Sodium. This month work related to analysis for carbon in sodium involved blank runs to check the performance of the analytical equipment, training of an analyst to make carbon determinations, and redesign of the extrusion vessel-type sampler with provision for rapid cooling and solidification of the sodium sample. Redesign of the extruder vessel has also necessitated redesign of the extruder mechanism which is used in the glovebox containing the furnace portion of the carbon analytical train.

The extrusion vessel sampler is being modified to investigate the efficacy of rapid quenching as a means of minimizing segregation of substances of interest in sodium samples. The segregation phenomenon has been observed in prior work with carbon in sodium. Recently, evidence of segregation of radiocesium in sodium samples has been observed at EBR-II. This latter subject is treated in Sect. II.A.7.c, following.

The extruder vessel is being equipped with a cooling jacket through which cold nitrogen gas (from liquid nitrogen) can be forced at a high rate.

As previously noted (see Progress Report for May 1967, ANL-7342, p. 31), difficulty was encountered in attempting to fill the extruder vessel in the present primary sampling system. Therefore, work is in progress to provide for filling extruder vessels by a flow-through, freeze-line technique, incorporating provision for rapid quenching of the sodium sample. Two parallel efforts are proceeding to provide capability for flow-through filling of extruder vessels. The first involves improvised end adapters for the extruder vessel, utilizing metal O-rings for sealing. This is an expedient to permit sampling of the primary sodium for carbon analysis and investigation of carbon segregation as soon as possible. The other effort involves design of end closures and the use of seals which will simplify handling of the extruder vessel sample for analysis. Commercially available seals have been ordered for this application. August delivery has been quoted by the vendor.

The flow-through sampler in the secondary sodium system has been put into operation, and the extruder vessel has been filled successfully. Samples of secondary sodium will be used in training the analyst for carbon determination.

In order to obtain data concerning carbon content of the EBR-II primary sodium, seven historical samples were shipped at the beginning of June to the Chemical Engineering Division, ANL-Illinois, for analysis for total carbon. Sample numbers and dates are tabulated below:

Historical Sample No.	Date Sampled
2	3/7/63
11	11/12/63
19	6/27/64
31	2/26/65
44	9/15/65
57	7/25/66
63	12/2/66

After a portion of each sample has been taken for carbon analysis, the remainder is to be retained for future purposes, as required. It must be emphasized that the results of analysis will not necessarily be representative of true carbon concentrations in the sample vessels and in the bulk primary sodium because of segregation phenomena. Nevertheless, these analyses are expected to give a "ballpark" estimate of carbon content.

c. Segregation of Radiocesium in Samples of Primary Sodium. During the investigation of Cs^{137} concentrations in samples of primary sodium, following the EBR-II fission product release incident (see Sect. II.A.1.a), evidence of segregation of the Cs^{137} was found. A sample of primary sodium in a 10-ml beaker was allowed to decay until substantially all the Na^{24} was gone. The sample was then counted on the multichannel analyzer to obtain energy peaks for the Na^{22} gamma (0.51 MeV from positron annihilation) and for the Cs^{137} gamma (0.66 MeV). An aliquot from the above sample was then taken by mechanically digging out a center portion. This was also counted for the Na^{22} and Cs^{137} energy peaks.

The ratio of Cs^{137} to Na^{22} for the aliquot was found to be far lower than for the total sample, a very strong indication that segregation of the Cs^{137} had occurred in the sample of sodium.

To investigate this phenomenon further, a Type 304 stainless steel extrusion cup was filled with sodium by the "cup and spigot" method in an argon atmosphere. The volume of the cup was 15 ml, with the top and bottom surfaces flush with the surfaces of the contained sodium.

The sample as received appeared as in drawing (a) of Fig. 7. The excess sodium was cut off and dissolved in ethyl alcohol for analysis. The brass orifice closure was removed, the cup was placed in the extruder, and the extrusion was started with the ram placed as shown in drawing (b).

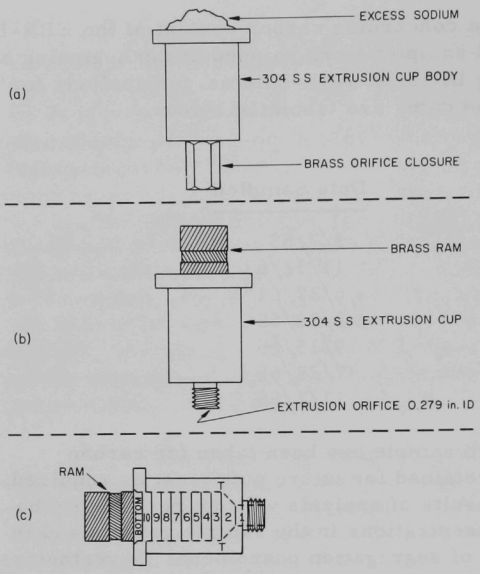

Fig. 7

EBR-II Extrusion Sample Vessel

The sodium was extruded in ten approximately equal aliquots, as shown in drawing (c). Sample 10 was undersize, since the ram stopped at the beginning of the taper TT. The "bottom" sample taken after 10 had a total size about equal to 1 and 2 together. This was dug out after ram was removed. As much sodium as possible was removed to obtain the "bottom" sample, but it was quite difficult and awkward; hence, some of this sodium remained in the vessel when the inside wall was washed down. This reduced to some extent the actual ratio of Cs^{137} to Na^{22} for the sample called the "vessel wall sample" because the sodium was depleted in Cs^{137} but not Na^{22}.

The amount of sodium in the vessel wall sample was found to be 0.23 g. The ram wash sample was found to contain 0.04 g sodium. The total amount of sodium was ~14.52 g.

The ratios of Cs^{137} to Na^{22} as found by summing the counts under the appropriate energy peaks are shown in Table XVII.

TABLE XVII. Ratios of Cs^{137} to Na^{22} for an Extruder-partitioned EBR-II Primary Sodium Sample

Sample (Refer to Fig. 7)	Cs^{137} to Na^{22}	Sample (Refer to Fig. 7)	Cs^{137} to Na^{22}
1	0.06	9	0.06
2	0.08	10	0.03
3	0.09		
4	0.09	Bottom	0.02
5	0.07	Excess Sodium	0.21
6	0.07	Ram Washings	0.69
7	0.09	Vessel Wall Washings	12.9
8	0.06		

Using the above data and a value of 1.5×10^{-2} μCi/g for the concentration of Na^{22} in the primary sodium, the following conclusions were drawn.

In this particular experiment, 75% of the Cs^{137} was found in a layer of sodium ~0.002 in. thick near the walls. This is the clearance between the ram and the inside of the vessel. The Cs^{137} was 185 times more concentrated in this layer than in the bulk of the sodium. The ram, in extruding the sodium, picked up some of the Cs^{137} concentrated in the wall layer of sodium. The Cs^{137} was about ten times more concentrated on the ram than in the bulk of the sodium. There was no significant axial segregation of the Cs^{137} in the sodium.

d. Analyses for Copper in EBR-II Primary Sodium. Analyses of copper provided by the ID Chemistry Laboratory are shown in Table XVIII.

TABLE XVIII. Analyses for Copper in Primary Sodium

Sample Date and Time	Sample Point	Copper (ppm)
5/17/1300	PI-A[a]	0.24
5/27/0945	PI-B[b]	0.24
5/27/1220	PI-A	0.34
5/27/1405	PI-B	0.44
5/27/1510	PI-A	0.56
6/1/1450	PI-A	0.57
6/4/1350	PI-A	0.22
6/5/1655	PI-A	0.23
6/6/1030	PI-A	0.18
6/7/2200	PI-A	0.14
6/8/2200	PI-A	0.14
6/9/1245	PI-A	0.16
6/19/1515	PI-A	0.22

[a]Sampling line from cold trap inlet piping.
[b]Sampling line from cold trap outlet piping.

e. Primary Sodium Plugging Temperatures. During June, the measured plugging temperatures of the primary sodium were consistently less than 240°F, with the bulk of the readings less than 225°F.

f. Primary Argon. On several occasions the primary-gas chromatograph showed a rapid increase in hydrogen concentration in the cover gas during the first 10 min after a subassembly was put into the transfer port. The hydrogen content then gradually decreased to its former level over a period of several hours. The data from the recorder charts are summarized in Table XIX.

TABLE XIX. Primary Argon Analysis by Continuous Gas Chromatograph

	Constituent (ppm V/V)		
	Hydrogen	Oxygen	Nitrogen
High	250	0	9,600
Average	4	0	4,000
Low	15	0	6,000

g. Data for EBR-II Fission Product Release Incidents

(i) Cs^{137} Analyses. Table XX gives the results of primary sodium analyses on samples collected prior to and after May 8, 1967. No Cs^{137} was detected in the sodium sampled April 24, 1967, and counted under the same geometry as the sample of May 8, 1967.

TABLE XX. Fission Products in Primary Sodium

At 1245 Sample Date	Cs^{137} (μCi/g Na)	Zr^{95}-Nb^{95} (μCi/g Na x 10^4)	I^{131} (μCi/g Na x 10^4)
4/24/67	$<5 \times 10^{-4}$	<5	<5
5/8/67	1.1×10^{-2}	<5	<5
5/19/67	1.5×10^{-2}	<5	<5
5/24/67		<5	~1
5/25/67	1.5×10^{-2}	<5	<5
6/1/67	1.6×10^{-2}	<5	<5
6/11/67	1.7×10^{-2}	<5	~1

From the Cs^{137} values, the total activity in the primary sodium was calculated. This value and the fraction it represents of the total Cs^{137} produced in an experimental pin of 5.8 a/o burnup and in a driver fuel pin of 1.0 a/o burnup are given in Table XXI.

TABLE XXI. Cs^{137} in Primary Sodium as Fraction of Total Produced in Experimental Pin and Driver Fuel Pin

Sample Date	Cs^{137} in Na (d/m x 10^{-13})	Cs^{137} in Na / Cs^{137} Produced in Experimental Pin	Cs^{137} in Na / Cs^{137} Produced in Driver Fuel Pin
5/8/67	0.7	0.25	1.80
5/19/67	1.0	0.33	2.50
5/25/67	1.0	0.33	2.50
6/1/67	1.0	0.33	2.50

From the information in Table XXI, it is obvious that the quantity of Cs^{137} in the primary sodium could not have come from a single pin of driver fuel.

Analysis of a sample of sodium taken from the upper end of a 1% burnup driver fuel pin gave 1 x 10^3 μCi of Cs^{137} per gram of sodium. There is approximately 1 g of bond sodium in each driver fuel pin. At 1% burnup, the Cs^{137} inventory of a driver fuel pin is 1.9 Ci, so the Cs^{137} in the bond sodium represents only ~0.05% of the total inventory.

(ii) Cover Gas. Quantitative estimates of Cs^{138}, Xe^{135}, and Xe^{133} activities in the cover gas were made following the May 24, 1967 fission gas release. These data, corrected for decay to release time, are given in Table XXII. The activity level of Xe^{135} in the 1300 hr sample, corrected for decay to release time, was about 450 times greater than the level from "tramp" uranium just prior to the release. No increases over the normal cover gas activity from "tramp" uranium was observed prior to the May 24 release.

TABLE XXII. Fission Gas Release of May 24, 1967

Sample Date and Time	Cs^{138} (μCi/ml)	Xe^{135} (μCi/ml)	Xe^{133} (μCi/ml)	$\frac{Xe^{135}}{Xe^{133}}$
5/24/1300	2.5 (±30%)	1.9 (±10%)	0.71 (±20%)	2.7
5/24/1615		1.5	0.70	2.2
5/24/1830		1.5	0.56	2.6
5/24/2200		1.7	0.6	2.8
5/25/0130		1.6	0.6	2.7
5/25/0535		1.8	0.67	2.7
5/25/0935		1.6	0.6	2.7

Note: Xe^{133} in the fuel was at about 50% of saturation when the gas release occurred. Both Cs^{138} and Xe^{135} were at 100% of saturation.

Above data corrected for decay back to release time.

The total Cs^{138}, Xe^{135}, and Xe^{133} activities in the cover gas were calculated from the data for the 1300 hr sample (given in Table XXII) and compared to their respective inventory in an experimental pin at release time. These data are given in Table XXIII.

TABLE XXIII. Fraction of Isotope Inventory in Experimental Pin Released to Cover Gas - May 24, 1967

Cs^{138}	Xe^{135}	Xe^{133}
0.058 (±30%)	0.042 (±10%)	0.031 (±20%)

Note: The error factor is due to the estimated uncertainty in the accuracy of the isotope measured in the cover gas.

On June 11, at 0223 hr, during 30-MWt power operation, the charged-wire fission product monitor indicated a fission product release. Gas samples were analyzed at intervals following the release, and the data, corrected to release time, are given in Table XXIV. An increase in Xe^{135} activity by approximately a factor of 5 was observed between the 0100 and the -237 hr primary agron gas sample.

Table XXIV. Fission Gas[a] Release of June 11, 0223 hours

Sample Date and Time	Cs^{138} (μCi/ml)	Xe^{135} (μCi/ml x 10^3)	Xe^{133} (μCi/ml x 10^3)
6/11/0100	Nondetectable	1.9	19.5
6/11/0237[b]	7.5×10^{-3} (±50%)	9.5 (±10%)	20.8 (±10%)
6/11/0325		10.0	20.2
6/11/0436		12.2	18.7
6/11/0900		18.1	18.6
6/11/1100		20.0	
6/11/1650		25.6	22.6
6/11/1950		24.3	23.6

[a]Estimated inventory of Xe^{133}, Xe^{135}, and Cs^{138} in an experimental fuel pin at the time of release: $Xe^{133} = 3 \times 10^8$
$Xe^{135} = 6.8 \times 10^8$
$Cs^{138} = 6.2 \times 10^8$.

[b]All values following the release are corrected for decay to release time.

The initial sample of primary argon gas following the release shows an approximately equivalent increase in Cs^{138} and Xe^{135} activities as would be expected from the calculated inventory. The expected equivalent increase in Xe^{133} activity (2-3 μCi/ml) is obscured by the statistics of counting.

As shown in Table XXIV, Xe^{135} activity continued to increase as a function of time for approximately 15 hr following the initial release. This ingrowth of Xe^{135} from I^{135} was not observed following the May 24 release. Both the magnitude of the release and the ingrowth of Xe^{135} from I^{135} suggest that the June 11 release may have been a small "bond" sodium release carrying recoil fission products rather than a true gas release from the capsule.

On June 19, at approximately 2229 hr at 10-MWt operation, the charged-wire fission gas monitor indicated a third gas release. Gas samples were collected at intervals and analyzed for Xe^{135} and Xe^{133}. The data, corrected for decay to release time, are given in Table XXV.

h. Secondary Sodium Sampling and Analysis. Flow of sodium was initiated on June 13 through the new sampling station and oxygen analyzer loop (without analyzer cells). Several containers for the Fuel Cycle Facility were filled, and two extrusion vessel samples were taken in the flow-through sampler. Testing of the oxygen analyzer has not been started pending completion of system checkout. A number of difficulties were encountered

in startup of the equipment, some of which have not yet been corrected. Some silver-soldered connections on remote valve operators for the flow-through sampler failed, galling of threaded fittings in the oven occurred, one heating element burned out, plugging of argon valves by splashing sodium or condensation of sodium vapor was noted, a leaking valve in a sodium line was discovered, and a cold section of a sodium line was found and corrected.

TABLE XXV. Fission Gas[a] Release, June 19, 2229 hr

Sample Date and Time	Xe^{133}[b] (μCi/ml)	Xe^{135}[b] (μCi/ml x 10^3)
6/19/2240	0.25	13
6/19/2305	0.27	7
6/19/2327	0.26	6
6/19/2350	0.29	5
6/20/0005	0.30	5
6/20/0035	0.31	5
6/20/0058	0.31	5
6/20/0125	0.31	4
6/20/0150	0.31	5
6/20/0300	0.32	5
6/20/0402	0.33	5
6/20/0510	0.34	5
6/20/0620	0.35	5
6/20/0718	0.35	6
6/20/0825	0.36	6

[a]Estimated inventory of isotopes in experimental pin at release time:
$Xe^{133} \cong 1 \times 10^8$ μCi;
Xe^{133} = very low--reactor just starting up after 8-day shutdown.
[b]All data corrected for decay to release time.

The installation of the plugging meter (for testing prior to installation in the FERD system) was completed, and the plugging temperature of the secondary sodium was measured as less than 225°F.

i. Secondary Argon. The continuous chromatograph, sampling argon from the surge tank, consistently indicated 10 to 15 ppm hydrogen and 1,000 to 1,800 ppm nitrogen. A minor perturbation was recorded on June 17 when some difficulty was encountered in getting the secondary sodium pump started after a power outage. The chromatograph indicated 15 ppm H_2 and 1,800 ppm N_2 before the power outage, and less than 10 ppm H_2 and 1,300 ppm N_2 after the pump had been back in service for several hours. Table XXVI presents a summary of data from the recorder chart.

TABLE XXVI. Analysis of Secondary Argon by Continuous Gas Chromatograph

	Constituent (ppm V/V)	
	Hydrogen	Nitrogen
High	15	1,800
Average	10	1,200
Low	<10	1,000

j. Expanded Sampling Capabilities for Primary and Secondary Sodium Systems. As noted above (see Sect. II.A.7.h), flow was started through the secondary sampling system. Initial operation has shown the need for some modifications to the system before it can be considered completely operational. With the installed heater capacity of the oxygen analyzer loop it was not possible to reach the recommended sodium to temperature at the analyzer cells. To correct this deficiency, a regeneration heat exchanger has been designed and appropriate heaters have been ordered. The heat exchanger will reduce the required heat input (at 1 gpm) from about 6 kW to about 1.9 kW. Plans call for installation of 2.8 kW with a 2.55 kW manually variable from 0 to 100 percent and 0.25 kW automatically controlled by sodium temperature. This arrangement should provide temperature control within ±2.5°F deviation at the analyzer cells. The manufacturer of the oxygen meter recommends temperature control within ±5°F deviation.

Machine work has been started to provide modified distillation sampler heads. These modifications will improve heating and temperature monitoring of the distillation cup. Improvements are also being made in the associated vacuum systems with the aim of a capability for holding less than 1-micron vacuum.

When these modifications have been completed, distillation equipment will be reinstalled in both the primary and the secondary sodium sampling systems.

As noted in Sect. II.A.7.b, work is in progress to adapt the extrusion sample vessels for flow-through freeze-line service. Also, pure nickel tubing has been ordered for taking freeze-line samples of sodium to be analyzed in the ID Chemistry Laboratory and elsewhere (e.g., RE, CEN, MET, CHEM Divisions at ANL-Illinois). The tubing sample seems to be the preferred form for shipping and storage. The capability for sampling and shipping in tubing is expected to expedite and improve analytical results provided by others in support of the EBR-II program. Delivery of the tubing is expected in late August.

k. Cleaning Operations for EBR-II Rotating Plug Seal Troughs

(i) Large Plug Seal. During June 2 and 3, the following amounts of material were removed from the large plug seal trough by the wire-brush technique described in the Progress Report for September 1966 (ANL-7255, pp. 6-7) and for October 1966 (ANL-7267, pp. 5-7):

Date	Weight of Material Removed (lb)	Arc through Which Plug Rotated during Cleaning
6/2/67	13.5	150°
6/3/67	20.0	90°
6/3/67	12.5	64°
6/3/67	74	204°
6/3/67	23	Cleanup spills, spatter, etc.
	Total 143	

The entire 143 lb of material was composited and saved as Sample No. 102.

The amount of oxidized material comprised only a few percent of the total weight, as judged by visual examination. No means is available to separate the oxidized material from the unoxidized alloy in the material removed for quantitative estimation of the amount of oxide. During the brushing operations, there was no evidence of extensive deposits of oxidized material.

(ii) Small Plug Seal. On June 13 and 14, brush-cleaning operations were performed on the small seal trough. Amounts of material removed are tabulated below:

Assigned Sample No.	Weight of Material Removed (lb)	Arc through Which Plug Rotated during Cleaning
103-A	6	60°
103-B	4	60°
103-C	3	60°
103-D	5	60°
103-E	11	60°
103-F	19	60°
103-G	4	60°
103-H (discarded)	16	Cleanup spills, splash, etc.
	Total 68	

Samples 103-A through G were packaged and stored.

As with the large plug seal cleanings, material appeared to be mostly metallic alloy.

(ii) Sampling of Alloy in Troughs. On June 2 prior to the cleaning operations described above, samples of alloy were taken from each seal trough to be analyzed for tin, bismuth, and sodium contents. Sample descriptions are tabulated below. Analysis results had not been received by reporting time. They will be reported next month.

Alloy Samples from LP Seal Trough	
Plug Orientation	Distance from Trough Bottom (in.)
Operate (0°)	2
Operate	7
120°	2
120°	7
240°	2
240°	7

Alloy Samples from SP Seal Trough	
Plug Orientation	Distance from Trough Bottom (in.)
Operate (0°)	2
Operate	7
120°	2
120°	7
240°	2
240°	7

8. Water Treatment Monitoring and Control

a. Treatment Data. Data for the power cycle streams are presented in Tables XXVII through XXIX.

TABLE XXVII. pH Values for Power Cycle Streams

Date	Condensate	No. 2 Heater (Deaerator Effluent)	Feedwater	Blowdown	Stream
6/1	9.2				
6/2	9.2				
6/3	9.3				
6/4	9.2		9.2		
6/5	9.2		9.2		
6/6	9.2		9.3		
6/7	9.2		9.3		
6/8	9.2	9.3	9.1	9.2	
6/9	9.3	9.3	9.3	9.1	9.2
6/10	9.2		9.3		
6/11	9.1		9.3		
6/22	8.8	8.8	9.1	8.9	8.9
6/23	9.1	9.1	9.2	8.9	
6/24	9.1		9.2		
6/25	9.2		9.2		
6/26	9.1	9.2	9.2	9.0	

TABLE XXVIII. Hydrazine and Dissolved Oxygen in Feedwater

Date	No. 2 Heater Effluent (ppb Dissolved O_2)	Boiler Feedwater	
		ppb Dissolved O_2	ppm Hydrazine
6/8	10-15	< 5	0.07
6/9	10	< 5	0.05
6/10			0.05
6/11			0.05
6/22	20	13	0.02
6/23	20	10	0.05
6/24			0.04
6/25			0.04
6/26			0.04

TABLE XXIX. EBR-II Condenser Cooling Water

Date	pH	ppm CrO_4	Cycles of Concentration	Date	pH	ppm CrO_4	Cycles of Concentration
6/1	6.3	12	2.0	6/14	7.5	8	2.1
6/2	6.5	13	2.0	6/15	7.6	8	2.0
6/3	6.5	12	1.9	6/16	7.9	6	1.8
6/4	6.7	12	1.9	6/17	8	5	2.1
6/5	6.5	12	2.1	6/19	7.4	4	1.5
6/6	7.1	13	2.2	6/20	6.4	12	1.6
6/7	6.8	15	2.5	6/21	6.9	12	1.6
6/8	6.9	12	2.4	6/22	6.7	13	1.8
6/9	6.7	12	2.7	6/23	7.3	15	2.0
6/10	6.7	15	2.8	6/24	6.7	11	2.4
6/11	7.0	13	2.8	6/25	6.5	17	2.7
6/12	6.4	12	2.5	6/26	6.7	13	3.1
6/13	7.6	7	2.1				

b. Treatment Equipment

(i) Acid Injection. The normal pH control system remained inoperative (see Progress Report for May 1967, ANL-7342, p. 36). Manual addition of sulfuric acid to the cooling water is continuing. Polyethylene tubing and fittings have been ordered to permit running a temporary line between the Power Plant and the injection point at the cooling tower.

The May report indicated that the existing line would be repaired when plant operation permits. However, further investigation has revealed that the perforated section is deeply submerged in the pump suction bay, perhaps in the 36-in. main cooling water header. Thus, there is no possibility of repair unless the cooling tower basin and the header can be completely drained. Furthermore, air-pressure testing showed that a plug exists somewhere in the acid line within the cooling water header. Thus, it appears that to return this line to service might require extensive

replacement of pipe. It is quite certain that considerable time would be required, during which the reactor could not be operated because the condenser would be without cooling water. In view of this, and also in view of the fact that this is the second failure which this line has sustained, the submerged acid line will be abandoned.

(ii) Chromate Reduction. The equipment for chromate reduction by sulfur dioxide is in service. However, results continue to be erratic, the apparent pounds of SO_2 required for reduction of one pound of CrO_4 varying between 2.2 and 5.3. A field engineer of Betz Laboratories, who supplied the reduction unit for testing, visited the site on June 9 to observe the operation of the unit and to take samples of influent and treated effluent for analysis by Betz. Testing of the unit will continue to determine the effects of operating variables and to ascertain whether equipment modifications are required.

9. Experimental Irradiations

a. Status of Experiments in EBR-II. The status of all experimental irradiations in EBR-II at the end of June is shown in Table XXX.

TABLE XXX. Status of EBR-II Experimental Irradiations, June 30, 1967

Sub-assembly	Date Loaded	Capsule Content and Number of Capsules( )		Experimenter	Approximate Accumulated Exposure (MWd)	Goal Exposure (MWd)
XG02	7/16/65	UO_2-20 w/o PuO_2	(1)	GE	10,644	13,600
		Stainless Dummies	(18)			
XG03	7/16/65	UO_2-20 w/o PuO_2	(2)	GE	10,644	19,450
		Stainless Dummies	(17)			
XG04	7/16/65	UO_2-20 w/o PuO_2	(2)	GE	10,644	39,000
		Stainless Dummies	(17)			
XG05	9/3/65	UO_2-20 w/o PuO_2	(9)	GE	9,917	14,750
		U-15 w/o Pu-10 w/o Zr	(1)	ANL		
		U-15 w/o Pu-10 w/o Ti	(1)	ANL		
		UC-20 w/o PuC	(3)	ANL		
		Structural	(5)	GE		
XA08	12/13/65	UC-20 w/o PuC	(8)	ANL	8,245	19,800
		Structural	(11)			
XO10	3/24/66	UO_2-20 w/o PuO_2	(4)	GE	7,575	19,600
		Structural	(11)	ANL		
		Structural	(4)	PNWL		
XO12	8/10/66	UO_2-20 w/o PuO_2	(19)	NUMEC	3,875	20,600
XO15	11/15/66	PuO_2-UO_2	(11)	NUMEC	2,220	11,000
XO16	1/13/67	Structural	(9)	ANL	900	3,000
		Structural	(10)	GE		
XO17	11/15/66	PuO_2-UO_2	(11)	NUMEC	2,220	6,500
		(Pu,U)C	(3)	UNC		
		MK-IA (Metal)	(5)	ANL		

TABLE XXX. (Contd.)

Sub-assembly	Date Loaded	Capsule Content and Number of Capsules ( )		Experimenter	Approximate Accumulated Exposure (MWd)	Goal Exposure (MWd)
XO18	12/6/66	Structural	(3)	GE	1,530	21,300
		Structural	(1)	PNWL		
		Structural	(2)	ANL		
		Structural and Heavy Metal Fission Yield Samples	(1)	ANL		
XO19	1/13/67	UO_2-20 w/o PuO_2	(7)	GE	900	7,500
		$(U_{0.8}\ Pu_{0.2})C$	(3)	UNC		
		Structural	(8)	PNWL		
		Graphite	(1)	PNWL		
XO20	1/13/67	Mixed Oxides	(9)	GE	900	25,000
		Mixed Carbides	(3)	UNC		
		Structural	(4)	PNWL		
		Structural	(2)	ANL		
		Graphite	(1)	PNWL		
XO21	2/27/67	Structural	(7)	PNWL	900	21,500
XO22	2/27/67	Structural	(7)	PNWL	900	8,000

b. Procurement and Inventory Control of Experimental Hardware. Arrangements are being completed for carrying out capsule hardware procurement, inspection, inventory, and distribution activities under this subtask.

Cost estimates were prepared for 30 sets of Mark-A capsule hardware for United Nuclear Corporation and 2 sets of Mark-B-7 capsule hardware for Idaho Nuclear Corporation. Also, the following experimental fuel capsules were received at Idaho Division:

GE, Group 3B	16 capsules
GE, Group E1H	19 capsules
ANL, Group M3	19 capsules

c. Other Work. A test proposal for investigating the Row-6 outlet temperature calls for increasing the flow in a subassembly from 73 to 90 gpm by enlarging the inlet holes to 0.314-in. dia. The flow holes in a Row-6 core-type lower adapter have been enlarged and the adapter is ready for use in a subassembly.

Prototype capsules and spacer wires have been received from PNWL for a prototype Mark-B-37A irradiation subassembly. The spacer wires are being attached to the prototype capsules. This Mark-B-37A prototype will be flow-tested for Rows 1 through 8.

10. Nondestructive Testing

a. Antimony-Beryllium Neutron Source. Fabrication of the Sb-Be neutron radiography source has been completed. Moderator materials loaded into the steel container are carbon (530 kg), beryllium oxide (1790 kg), and beryllium (148 kg). A criticality review for installing the source in FCF is scheduled for July 10, 1967.

Construction of handling fixtures and other needed hardware for the neutron radiography facility in FCF was not started in June. However, the construction drawings were completed, and the projected date for completion of the installation in FCF is still October 1, 1967.

The five dyprosium foils for neutron image detection were received in June. The surface of these foils did not have the smooth appearance that other dysprosium foils at ID have. The supplier has been contacted, and he requested that photographs be sent to him for inspection.

A second shipment of antimony oxide for gamma sources was received. The results of X-ray diffraction showed that the material was essentially pure antimony tetroxide (Sb_2O_4). A sample of the Sb_2O_4 was heated to approximately 900°C in a Type 304 stainless steel capsule in which the pressure could be measured. The sample remained at temperature for 6 hr. No evidence of pressure increase over that effected from the increased temperature of the contained gas was experienced. The sample has been sent to Idaho Nuclear Corporation for analysis by X-ray diffraction to determine whether any chemical changes occurred during heating.

b. Development of Isotopic Neutron Source. The computer study of the Am-Cm-Be neutron source for neutron radiography has been completed for all moderator materials except zirconium hydride. This material can upscatter neutrons, and cross sections to account for this have not yet been obtained. Beryllium oxide provided a higher neutron flux than any other moderator considered. A peak thermal flux of about 5×10^7 nv can be obtained from a source emitting 10^{10} neutrons per second.

General Atomics has tentatively agreed to run some problems on their GAM-II program. The cross-section library extends up to 14 MeV, so group cross sections can be generated for accelerator sources. Further negotiations will be conducted in July.

c. Neutron-sensitive Vidicon Development. A vidicon pickup tube in which boron nitride was substituted for the normal photoconductive target was tested in a camera that had been modified to control the integration time between target beam scans. There was considerable noise in the video signal, and a cadmium strip taped to the tube faceplate could not be observed.

Three solid-state neutron detectors were tested at TREAT. Boron nitride was the target material for each detector. One detector had a 1-in.-sq electrode divided into 16 equal areas. Each section could be interrogated individually by mechanical switching. Each section of the electrode responded to changes in the reactor power very well, but agreement of various sections at a given neutron flux level was poor. It is believed that uneven electrode pressure is the reason for the lack of agreement. This will be investigated further during July.

Raytheon did not supply a recording tube as previously agreed, but furnished a sample of the target material for testing in a greatly simplified tube. The device, about 50% complete, will be tested in July. The test will be essentially a measure of the rate of charge leakage from the target material in a neutron field.

d. Other Nondestructive Tests. Work on the oscillator for the pulsed eddy-current system was delayed because of work on equipment for the FCF cold line. Construction of the conveyor for the eddy-current machine has been started by INC. It should be finished in late July or early August.

11. Handling and Examination

HFEF data were prepared for HFEF on the heat-removal requirements for high-burnup, short-cooled subassemblies to be transferred between the reactor plant and HFEF.

a. Materials Surveillance Subassembly. The first of the EBR-II materials surveillance subassemblies, designated SURV-1 was removed from the primary tank last month. It has been in reactor position 12B1 (cumulative exposure of 11,541 MWd).

Test samples taken from this subassembly will be investigated at Idaho and at Illinois. ANL-ID is in the process of analyzing the hardness and corrosion specimens. Some of the samples to be evaluated by Illinois Divisions have been loaded in a cask and are to be shipped early in July. Two cask shipments will be required for these samples.

b. Testing of Procedures for Subassembly Sodium Removal. A program is in progress to determine the effects of subassembly cleaning procedures upon stainless steel cladding. The program comprises three major categories of work which, when completed, would provide definitive information as to the acceptability of returning experimental capsules to the reactor after cleaning for nondestructive examination and testing.

(i) Metallographic Examination of Capsule-wall Material (Type 304 Stainless Steel) from Capsules Irradiated in Subassembly XG06. These irradiated capsule specimens have been subjected to conditions typical of medium-exposure test capsules. They have been in the EBR-II core for approximately 18 months and received a total neutron exposure of about 3.5×10^{22} nvt. Normal moist, inert gas oxidation and water-wash procedures were used for sodium removal in the Interbuilding Coffin. After removal from the experimental subassembly some of the capsules were stored for about 11 days in water. Results of examination of capsule material will be compared with examination results for unirradiated Type 304 stainless steel. This work will be performed by the General Electric Company.

The metallography, which is the primary part of this work, has not been started because the necessary hot cell is in use for higher priority fuel examinations.

(ii) Cyclical Testing of Stressed Capsules (Type 304L Stainless Steel) at EBR-II. This work involves metallographic comparisons of as-received Type 304L stainless steel tubing with samples from pressurized tubes which will be exposed to EBR-II primary sodium, cleaned by standard EBR-II procedures and equipment, stored in air, and returned to the primary tank. Four cycles, into the storage basket in the primary tank and out again, are planned, followed by a fifth cycle which will involve installation of the capsules in Row 7 of the reactor for exposure up to 6×10^{21} nvt. Specimens will be examined after each wash cycle. Three hoop stresses will prevail during water washing. Higher stresses will exist while the capsules are in the 700°F sodium environment. All components for the pressurized capsules were received at Idaho. Assembly and pressurization of the capsules will be implemented early in July followed by the initial sodium exposure in EBR-II.

12. Fuel Cycle Facility (FCF)

a. Operations

(i) Hot-line Operation. Normal production activities were carried out throughout the month. Thirteen alloy preparation runs were made with unirradiated feed stocks to supplement the irradiated fuel inventory. Process operations are summarized in Table XXXI.

The samples from the materials test subassembly "Surveillance I" have all been removed from their containers and identified. In accordance with the procedure agreed upon, the samples designated for analysis in Illinois have been packaged and loaded in a cask for shipment. Work on the samples to be analyzed in Idaho has begun.

TABLE XXXI. Production Summary

	6/1/67 through 6/30/67	Total This Year
1. Subassemblies received:		
Core Control, Safety (for processing)	1	40
Other (Blanket)	7	115
2. Subassemblies dismantled (for processing); includes one for reassembly in new hardware	0	45
3. Subassemblies dismantled (for examination, etc.); includes 2 refrabricated subassemblies with bad hardware	2	31
4. Subassemblies fabricated (includes those made with unirradiated fuel)	18	91
5. Subassemblies transferred to reactor	16	68
6. Elements decanned:		
From irradiated subassemblies	0	4162
Rejects	170	484
Other	-	-
Total Decanned	170	4646

Melt Refining

	Irradiated Fuel	Recycle Material	New Fuel
7. No. of runs	1	7	13
8. Average pour yield, %	90.8	94.1	96.9

Processing

	6/1/67 through 6/30/67	Total This Year
9. Injection-casting runs (total number)	20	90
10. Elements processed:		
Accepted	1609	8017
Rejected	322	1041
11. Elements welded:	1844	8051
Rewelded:	2	9
12. Elements leak tested:		
Accepted	1857	7454
Rejected	24	136
13. Elements bonded (including recycle)	1941	9498
14. Elements bond tested:		
Accepted	1571	7655
Rejected	235	1320
15. Elements to surveillance	6 from 1 subassembly	407 from 40 subassemblies

Waste Shipments

16. Cans to burial ground	2	62
17. Oxide and glass scrap to ICPP	4	35

The problem with cracking of melt-refining crucibles (see Progress Report for May 1967, ANL-7342, p. 44) has been resolved by tightening the manufacturing specifications to include the following statement: "These crucibles must be structurally sound, containing no cracks, striations, or excessive graininess. They shall also have a minimum weight of 9,100 g per crucible."

The "bare pin" subassembly (L-418X) was received from the reactor and dismantled. Special handling procedures, which included sodium oxidation but not washing, were used to assist in obtaining maximum information from the experiment.

In preparation for the installation of the Vertical Assembler-Dismantler (VAD) machine, the original dismantling equipment was removed from the air cell. Installation of the VAD is scheduled for early July.

Production activities were hampered during the latter part of last month because of the unacceptable Mark-IA restrainers received late in May. As an expedient solution to the restrainer problem (see ANL-7342, pp. 45-46), acceptable restrainers were fabricated by cutting the top knobs off the unacceptable restrainers and welding knobs from acceptable Mark-I restrainers that were available. Approximately 5,000 restrainers (or a 3-month supply) were obtained in this manner. Specifications for replacement restrainers are being amended to include a limitation on the slag inclusions present. Material for the replacement order is being obtained.

Central Shops continues to develop manufacturing procedures for the Mark-IB restrainers. Shipment of samples for approval is expected by early July.

(ii) Cold Line Operation. A cold or unirradiated fuel fabrication line is being installed outside the Air and Argon Cells of the FCF. This line will be used to augment the fuel-production capacity of the FCF and to serve as back-up to it. It is expected to be in operation during the first half of FY 1968, with a production rate of about eight subassemblies per month. With initiation of the cold fuel production, transfer of spent subassemblies in excess of those necessary for remote production will be made to the Idaho Chemical Processing Plant (ICPP) for storage and processing.

The following is the status of the various components that will be used in the cold line for production of unirradiated fuel.

(α) Alloy Preparation Furnace. Although the problem of cooling of power leads to the induction coil was resolved, the leads had to be rebuilt because they could not be balanced with the capacitor work station.

A test run without uranium has been completed. After minor adjustments have been made, several depleted uranium ingots will be cast.

(β) Injection-casting Furnace and Pin Processing. Installation of piping and accessories is almost complete. Electrical work is about 25% complete. All equipment except the injection-casting control consoles are complete, but not checked out.

(γ) Glovebox and Element Assembly. Installation of the glovebox and purification system is 95% complete. All equipment to go in the glovebox is ready. Several acceptable welds were made on empty jackets with the restrainer welding machine.

(δ) Fuel-element Process Equipment. The leak detector and valve cabinet are completely set up and the system is being debugged. Controls for the bonding furnace are being checked. No progress was made during this month on installation of the bond tester.

(ε) Assembly Machine. Detail drafting is 98% complete and, at the end of the month, those drawings that were finished were turned over to Central Shops for fabrication. Delivery date of September 15 for all components has been requested.

(ζ) Installation. Installation of the degreaser in the new addition to the Inspection and Test Facility is over 95% complete. The contractor is expected to be 90% complete (cold-line work) by July 1 and 100% by July 14.

With the procurement of EBR-II driver fuel elements by either cold-line production or from commercial vendors, the inventory and usage of driver fuel elements is expected to increase beyond that which can be stored or processed in the FCF. Some irradiated driver fuel elements will be reprocessed at the Idaho Chemical Processing Plant (ICPP). To allow sufficient cooling time and until sufficient irradiated driver fuel has been accumulated for a reprocessing run, ICPP plans to store the fuel in a water basin.

A top loading and unloading cask has been designed to transfer subassemblies between the FCF and the ICPP. Because its design is relatively simple, the cask can be readily fabricated. It will accommodate one 15-day-cooled subassembly and will contain water for natural-circulation cooling of the subassembly. The completed cask drawings have been submitted to Central Shops, Argonne, Illinois, where the cask will be fabricated. Delivery of the cask to the FCF, Idaho, by September 15, 1967, has been requested.

ICPP in-house corrosion tests are in progress with five of the six irradiated fuel elements, being used for this purpose, shipped to them last month. The tests are being carried out to determine if, after in-reactor exposure of the fuel element to sodium, the corrosion rate of the stainless steel cladding is accelerated during storage in the water basin. It was reported that the five fuel elements selected for the corrosion studies were tested for cladding defects and none were found. Under-water storage (in the ICPP basin) of the five elements is in progress.

(iii) Maintenance and Repair. Routine maintenance and repair is required to keep the existing equipment in operating condition and hence to prevent production interruptions.

No major repairs were required during this month and the equipment in general ran quite well.

At this time, we are initiating a study to determine if a computer program can be worked out for the equipment maintenance. Because of limited information on equipment life, the general approach to date has been to operate equipment until some component fails and then to perform a complete decontamination and overhaul. A study of time and cost experience history may indicate an alternate to this approach.

(iv) Operator Training. The form of training utilized by FCF operations is a combination of on-the-job training augmented by a series of lectures. These lectures include safety, accountability, criticality control, and general operating procedures in addition to specifics for cell processes and equipment. Manipulator training sessions were begun last month for two new employees. So far, three sessions have been completed.

Periodically, several technicians are rotated in job assignments to gain additional on-the-job training and knowledge of other FCF operations. Last month, five technicians were rotated and this month were undergoing on-the-job training to gain new knowledge and experience.

(v) Operating Manuals and Reports. As a part of the overall operating and training program, new manuals are being prepared and the current manuals are being updated on all phases of the operation. In general, emphasis or priority in the following order is being given to those sections of operations which are related to personnel safety, could cause damage to the facility, and affect only individual components of equipment.

In the past month, 3 new sections, 9 parts of new sections, and 4 revised sections have been completed and submitted for review and acceptance. Five sections, revisions, and parts of sections have been issued as accepted portions of the FCF Operating Manual.

(vi) Product Analysis. Two basic types of analytical effort are included in this area. The first is the chemical analysis required for quality assurance of all reactor fuel. This includes analysis for specific trace elements which build into the fuel during recycle, analysis of samples of cell atmosphere, equipment contamination samples, etc. The second effort is that of postirradiation analysis of the fuel used in the reactor. This is a continuing effort to correlate process and product variations with postirradiation fuel behavior.

(α) Chemical Analysis. The numbers of fuel-production and surveillance analyses accomplished are tabulated below. No significant deviations from the normal were observed.

Analyzed for	Surveillance Subassemblies	Production Subassemblies
U (total and isotopic)	3	22
Pu (total and isotopic)	11	10
Si	6	9
Al	-	12
Rh	-	3
Fe	0	28
Mo	0	16
Ru	-	14
Zr	-	8
Pd	-	2
Burnup (La)	5	-
Total	25	124

An atomic absorption spectrophotometer had been received in the laboratory, and its installation and checkout are underway. It will be set up adjacent to the analytical caves for use on both irradiated and unirradiated samples. It is anticipated that its use will accelerate the determination of trace elements and noble metals in fissium alloy which are now determined by wet chemical techniques.

(β) Postirradiation Analysis of EBR-II Fuel. A continuing program to evaluate the irradiation performance of Fuel Cycle Facility-produced, EBR-II driver-fuel alloy is being carried out in the FCF. This program consists of determining the irradiation swelling that has occurred in U-5 w/o Fs alloy of EBR-II driver fuel elements as a result of service in the reactor.

Volume changes of fuel pins have been calculated for elements from a total of 20 subassemblies. These data are presently being evaluated and prepared for reporting.

b. FCF Process Analysis and Testing

(i) Operational Analysis. One purpose of this program is to identify the actual costs of individual steps of the fuel refining and fabrication, and to identify the various components and pieces of equipment that are used in conjunction with these processes, as well as to segregate the amount of time used by these various components for each step of the process. Studies will be made to computerize the accountability control system. Comments have been solicited from various cognizant staff members to aid in the organization of a computer-oriented data-retrieval system which could be applied to process variable analysis, performance analysis, and data accumulation for reporting. In addition, a long-range program to follow the effect of recycling of the fuel has been inaugurated.

A proposal for computerized accountability control system has been prepared and is being studied.

(ii) Reporting. The accumulation and consolidating of process and analytical data continued to enable ready retrieval for the preparation of reports.

(iii) Test and Analytical Methods. Various methods, procedures, and equipment are being developed to test the analytical means of determining the results of the processing and refining of the fuel within the fuel cycle.

(iv) Advanced Process Methods. A study task force is being designated to review material describing advanced fuel cycles. FCF operating experience and pertinent operating data will be included in the advanced cycle studies. Evaluations of proposed operational sequences will be prepared.

c. FCF Equipment Improvements

(i) Processing Equipment. The vertical disassembly-assembly machine (VAD) was received, set up and tested in the mockup area. Operator training and equipment modifications were carried on throughout the month. Installation of the VAD machine in the Air Cell to replace the original dismantling equipment is scheduled for next month.

A pneumatic-transfer tube system is being designed to be installed between the Air Cell and the analytical caves to facilitate the transfer of samples between the Fuel Cycle Facility and the Analytical Laboratory. Drawings have been completed and are now being checked. Purchase orders for procurement of fabricated items has been initiated. The project is currently on a schedule which calls for completion by the second quarter of FY 1968.

A nondestructive method of examining experiments and driver fuel is neutron radiography. Equipment to provide for this is being designed to be installed in the Argone Cell of the Fuel Cycle Facility; design has been completed and detailed drafting is nearly complete. Checking of the drawings is proceeding, and it is anticipated that the first drawings will go to the shop during the coming month. Based on present evaluation, this project should be completed during FY 1968.

(ii) Auxiliary Equipment. One of the major problems with the maintenance and/or repair of the Argon Cell gas-recirculating fans is the level of contamination within the fan housing as it effects access to the equipment. One means of reducing this level of contamination would be to filter the gas in the Argon Cell prior to its entrance into the fan boxes.

A full-sized mockup of a system to provide such filtering has been built and is being tested. It was moved from the Laboratory and Service Building basement where it was built to an outside location (noise level is very high). Only a limited amount of data has been accumulated.

Present operations of the Fuel Cycle Facility require that all material that is transferred into or out of the Argone Cell must traverse the entire length of the Air Cell passage. To alleviate this extensive material handling in the Air Cell, a modification is being made in the Transfer Cell between the Air and the Argon Cells. This modification will allow unirradiated new process materials to be introduced directly into the Transfer Cell and from there into the Argon Cell without traversing the length of the Air Cell. This transfer-cell modification can also be used for transfer out of samples or of low-level-contaminated material from the Argon Cell. The modification will include a transfer lock, a viewing window, and a pair of master-slave arms inserted into the wall of the transfer cell in the basement of the Fuel Cycle Facility.

The plug containing the shielding window and transfer lock was checked prior to installation and found to require extensive reworking which will delay actual installation for a month.

As a means of decreasing the interdependency of the schedules of the Fuel Cycle Facility, outside reprocessing plant, and the Reactor, more storage capacity for subassemblies is desirable. A major interruption in the flow of subassemblies would result in a stoppage of these operations. An interim-storage facility providing for a two-month-holdup capacity would insure that creditable interruptions could be compensated for.

In the preceding monthly report (see Progress Report for May 1967, ANL-7342, p. 53), it was reported that, owing to insufficient storage capacity and shielding problems, it would not be feasible to utilize the existing storage pits in the passageway between the reactor building

and the Fuel Cycle Facility. Alternative approaches for providing the additional interim storage capacity are being examined. One promising approach involves constructing a new wing in which up to 40 complete subassemblies would be stored in shielded and cooled, floor storage pits. The new wing would be located near the FCF passageway. Design concepts of this storage facility are now being developed.

A shielded cask employing bottom loading and discharging of a subassembly will be used (1) to transport subassemblies to and from the new facility, (2) to charge and remove a subassembly from a storage pit, and (3) as an alternate cask for the transfer of subassemblies from the FCF to the ICPP for storage and subsequent reprocessing. The cask will handle one subassembly (15-day cooled) and will provide cooling of the subassembly. Design concepts of this cask are being coordinated with those of the new storage facility.

(iii) Repair and Decontamination. A facility for the decontamination and repair of the electromechanical manipulators is needed. This facility could be most advantageously located in the wind-and-weather enclosure on the roof of the Air Cell above the existing shielded plug opening.

Preliminary concepts have been proposed and approved. The engineering on this project is very near completion, and detailed drawings will be started this month. The job is estimated to be 10% complete.

Removal of equipment items from the Argon and Air Cells presents problems in spread of contamination and personnel exposure. In order to alleviate these problems, a shielded, mobile, decontamination chamber is being designed. This chamber will mate with a special hole in the transfer tunnel between the Argon and Air Cells. It will provide 3 in. of lead shielding, a high-pressure liquid washing system, master-slave manipulators, and filtered ventilation system. A 1500-lb-capacity hoist on an extendible boom will enable heavy items to be introduced to or removed from the chamber. The chamber itself will be mobile, permitting material to be moved from the transfer tunnel to a special repair room, which will also be built as part of this project. Preliminary decontamination will take place in the mobile unit with final cleanup in the repair room.

The project is currently in the final design stages, work having been started on detail drawings. Present schedules indicate this project will be completed in FY 1968.

13. Nuclear Instrument EBR-II Test Facility

A test loop is required for testing of instruments in a neutron, gamma, and temperature environment that will be typical of the Fast Flux Test Facility (FFTF) and liquid metal fast breeder reactors. The spare

out-of-core 01 instrument thimble in EBR-II will be utilized for this instrumentation development program.

The experimental program will be divided into two phases. Heating of the existing 01 thimble and its contents to the 700°F bulk sodium temperature in EBR-II will be the first step. This phase of the program will require a completely new thimble insert to hold the newly developed high-temperature nuclear detectors. As presently installed, the thimble cooling system will allow a gradual reduction and complete shutoff of air to the 01 thimble while flow to all other thimbles may be adjusted as desired. Some minor changes to power supplies, instrumentation, and reactor high-temperature shutdown circuity will also be required. This phase of the program is estimated to require ten man-months of effort.

The second phase of the program will be the continued testing of instruments and cables from 700°F up to 1200°F. This will require a complete redesign and replacement of the existing 01 thimble, which presently contains aluminum baffling that is inadequate for the elevated temperatures. A new heating system will be necessary, as well as a cooling system, to allow a range of temperatures in the thimble from about 100 to 1200°F. The present coolant system may be adequate with some modifications. Preliminary investigations indicate an external gas-heating system would impose severe thermal problems on the upper thimble area of attachment of the tank cover. A new thimble design, utilizing small electric heaters to provide a 1200°F atmosphere only near the thimble bottom at the instrument and cable, appears to be most feasible at this time. This high-temperature phase of the program is estimated to require about two and one-third man-years of effort.

14. Hot Fuel Examination Facility

Various ways of expediting the establishment of the project staff to the level required to generate a reasonably detailed and reliable cost estimate by November are being explored. The conceptual design effort has been divided into tasks, and preliminary descriptions have been prepared.

Conceptual design studies of various cell configurations and manipulator support systems are being continued. A flow diagram has been prepared of the in-cell operations to be performed. Work stations requirements are being investigated.

Several new configuration concepts of the Hot Fuel Examination Facility (HFEF) have been generated and are being evaluated. The most promising is a configuration involving three separate cells: a "high level" cell which would be primarily used for the assembly and disassembly of fuel

and loops; a "low level" cell primarily for metallographic and physical examination of samples; a decontamination cell. All three cells are on one level and interconnected by a common transfer tunnel. Equipment, vertical loops, and fuel subassemblies would be brought from outside of the HFEF complex directly into any one of the cells (or from cell to cell) through this tunnel. Inexpensive movable transfer boxes on a rail system in the tunnel permit the maintenance of separate atmospheres or contamination levels in each cell and also permit a number of transfers to take place at the same time.

This concept appears to have many advantages over a multiple-storied complex, especially in view of the tight schedule involved. Because the cells are relatively independent of each other, they can be designed, constructed, and checked out in the most efficient manner possible. Changes in the design, size, or configuration of one cell do not affect the other cells. Also, the separate cell-tunnel approach is very conducive to future expansion and facility upgrading.

Unique construction methods are also being investigated in an effort to cut costs and allow flexibility in equipment design and facility construction as the project progresses.

B. Physics Development

1. ZPR-3

Work was completed this month with Assembly 49, and the approach to critical for Assembly 50 is in progress. These two assemblies are the second and third in a series of simple plutonium assemblies planned for ZPR-3. Assembly 48, the first in the series, contained plutonium, depleted uranium, sodium, graphite and stainless steel. The composition of Assembly 49 was similar except that all of the sodium was removed. Assembly 50 has additional graphite substituted for the sodium but is otherwise the same as Assembly 48. The aim of the experimental program in each assembly is to provide a set of integral data that can be used to check the accuracy of cross-section sets and analytical techniques.

a. Assembly 49. Central perturbation measurements have been completed with a set of samples which included the following materials: manganese, boron-10, chromium, aluminum oxide, tantalum, iron, stainless steel, nickel, graphite, molybdenum, enriched uranium, depleted uranium, plutonium, aluminum and polyethylene. Sets of enriched uranium, depleted uranium, and manganese foils were irradiated in a central drawer to determine the variation of reaction rates throughout the cell-plate arrangement. The U^{238} Doppler coefficient was measured by means of the hot-sample technique. On the completion of these measurements sodium was added in steps to a 74-drawer central region over the full core length to measure the sodium worth and to return to the Assembly 48 central spectrum for additional foil scans in the central cell. The analysis of the Assembly 49 data is in progress.

b. Assembly 48B. The general arrangement of Assembly 48B has been described (see Progress Report for March 1967, ANL-7317, p. 33). The fuel loading of the machine was as follows:

	$Pu^{239} + Pu^{241}$ (kg)
Central high Pu^{240} zone	20.56
Outer low Pu^{240} zone	249.46
Total	270.02

Corrections to the loaded mass for the irregular outline of the core and the higher fuel loading of the control rods are being evaluated. The composition of the high Pu^{240} zone is given in Table XXXII.

Measurements were made of the reactivity change produced by the removal of sodium from the front 4 in. of drawers in both halves of the machine. The location of the drawers used is shown in Fig. 8, and the results given in Table XXXIII.

TABLE XXXII. Composition of High Pu^{240} Zone

	10^{22} atoms/cm^3		10^{22} atoms/cm^3
Pu^{239}	0.1436	Fe	1.0223
Pu^{240}	0.0311	Cr	0.2543
Pu^{241}	0.0059	Ni	0.1113
Pu^{242}	0.0007	Mo	0.0206
U^{235}	0.0016	Al	0.0118
U^{238}	0.7405	Mn	0.0106
C	2.0767	Si	0.0125
Na	0.6231		

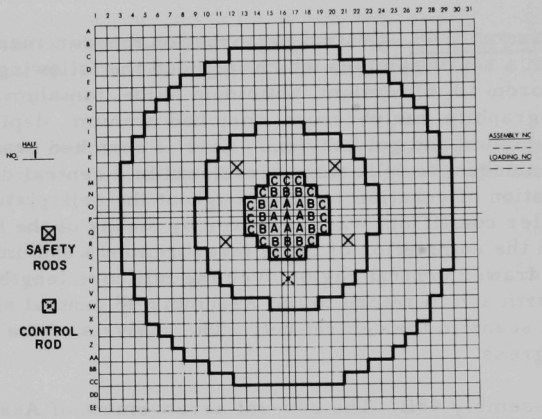

Fig. 8. The Arrangement of Assembly 48B for Sodium-removal Measurements

TABLE XXXIII. Sodium-removal Measurements in Assembly 48B

No. of Drawers	Drawer Designation	Sodium Removed (kg)	Reactivity Change (Ih/kg)
18	A	1.32	8.4 ± 1.1
24	B	1.76	7.4 ± 0.9
42	A + B	3.08	7.8 ± 0.5
32	C	2.346	1.0 ± 0.7
74	A + B + C	5.426	4.7 ± 0.3

Fission-ratio measurements were made at the center of Assembly 48B, using the spherical aluminum wall back-to-back chambers. The results are given in Table XXXIV.

TABLE XXXIV. Central Fission Ratios in Assembly 48B

U^{233}/U^{235}	1.439 ± 0.014	U^{234}/U^{235}	0.198 ± 0.003
Pu^{239}/U^{235}	0.964 ± 0.010	U^{236}/U^{235}	0.066 ± 0.001
Pu^{240}/U^{235}	0.229 ± 0.003	U^{238}/U^{235}	0.0297 ± 0.0005

2. ZPR-6

a. The Effect of Varying the Concentrations of U^{238} on the Sodium-void Coefficient. The influence of the concentration of U^{238} on the sodium-void coefficient in Assembly 5 of ZPR-6 was measured. The normal materials concentrations in Assembly 5 were altered for this experiment in the following manner:

(i) The atomic concentration of U^{238} per unit volume was essentially halved in a region 30 cm in radius and throughout the axial height of the core (142 cm).

(ii) Cans of sodium, 1/4 in. thick, were added to fill the empty space that resulted from the removal of depleted uranium plates.

(iii) The concentration of U^{235} was decreased by 25% to counteract the increase in reactivity of the system due to the removal of U^{238}.

The atomic concentrations of the materials in the uniform and modified loadings of Assembly 5 are shown in Table XXXV. The reflector for both loadings was depleted uranium. The radial and axial thicknesses of the reflector were 27 and 30 cm, respectively.

TABLE XXXV. Material Concentrations in the Uniform and Modified Loadings of Assembly 5 of ZPR-6

	Concentrations (atoms/cc x 10^{-24})	
Material in Core	Uniform Loading	Modified Loading[a]
U^{235}	0.00153	0.00115
U^{238}	0.01056	0.00615
N	0.00920	0.01120
Fe	0.00904	0.00992
Ni	0.00113	0.00125
Cr	0.002386	0.00264
C	0.01293	0.01293

[a]The modified loading comprised a region 30 cm in radius and 142 cm long about the center of the core. The rest of the core had the same composition as the uniform loading. This region extended to 76 cm radially.

The measurements consisted of determining the reactivity worth of the sodium-filled cans in sections 4 in. long in each half of the reactor relative to empty cans which were identical to the sodium containers. The sodium-void effect was measured in 9 central drawers per half (equivalent outer radius of 9.37 cm) as a function of the axial dimension. The results are given in Table XXXVI. The physical location of each section is given in Fig. 9. The uncertainties in the values of the sodium-void coefficient for the uniform loading are typically 0.15 Ih.

TABLE XXXVI. Comparison of Measured Sodium-void Coefficients in Uniform and Modified Loadings of Assembly 5 of ZPR-6

	Measured with (Ih/kg)	
Section Voided[a]	Uniform Loading	Modified Loading
A	1.15	-
A + B	1.12	-0.221 ± 0.070
C	0.97	-0.281 ± 0.044
D	0.44	-0.585 ± 0.127
E	-0.20	-1.029 ± 0.127
F	-1.02	-1.254 ± 0.024
H	-1.54	-1.967 ± 0.054
A → H	-0.293	-1.195 ± 0.008

[a]For the position of each section see Fig. 9.

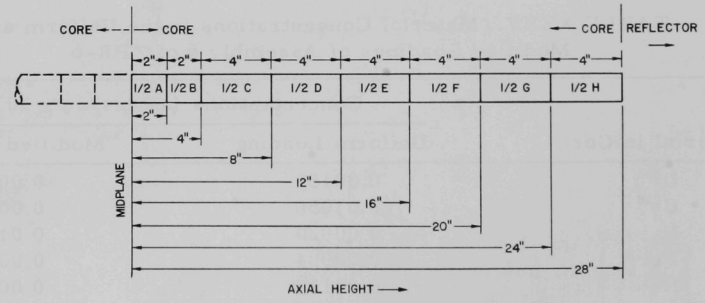

Fig. 9. Sections Where Sodium was Removed at Center of Assembly 5 of ZPR-6

b. Fission- and Capture-rate Traverses in Uniform and Modified Loadings in Assembly 5 of ZPR-6. Fission-rate traverses of U^{238}, and fission- and capture-rate traverses of U^{238}, were measured in both the uniform and modified loadings of Assembly 5 to determine the degree of power flattening in the modified loading and to make comparisons with calculations. In general, the calculated and experimental results are in good agreement. Figure 10 shows that considerable flattening in the power distribution takes place in the modified core.

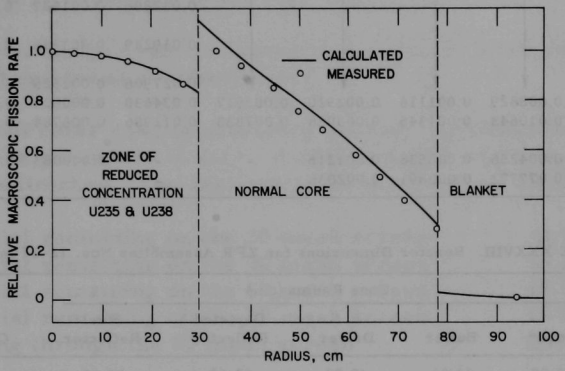

Fig. 10. Measured and Calculated Macroscopic Fission Rates of U^{235} in Modified Loading of Assembly 5--ZPR-6

3. ZPR-9

Assembly 17, which was the final core in the series of soft-spectrum cores, has been removed from ZPR-9, and Assembly 18 has been loaded. Assembly 18 is identical to Assembly 12 of ZPR-9. It is a small zoned core (the central core radius is 26 cm) with a central spectrum similar to that in Assembly 5 of ZPR-6. Doppler measurements designed to check the effect of different sample environments are now underway on Assembly 18.

Shown in Table XXXVII are the material concentrations of Assemblies 12 through 17. The radial zone dimensions and critical mass of each Assembly are given in Table XXXVIII. The axial length of each zone was 36 in. with a 5-in. depleted uranium plus an 8-in. steel reflector region on each end, making an overall axial length of 62 in.

TABLE XXXVII. Material Compositions for ZPR-9 Assemblies Nos. 12-17 Inclusive

Type of Zone Material	Atomic Atom Densities (atoms/cm^3 x 10^{24})							
	Fe	Ni	Cr	Na	C	U^{235}	U^{238}	H
Core of Assembly 12	0.009086	0.001148	0.002593	0.009028	0.012986	0.001547	0.010633	-
Core of Assembly 13	↓	↓	↓	↓	0.014920	0.001541	0.007389	0.006754
Core of Assembly 14	↓	↓	↓	↓	0.016363	0.001539	0.006580	↓
Core of Assembly 15	↓	↓	↓	↓	0.017806	0.001537	0.005771	↓
Core of Assembly 16	↓	↓	↓	↓	0.019249	0.001536	0.004963	↓
Core of Assembly 17	↓	↓	↓	↓	0.027906	0.001525	0.000110	↓
Buffer	0.008829	0.001116	0.002520	0.003917	0.034630	0.000020	0.009704	-
Driver	0.010643	0.001345	0.003038	0.007833	0.012986	0.006784	0.005335	-
Depleted Reflector	0.004256	0.000538	0.001215	-	-	0.000083	0.040034	-
Steel Reflector	0.077772	0.000891	0.002036	-	-	-	-	-

TABLE XXXVIII. Reactor Dimensions for ZPR Assemblies Nos. 12-17 Inclusive

Assembly No.	Zone Radius (cm)					Total Critical Mass (kg)
	Core[a]	Buffer	Driver	Depleted Reflector	Steel Reflector	
12	25.87	32.51	40.83	52.43	80.00	579.6
13	25.87	↓	37.85	↓	↓	402.8
14	25.87	↓	37.35	↓	↓	374.1
15	25.87	↓	36.97	↓	↓	352.9
16	25.87	↓	36.62	↓	↓	333.1
17	27.46	-	-	↓	↓	126.7

[a]Nominal 115 kg U^{235} in 25.87-cm core region.

4. ZPPR

Construction activities of the ZPPR facility continued this month. The construction contractor has been concentrating on the cell ring beam and fill for this period. Heavy rains during the early part of the month have delayed and hindered progress. The earth fill has been completed up to the bottom of the cell ring beam, the ring beam forms are complete, and the installation of cable sleeves is now in progress.

The roof of the support wing has been completed except for the final patching and gravel coat. The air-handling equipment in the fan loft of the support wing is being installed. The support wing is estimated to be about 70% complete.

The instrument and control wiring is now being installed between the seal pit in the access corridor and the cable routing room. The bulk head seals in the connecting tunnel between the support wing and the

workroom are being installed, and the corresponding wires are being pulled into place on the cable trays.

ANL personnel have visited the seal-door manufacturer and have reviewed the operation of the doors. The mechanisms appear to work satisfactorily, but some adjustments will probably be necessary in the field, since the doors and frames must be compatible. Since the doors and frames were made by different manufacturers, some interferences may exist. These are expected to be corrected in the field by the contractor.

A Mason-Hanger representative inspected the worktable at the vendor's plant and found it satisfactory.

The roof filter sand is now being graded. Approximately 50 cubic yards have been processed to date. A check sample was taken when about 10 yards were finished. The analysis of the sand was as follows:

Material remaining on the 20 mesh screen	2.1%
Material remaining on the 30 mesh screen	35.2%
Material remaining on the 40 mesh screen	45.0%
Material remaining on the 50 mesh screen	16.9%
Passing through the 50 mesh screen	Balance

This is not the final analysis since further washing of the sand is necessary to meet the cleanliness specification. During the processing, there will be a minor increase in the fines but should be quite acceptable for the ZPPR filter sand.

The Final Safety Analysis Report was reviewed by the Laboratory's Reactor Safety Review Committee on June 27. Minor revision will be made before the report is submitted to the AEC.

The month's end status of reactor components is as follows:

Poison Rod Drives: The poison rod drives were accepted and are being stored at ANL-Idaho.

Personnel Shields: The shields were received with the exception of the tractors, which are scheduled to be shipped at the end of the month.

Matrix Alignment: All matrix alignment items have been received and accepted.

Rod Drive Mounting Plates: Several visits were made to the vendor's plant because of difficulties in the manufacture of the mounting plates. Voids in the castings are only discovered during machining operations and may be

cause for rejection. The plates have been rough machined, and it was suggested to the manufacturer that he verify the integrity of the plates prior to final machining and hole drilling. The new schedule indicates delivery in August. The vendor was instructed to ship the plates only after inspection and acceptance by ANL has been obtained at his plant.

Fuel Control Drawers: The fuel control drawers were rejected by ANL due to out-of-tolerance dimensions. The manufacturer has fabricated new drawers, which were shipped June 29 to ANL for inspection.

Boron Fabrication: The first batch of plates was made at too low a temperature, resulting in out-of-tolerance pieces. Examination of the process indicated an improper reading of the temperature. This has been corrected, and heat pressing of the plates will be resumed on July 5.

Alpha Air Monitors: A review of the requirements of alpha air monitoring by ANL indicated that the same specifications can be used to cover the five monitors. The bid packages are now being prepared.

Outlines and preparation for the installation of the reactor components have been started. Information required for the reactor operating manual is now being assembled.

C. Component Development

1. Sodium Technology and Development

a. Fuel-pin Thermocouple. Thermocouples are being developed to indicate fuel-pin temperatures up to 2800°C in FFTF. For this development, previous experience with fuel-pin thermocouples has been evaluated, technology is being established to assure satisfactory design and performance, thermocouple assemblies and materials will be tested and evaluated extensively both out-of-pile and in-pile, and thermocouple fabrication techniques and specifications will be formulated.

(i) Electrical Insulators. The resistivities of two different 99.9%-pure vitrified-thoria insulators were measured up to 2830°C in a furnace containing dry (<2 ppm H_2O) stagnant helium at atmospheric pressure. The 3-in.-long insulator beads had a 0.201-in. OD and a 0.132-in. ID; they were assembled in the shape of coaxial probes and had a 0.206-in.-ID tantalum outer tube and a 0.127-in.-OD tantalum center wire. The resistivity data were obtained with a transistor curve tracer.

The two resistivity probes, identified as TR-1 and TR-2, yielded essentially the same resistivity values below 2000°C, but TR-1 indicated somewhat higher resistivity than TR-2 above 2000°C. Some typical

measured values are: 31 ohm-cm at 2810°C and 51 ohm-cm at 2520°C for TR-1, and 7 ohm-cm at 2810°C and 35 ohm-cm at 2535°C for TR-2. The cause of these discrepancies is being investigated. These resistivities are very much higher than those measured for 99.8% crushable thoria.

An analysis of all the resistivity data obtained and the potential usefulness of vitrified thoria as an FFTF fuel-pin-thermocouple insulator will be presented in the next progress report.

Six other vitrified-thoria insulators were heated to 2200-2700°C for up to 3 hr while suspended on a tantalum wire in dry stagnant helium at 1 atm. These samples changed from the as-received light yellow to a dark gray after heating; linear shrinkage varied from 2 to 10%. These material changes were expected. The samples will be analyzed to determine the extent of any stoïchiometric changes or contamination.

(ii) Thermoelement Properties. Long-term thermoelectric stability tests of bare wire W-3% Re/W-25% Re thermocouple assemblies have begun. Goal of the initial test is 240 hr at 2500°C.

(iii) Material Compatibility. Capsules TU-1 and TU-2, as well as tantalum tubing samples T-1 and T-2, have been examined metallographically. All samples appear to be identical in appearance and verify the conclusion that there has not been any reaction between the tantalum and the UO_2. The cause of the leak in capsule TU-2 (see Progress Report for May 1967, ANL-7342, p. 64) can be attributed to either a local defect in the as-received tubing or as an exceptionally large grain-boundary crack across the entire thickness of the tubing wall. In either case, this mode of failure is rare.

(iv) Preliminary In-pile Tests. Mainly because it can give the largest integrated doses of fast (>0.1 MeV) neutrons in the shortest time, the Engineering Test Reactor (ETR) has been selected as the first choice for the irradiation of FFTF-type fuel-pin thermocouples. If space is not available in the ETR, the HFBR at Brookhaven is the second choice. The CP-5 reactor at Argonne might be used for very short-term prooftesting of irradiation-capsule designs for the other reactors.

b. In-core Flowmeter. So that sodium flow through individual FFTF subassemblies or process tubes can be measured, technology is being established to assure that small magnetic, turbine, or other types of flowmeters can be obtained for use in severe temperature and radiation environments. Performance and reliability will be demonstrated in out-of-pile and in-pile tests.

(i) Thermal and Mechanical Tests of Magnetic Materials. Thermal tests of the Alnico alloys are continuing. Rod-magnet samples of

Alnico-5, -6, and -8 have been prepared, and the material and irreversible effects of these alloys for various length-to-diameter (L/D) ratios are being determined. In addition, several stainless steel-clad samples have been prepared. These clad samples, which are identical to those to be used for the in-pile test, will be heated in the same manner as the unclad samples. The results will indicate differences between the two types of samples and will determine whether thermal stabilization of the magnetic material for the in-pile tests can, in fact, be performed after the samples have been sealed in the cladding.

The coils for the B-H tester have been calibrated. The circuits for this apparatus have been designed and are being fabricated. This instrument will be pulse-operated from a capacitance-discharge energy source. The H pickup coils are used with matching integrators to provide simple integral calibration factors on the oscilloscope readout device. This technique of measuring magnetizing force compensates for the self-demagnetizing effect of the magnet itself, particularly when short magnet samples are considered.

A magnetizer and demagnetizer are available for use with all out-of-pile test-magnet sample sizes and alloys. Even the relatively difficult-to-work-with Alnico-8 alloy can be completely demagnetized and remagnetized.

Further discussions have been held with a magnet manufacturer to learn how to design manufacturable flowmeter magnets made of Alnico-8. As a rule of thumb, no dimension of the magnet can be greater than 2.5 to 3 times the smallest dimension. This means that segmented magnets would have to be used. This possibility is being studied further.

The Schonstedt HSM-1 magnetometer has been received. The sensor and a magnet sample holder have been attached to a wooden table constructed without the use of iron nails or other ferromagnetic parts; preliminary magnetic-moment measurements have been made.

With the present test setup and that anticipated for the hot-cell tests, the distance between the magnet and magnetometer sensor is 27.15 cm. An uncertainty in this distance of 0.079 cm results in an error in the magnetic-moment measurement of about 0.9%. As other system errors are considerably less, this is the largest contribution to the overall accuracy of the method.

The greatest precision in the measurement is obtained if the magnetometer is nulled for each of the 180° magnet positions used for the determination. Changes in ambient magnetic-field conditions during the period between the two instrument balances also affect the precision of the moment measurement. If certain gross disturbances in the

experimental area can be avoided, the magnetometer can be nulled to a precision of one gamma (10^{-5} gauss). Repeatability of the difference in the two balances required for a moment measurement is about 10 gammas. For the test distance of 27.15 cm, ten gammas is equivalent to 1 cgs unit of magnetic moment. Thus, for magnets having magnetic moments of about 1000 cgs units, which is typical of the rod magnets being tested, the precision of the measurement can be as good as 0.1%. Using the magnetometer under typical field conditions, however, the repeatability of the measurement appears to be slightly better than 0.3% of the induction from all causes when the magnet holder and magnetometer sensor are rigidly fixed in position.

Soft magnetic materials close to the test magnet or magnetometer sensor can also cause difficulties, even when these objects are in fixed positions. As the test magnet is turned 180°, the change in the induced field in the object subtracts from the change in the field due to the magnet itself, causing measurement errors. This effect has been found to be greater when objects are placed near the sensor than when objects are placed near the test magnet itself.

The magnetic moment of a 1/4-in.-dia by 2-in.-long Alnico-8 rod magnet was measured as 961 cgs units. The calculated moment based on published B-H and permeance coefficient curves was 947 cgs units. The variation in the magnetic properties of these materials is well over the 1.5% discrepancy found here.

(ii) Magnetic-flowmeter Prototype. The sodium calibration loop has been partially modified to allow operation of the preliminary prototype flowmeter up to 1200°F. The loop and flowmeter have operated up to 700°F, and higher-temperature operation is anticipated soon. A two-point calibration of the flowmeter at 400°F indicates a change in sensitivity after the loop modification. The cause of the sensitivity decrease is being investigated.

(iii) Magnet Irradiation Tests. Plans for magnet irradiation in EBR-II have been approved in principle, and preparation of the experiment description and hazard analysis report is continuing. The magnet samples will be clad in stainless steel covers made by machining solid rods to the proper size and then welding one end plug in place. This operation will be performed in a glovebox to provide a controlled helium backfill inside the magnet capsule. Test samples have been fabricated and marked by electroetching. The initial samples were not leaktight. The exact cause of the leaks is being studied. Detailed design of the irradiation capsule is continuing.

Development of techniques to handle and identify the irradiated magnets in the hot cell is continuing. A magnet charger for the

demagnetized samples has been constructed. A mockup of the hot cell is being constructed so the magnetometer can be tested in the presence of the amount of steel used in the actual hot cell. Handling techniques also will be prooftested in the mockup.

c. Fission-gas Pressure Transducer. To obtain an indication of the fission-gas pressure buildup in individual fuel pins while they are operating in the reactor, commercially available pressure transducers are being reviewed and evaluated for conditions expected in the Fast Flux Test Facility (FFTF), and will be tested out-of-pile and in-pile.

(i) NaK-filled Capillary System. The prototype system (see Progress Report for April 1967, ANL-7329, pp. 37-38) is being subjected to a 3-month life test. The bellows end only has been heated to 1200°F, and twice a day, except weekends, it is pressure-cycled to 100 psig. The pressure is gradually reduced to 30 psig in 8 hr, the bellows is repressurized to 100 psig, reduced to near 0 psig in 16 hr, and then the entire cycle is repeated. Since the start of the test, no apparent malfunction of the instrument has been encountered.

In an attempt to construct a subminiature version of the NaK-filled system, a 1/8-in.-OD nickel bellows has been welded to a 10-ft-long capillary tube of 0.020-in. OD and 0.012-in. ID. The first weld attempt was not successful, but a change in the end fitting from Type 304 stainless steel to Inconel led to a satisfactory weld. The weldments are being completed in preparation for filling with NaK.

d. Signal Lead Connector. To develop remote connectors for electrical and fluid signal leads for in-core instrumentation, connector leadwire assembly designs and test procedures will be reviewed, changes made to meet FFTF design criteria, new connector concepts considered, out-of-pile test programs established, and methods for terminating the sensor leads inside the reactor vessel, both above and within the sodium, will be studied and developed.

A test run of 17 days has been completed. Temperatures were cycled daily, except for weekends, during which temperature was held at ~300°C. The range of cycling was ~250°C, with a maximum of 600°C. Leak-rates, which were measured several times each day, were very low with the connector immersed in sodium as well as with the sodium withdrawn (dry measurements were made only four times during the whole run). Pressure decay inside the connector was too small to be statistically significant. A few measurements indicating substantial rates of pressure decay were suspect and probably due to leaking connections outside the test tank. Several such leaks were actually confirmed and corrected.

Insertion of a probe through the tube from the external gas system into the connector cavity did not reveal any sodium inside the connector. The connector assembly was unlocked and the seal at the gasket was broken seven times during this test run. After the connector was locked again it appeared tight all seven times. The run was terminated when the central bellows of the test rig leaked; inspection revealed that a substantial quantity (~25 cm^3) of sodium had entered and accumulated in the pocket below the gasketed cavity, although connector components and the gasket appeared to be in excellent condition. It seems likely that this sodium entered the cavity as drippings while the seal was broken. A connector with 12 drain holes around the gasket (instead of the present four) will be used in the next run in an attempt to confirm this interpretation. If the postulated explanation is correct, improved drainage before the connector is opened would tend to reduce or eliminate sodium entry. The faulty bellows and the connector locking arm of the test rig are being repaired and the pressure-measuring system is being refined.

e. Failed-fuel Locater. To find a method for determining which subassembly within a shutdown reactor core has one or more failed fuel pins, the feasibility of sensing the fission-gas release from the subassembly is being investigated. To prove the principle, a scheme will be demonstrated for efficiently disengaging noble gases from a continuously circulating liquid-sodium system at 1200°F. The equipment will include devices for disengaging the gas, trapping sodium vapor, viewing, monitoring radiation, and for injecting gas.

The test system (see Progress Report for May 1967, ANL-7342, p.68) is operational, and a test has been conducted. For this test, a modified helium-leakrate detector calibrated for 5 cm^3/min was installed on the sodium-fill line and was charged with helium for 5 min into a small chamber in this line. With 25 cm^3 of helium isolated in this chamber, argon at 2 psi was introduced into the line to force the helium through the 1100°F sodium and into the sodium-vapor atmosphere in the sodium reservoir. When 2 psi gas pressure registered on the tank gauges, the bleed-off valve located after the recirculating fan was opened, and escaping gas was sampled by a helium leak detector. Helium was detected in 4.2 sec. Inasmuch as 25 cm^3 of helium were added to the 208,538-cm^3 tank, the volume ratio was $\sim 120 \times 10^{-6}$. The helium leakrate measured was 22.89×10^{-10} cm^3/sec.

The system has been cooled so that all helium can be purged from the tank. Once the system is again free of helium, much smaller quantities of helium will be injected to determine the smallest detectable volume ratio.

D. Fuel Development

1. Metallic Fuels

a. Irradiation of Uranium-Plutonium Ternary Alloys. Elements of 15-U-15 w/o Pu-10 w/o Zr were awaiting insertion in EBR-II for a target burnup of 10 a/o at 630°C. Three of the jackets are of Type 316 stainless steel, six are of Type 304 stainless steel, and six are of V-20 w/o Ti. Two fuel elements of U-15 w/o Pu-10 w/o Zr and U-15 w/o Pu-10 w/o Ti (see Table XXXIX) are still under irradiation. Little additional burnup has accrued since May because the reactor has operated only intermittently and at low power.

TABLE XXXIX. Status of Metal-fuel Irradiations in Progress

		Design Parameters					Operating Conditions			
									Burnup to Date	
S/A No.	Specimen No.	Fuel Composition (w/o)	Effective Density (%)	Cladding Composition (w/o)	Cladding OD (in.)	Cladding Thickness (in.)	Max kW/ft	Max Cladding Temp (°C)	a/o	fiss/cc x 10^{-20}[a]
XG05	ND 24	U-15 Pu-10 Zr	63.6	V-20 Ti	0.208	0.015	10.0	535	5.1	11.7
XG05	NC 17	U-15 Pu-10 Ti	66.7	V-20 Ti	0.204	0.016	10.0	540	5.3	12.2

[a]Based on effective density.

Group M-3 (see Table XVIII, p. 70, of Progress Report for May 1967, ANL-7342), consisting of fifteen U-15 w/o Pu-10 w/o Zr fuel elements, is still at EBR-II waiting to be put into the reactor. The data for safety evaluation and the radiographs of the group have been submitted to the EBR-II staff.

The jacket materials for Group M-4 are being procured. This group consists of 40 elements of U-15 w/o Pu-(10-12 w/o)Zr with 93% enriched uranium. The fuel dimensions are a length of 14.22 in. and a diameter of 0.163 in. Fuel pins will be jacketed in tubing 0.220 in. in OD by 0.188 in. in ID. Jacket materials are Type 304, 316, and 318 stainless steel, Inconel 625, Hastelloy-X, V-15 w/o Ti-7.5 w/o Cr, and V-15 w/o Cr-5 w/o Ti. Burnups are aimed at 10 a/o with interim examinations at 4, 6, and 8 a/o.

2. Oxide Fuels

a. Mixed-oxide Fuel-performance Studies. Metallic inclusions in vibratorily compacted, hypostoichiometric, Dynapak UO_2-20 w/o PuO_2 irradiated in EBR-II to a burnup of 2.9 a/o (U + Pu) at a maximum jacket temperature of 605°C was reported (see ANL-7342, pp. 70-71) to consist mainly of ruthenium and molybdenum, with smaller amounts of technetium, rhodium, and palladium. A gray phase located in grain boundaries in the sintering transition zone contained significant amounts of what was thought to be barium, strontium, and cesium.

Description and operating conditions for two fuel elements undergoing postirradiation examination and ten elements being irradiated in EBR-II are listed in Tables XL, XLI, and XLII. Reactor operating conditions, calculated from data published in the Guide for Irradiation Experiments in EBR-II, have been adjusted in accordance with revised EBR-II flux values, as well as a number of analytical burnup results on experimental rods. The best-known values at the present time, for linear heat generation rates and cladding temperatures, are listed in the tables.

TABLE XL. Design Parameters and Operating Conditions for Mixed-oxide Elements Irradiated in EBR-II and Now Undergoing Postirradiation Examination

	Element Number	
	SOV-5	SOV-6
Fuel Composition	UO_2-20 w/o PuO_2	UO_2-20 w/o PuO_2
Fuel Synthesis	Pneumatically Impacted	Pneumatically Impacted
Fuel Form	Vibratorily Compacted	Vibratorily Compacted
Fuel Diameter, in.	0.254	0.254
Fuel Length, in.	11.5	11.5
Effective Density, %	83.4	83.3
Cladding Material	Type 304 SS	Type 304 SS
Cladding OD, in.	0.296	0.296
Cladding Wall, in.	0.021	0.021
Max Heat Rating, kW/ft	17.2	18.4
Max Cladding Temp, °C	565	580
Burnup (est), a/o	2.7	2.9

TABLE XLI. Status of Irradiations of Vibratorily Compacted (U-20 w/o Pu)O_2 in Progress in Subassembly XO11 of EBR-II

	Design Parameters				Operating Conditions			
							Burnup to Date	
Specimen Number	Effective Density (%)	Cladding Composition	Cladding OD (in.)	Cladding Thickness (in.)	Max kW/ft	Max Cladding Temp (°C)	a/o	fiss/cc x 10^{-20}[a]
SOV-3	83.1	304 SS	0.296	0.021	21.4	605	3.2	6.6
SOV-7	85.1	304 SS	0.296	0.021	21.3	605	3.1	6.5
SOV-1	79.9	304 SS	0.296	0.021	20.0	590	3.1	6.1
HOV-10	84.8	Hastelloy-X	0.295	0.016	22.8	605	3.0	6.3
HOV-15	79.8	Hastelloy-X	0.295	0.016	21.4	590	3.0	6.0
HOV-4	80.0	Hastelloy-X	0.295	0.016	22.9	605	3.1	6.2
TVOV-1	76.8	V-20 w/o Ti	0.298	0.022	19.6	575	3.1	5.8

[a]Based on effective density.

TABLE XLII. Status of Type 304 Stainless Steel-clad Cermet-fuel Irradiations in Progress in Subassembly XO11 of EBR-II

	Design Parameters					Operating Conditions			
								Burnup to Date	
Specimen No.	Fuel Composition (w/o)	Fuel Form	Effective Density (%)	Cladding OD (in.)	Cladding Thickness (in.)	Max kW/ft	Max Cladding Temp (°C)	a/o	fiss/cc x 10^{-20}[a]
5P-9	SS-40 PuO_2	COEX[b]	98.0	0.301	0.015	10.4	480	3.7	2.8
5P-12	SS-27 PuO_2	COEX	98.7	0.294	0.015	6.7	440	3.7	1.8
5U-14	SS-27 UO_2	COEX	97.9	0.298	0.013	5.8	430	2.8	1.4

[a]Based on effective density.
[b]COEX = Coextrusion of Core and Cladding.

b. Dynapaked UO_2-20 w/o PuO_2 Mixed Oxide. Mixed oxide (fully enriched UO_2-20 w/o PuO_2) Dynapaked at 1250°C, crushed and sized to grain sizes from 10 mesh to -325 mesh, was homogenized in preparation for making vibratorily compacted fuel pins for irradiation. The material as received had two distinct phases: $U(Pu)O_2$ having a cell parameter of 5.469 Å, and $Pu(U)O_2$ with 5.401 Å. Oxygen-to-metal ratio as determined by oxidation/reduction in He-1 v/o O_2 and a ten-to-one ratio of CO_2 at 700°C on -35 +50 mesh material was 2.00. The ideal objective was to heat at a temperature and in an atmosphere such that a homogeneous solid solution would be formed and the oxygen-to-metal ratio would be reduced to 1.97 to 1.98, but this was practically not possible.

A 4.5-hr heat at 1375°C in flowing helium had no effect on -10 +18 mesh material other than to sharpen the X-ray reflections for the two phases. Some of the same material reheated for 3 hr in vacuum at 1600°C reacted only enough for the X-ray reflections from $U(Pu)O_2$ to be discernible. Equilibrium was not reached, as there was a feathering-out on the upper edges of the X-ray reflections and the unit-cell parameter was 5.469 Å, which is too high for a homogeneous solid solution of this composition. The oxygen-to-metal ratio of this twice-heated material was 1.98, with a total weight loss of 0.145%. If only oxygen is lost with an oxygen-to-metal ratio change from 2.00 to 1.98, the weight change is 0.10%.

Twenty batches of the various sized fractions with a combined weight of approximately 3 kg were heated in vacuum at 1600°C for 4 hr. Partial results indicate that the oxygen-to-metal ratios will be the same, 1.98, for all of the fractions. However, X-ray results with a -325 mesh batch indicated two solid solutions were formed with about equal intensities and unit-cell sizes of 5.449 Å and 5.468 Å. On the basis of the X-ray results there is a possibility of a variation in plutonium content from the coarse to the fine fractions.

X-ray data and oxygen-to-metal ratio (obtained both by oxidation/reduction and inert gas fusion) will be determined on a batch of each size fraction. All of the material has been transferred to Building 350 for fabrication into fuel pins.

3. Vibratory Compaction of Oxide and Carbide Fuel

The development of both oxide and carbide fuels requires capability of fuel-element fabrication by vibratory compaction. Pilot-scale equipment to attain this capability has been developed and built. During this reporting period the glovebox enclosure to house fabrication equipment has been erected. The installation work is about 90% complete at this time. Electrical and piping work is complete. Remaining work involves the assembly and installation of subhood panels, checkout of all systems and circuits, and

leak testing and leak repair. Pressure testing and leak detection to determine the leaktight integrity of the glovebox and piping is under way.

4. Carbide Fuels

a. Compatibility of (U, Pu) Carbides with Potential Jacketing Materials

(i) Vanadium Alloys. Specimens of V-15 w/o Ti-7.5 w/o Cr and V-5 w/o Ti-15 w/o Cr, cut from 0.25-in. rods, were examined metallographically after contact with $(U_{0.8}Pu_{0.2})C$ for 1000 hr at 800°C. The latter alloy showed no evidence of interaction under these conditions, as was previously found[2] when a preliminary test with this alloy in the form of 30-mil sheet rolled from a small, arc-melted button was tested under the same conditions. The V-15 w/o Ti-7.5 w/o Cr alloy, however, when etched, was observed to be affected by the (U, Pu)C to an average depth of 70 to 75 μ. The material in the reaction band appears to contain a great number of fine precipitates, and the original grain boundaries are much less distinct when compared to the unaffected material. This effect is very similar to that observed with V-20 w/o Ti when tested with (U, Pu)C.

(ii) Type 304 Stainless Steel. A 15-to-30 μ band that has been previously observed in Type 304 stainless steel after contact with stoichiometric and hyperstoichiometric (U, Pu)C in 1000- and 4000-hr tests[3] was analyzed by means of an electron microprobe. The iron content of the band (70 w/o) was about 3 w/o higher, whereas the chromium content (15 w/o) was about 3 w/o lower than that of the unaffected steel. The nickel content was unchanged. In addition, a number of small precipitates consisting of approximately equal percentages of iron and chromium were found in the band. Based on etching characteristics of these precipitates, they are believed to be carbides. There was no evidence of uranium or plutonium in the affected band.

b. Mixed-carbide-fuel Irradiations in EBR-II. Description and operating conditions for three elements undergoing postirradiation examination and 15 elements being irradiated in EBR-II are listed in Tables XLIII and XLIV.

Element No. SMP-1, containing pellets in a jacket of Type 316 stainless steel, was sectioned to provide samples for metallography and burnup analysis. Neutron radiographs and gamma scans of this element had indicated that the pellets were loose inside of the jacket. However, when removal of pellets from short sections of the element was attempted by pushing with a ramrod, the pellets emerged in fragments. Pellets also were fragmented when removal was attempted after slitting a short section

[2]Progress Report for October 1966, ANL-7267, p. 38.
[3]Progress Reports for April 1966, ANL-7204, p. 17; January 1967, ANL-7302, p. 51.

of the element longitudinally and then prying the jacket apart like a clam shell. The metallography samples, apparently intact and not impaired by fragmentation, will be impregnated with epoxy to prevent cracking during grinding and polishing operations.

TABLE XLIII. Design Parameters and Operating Conditions for Carbide Elements Irradiated in EBR-II and Now Undergoing Postirradiation

	Element Number		
	SMP-1	VMV-1	SMV-1
Fuel Composition, w/o	$(U_{0.8}-Pu_{0.2})C$	$(U_{0.8}-Pu_{0.2})C$	UC-20 w/o PuC
Fuel Synthesis	Arc Melted	Arc Melted	Arc Melted
Fuel Form	Pellets	Vibratorily Compacted	Vibratorily Compacted
Fuel Diameter, in.	0.253	0.253	0.257
Fuel Length, in.	13.4	14.0	14.0
Effective Density, %	81.4	85.9	80.0
Cladding Material	Type 316 SS	Vanadium	Type 316 SS
Cladding OD, in.	0.306	0.301	0.306
Cladding Wall, in.	0.024	0.024	0.025
Max Heat Rating, kW/ft	17.1	26.1	21.3
Max Cladding Temp, °C	575	645	630
Max Burnup, a/o	2.02*	3.02	2.59

*Estimated.

TABLE XLIV. Status of Mixed-carbide-fuel Irradiations in Progress in EBR-II

		Design Parameters						Operating Conditions			
										Burnup to Date	
S/A No.	Specimen No.	Fuel Composition (w/o)	Fuel Form[a]	Effective Density (%)	Cladding Composition	Cladding OD (in.)	Cladding Thickness (in.)	Max kW/ft	Max Cladding Temp (°C)	a/o	fiss/cc x 10^{-20}[b]
XG05	SMV-2	UC-20 PuC	VIPAC	83.8	304 SS	0.296	0.021	24.0	675	4.8	13.2
XG05	HMV-5	UC-20 PuC	VIPAC	80.0	Hast.-X	0.295	0.015	26.6	685	5.0	13.1
XG05	NMV-11	$(U_{0.8}-Pu_{0.2})C$	VIPAC	82.9	Nb-1 w/o Zr	0.284	0.012	25.5	635	5.0	13.7
XO08	NMP-2	$(U_{0.8}-Pu_{0.2})C$	PELLET	81.6	Nb-1 w/o Zr	0.284	0.013	17.4	545	3.0	8.2
XO08	NMV-4	UC-20 PuC	VIPAC	80.0	Nb-1 w/o Zr	0.283	0.013	27.0	645	4.4	11.6
XO08	NMV-7	UC-20 PuC	VIPAC	80.0	Nb-1 w/o Zr	0.283	0.013	26.0	630	4.0	10.6
XO08	NMV-12	$(U_{0.8}-Pu_{0.2})C$	VIPAC	85.5	Nb-1 w/o Zr	0.284	0.014	26.7	645	4.4	12.4
XO08	HMV-1	UC-20 PuC	VIPAC	80.0	Hast.-X	0.295	0.015	25.2	660	3.9	10.4
XO08	HMV-4	UC-20 PuC	VIPAC	80.0	Hast.-X	0.295	0.016	27.2	690	4.3	11.4
XO08	HWMP-1	$(U_{0.8}-Pu_{0.2})C$	PELLET	81.4	Hast.-X + W	0.296	0.020	16.9	565	3.0	8.1
XO08	HWMV-1	$(U_{0.8}-Pu_{0.2})C$	VIPAC	82.9	Hast.-X + W	0.295	0.018	26.4	685	4.4	12.0
XO15	NMP-1	$(U_{0.8}-Pu_{0.2})C$	PELLET	81.6	Nb-1 w/o Zr	0.284	0.013	16.5	535	0.50	1.3
XO15	NMV-3	UC-20 PuC	VIPAC	80.0	Nb-1 w/o Zr	0.284	0.013	26.0	635	0.74	2.0
XO15	HMV-2	UC-20 PuC	VIPAC	80.0	Hast.-X	0.295	0.015	27.0	685	0.81	2.1
XO15	TVMV-1	$(U_{0.8}-Pu_{0.2})C$	VIPAC	83.7	V-20 w/o Ti	0.298	0.021	23.4	640	0.65	1.8

[a]VIPAC = Vibratorily Compacted into Cladding; PELLET = Pressed and Sintered Pellets.
[b]Based on effective density.

5. Fuel Cladding and Structure

a. Development of Refractory-metal Alloys for Service in Oxygen-contaminated Sodium. The weight gain of V-20 w/o Ti (TV-20) during a 155-day exposure at 550°C in sodium containing about 8 wt ppm of oxygen was reported (see Progress Report for May 1967, ANL-7342, Table XXVII, p. 80) to be about one-third the value obtained at 650°C. A rather similar weight gain was exhibited by V-15 w/o Ti-7.5 w/o Cr, but V-5 w/o Cr and V-15 w/o Cr-5 w/o Ti gained about one-third to one-half as much weight. Small weight losses occurred in shorter tests at 450°C.

The behavior of V-20 w/o Ti, V-15 w/o Ti-7.5 w/o Cr, V-15 w/o Cr- 5 w/o Ti, and V-10 w/o Cr in sodium are being investigated

at 450°C in static or dynamic systems. Two oxygen-refreshed autoclave systems (cold traps at 110 and 175°C) have operated for nearly two months at this temperature. Weight losses have been recorded for both systems after the initial one-week exposure. The weight loss of TV-20 is significantly less than that of the other alloys in both systems. In the system with the higher oxygen concentration (cold trap at 175°C), TV-20 has lost 0.8 mg/cm^2 in 60.5 days; in the other system (cold trap at 110°C) it has lost the same amount in 49.6 days of exposure.

The sodium is being analyzed for oxygen by means of the distillation technique. The residue from the distillation is first titrated to phenopthalein endpoint (pH 8.3-10) and then to a methyl red endpoint (pH 4.2-6.3). If only Na_2O were present, extremely little additional acid would be required for the second endpoint. In fact, however, about 15 to 25% additional acid is required. An effort is being made to identify the unknown material. There is evidence to indicate that at least part of the residue is sodium carbonate.

A dynamic experiment has also been started (at 450°C, cold trap at 110°C, flow of 6.1 m/sec) with the above-mentioned alloys. After 13.7 days, small weight losses ($\leq$0.1 mg/cm^2) have been recorded for all but the V-15 w/o Cr-5 w/o Ti alloy, which shows small gains.

b. Compatibility of U-5 w/o Fs with Type 304 Stainless Steel. In diffusion-couple (sandwich) studies, liquid-phase formation has been determined to occur at 715 ± 15°C in interdiffusion layers formed between U-5 w/o Fs alloy and 304 stainless steel. At 700°C compounds based on U_6Fe and UFe_2 have been clearly determined from microprobe analyses to form in interdiffusion layers. Liquid-phase formation at 730°C occurs in a zone between the U_6Fe and UFe_2 layers.

c. Effect of Fast-neutron Irradiation on Jacket Materials. Type 304 stainless steel and Hastelloy-X have been irradiated concurrently with V-20 w/o Ti and V-15 w/o Ti-7.5 w/o Cr alloys to evaluate the mechanical properties of jacket alloys as affected by fast-neutron irradiation at elevated temperatures. Room-temperature tensile properties and chemical analyses of as-received Type 304 stainless steel and Hastelloy-X are given in Tables XLV and XLVI, respectively. Preliminary results of tensile tests

TABLE XLV. Room-temperature Tensile Properties of As-received Hastelloy-X and Type 304 Stainless Steel

Material	0.2% Yield Strength	Tensile Strength	Total Elongation	Reduction in Area
304 SS	95,000 psi (45.8 kg/mm^2)	94,500 psi (66.6 kg/mm^2)	56.2%	74.9%
Hastelloy-X	42,850 psi (30.2 kg/mm^2)	108,350 psi (76.3 kg/mm^2)	47%	Not Available

TABLE XLVI. Chemical Analyses of As-received Hastelloy-X and Type 304 Stainless Steel

Element	Material		Element	Material	
	Hastelloy-X (w/o)	Type 304 SS (w/o)		Hastelloy-X (w/o)	Type 304 SS (w/o)
Fe	18.09	Balance	Co	1.77	0.11
Ni	Balance	9.05	Mn	0.063	0.98
Cr	22.19	18.28	Mo	8.90	0.29
C	0.10	0.047	P	0.001	0.34
W	0.61	-	S	0.004	0.018
Si	0.40	0.46	Cu	-	0.34

conducted at temperatures between 20 and 650°C with specimens of Type 304 stainless steel and Hastelloy-X irradiated between 538 and 704°C to a nominal fluence of 5 x 10^{21} n/cm^2 are given in Tables XLVII and XLVIII.

TABLE XLVII. Tensile Properties[a] of Type 304 Stainless Steel Irradiated to a Nominal Fluence of 5 x 10^{21} n/cm^2 at Temperatures between 538 and 704°C

Condition	Test Temp (°C)	0.2% Yield Strength (kg/mm^2)	Ultimate Tensile Strength (kg/mm^2)	Total Elongation (%)
Unirradiated	Room	45.5	71.6	64.8
Unirradiated	Room	45.7	71.5	65.8
Unirradiated	400	37.4	48.8	24.8
Unirradiated	550	34.8	48.2	33.2
Unirradiated	550	36.2	47.6	25.7
Unirradiated	650	33.5	45.2	30.1
Unirradiated	650	36.0	47.6	29.5
Unirradiated, 30 days--550°C	Room	43.7	74.6	84.2
Unirradiated, 30 days--550°C	400	33.5	49.3	37.2
Unirradiated, 30 days--550°C	550	33.6	50.3	32.4
Unirradiated, 30 days--550°C	650	34.1	50.2	33.5
Irradiated	Room	55.0	78.8	82.1
Irradiated	Room	54.7	77.0	80.4
Irradiated	400	46.6	59.8	23.0
Irradiated	400	50.5	59.8	21.8
Irradiated	550	48.5	59.0	24.2
Irradiated	650	47.4	57.8	25.2
Irradiated	650	47.6	57.1	25.4

[a]Tested at crosshead speed of 0.05 cm/min ~2.5% per min.

TABLE XLVIII. Tensile Properties[a] of Hastelloy-X Irradiated to a Nominal Fluence of 5 x 10^{21} n/cm^2 at Temperatures between 538 and 704°C

Condition	Test Temp (°C)	0.2% Yield Strength (kg/mm^2)	Ultimate Tensile Strength (kg/mm^2)	Total Elongation (%)
Unirradiated	Room	32.5	69.2	71.0
Unirradiated	Room	33.6	71.0	67.7
Unirradiated	400	22.0	60.8	67.4
Unirradiated	400	24.0	65.7	69.4
Unirradiated	550	24.0	65.7	69.4
Unirradiated	550	24.6	63.2	70.5
Unirradiated	650	23.0	58.1	69.5
Unirradiated, 30 days--550°C	Room	37.9	77.7	58.3
Unirradiated, 30 days--550°C	400	26.7	63.7	61.2
Unirradiated, 30 days--550°C	550	24.8	63.3	65.8
Unirradiated, 30 days--550°C	650	26.3	63.1	56.9
Irradiated	Room	49.5	80.0	58.8
Irradiated	400	40.4	68.2	55.7
Irradiated	400	40.4	67.2	60.2
Irradiated	550	40.2	63.2	49.4
Irradiated	550	41.0	66.0	50.4
Irradiated	650	39.7	66.3	51.7
Irradiated	650	38.9	66.7	58.6

[a]Tested at crosshead speed of 0.05 cm/min ~2.5% per min.

Irradiation of Type 304 stainless steel or of Hastelloy-X to a nominal fluence of 5 x 10^{21} n/cm^2 at temperatures between 538 and 704°C increased the tensile (ultimate and yield) strengths and reduced the elongation at a given temperature.

(i) Type 304 Stainless Steel. Annealing the Type 304 stainless steel for 30 days at 550°C reduced the yield strength slightly but did not

affect the strength test-temperature relationship. The ductility of the stainless steel was increased at all test temperatures by the annealing treatment. The largest increase was at 400°C, where a 50% increase in percent total elongation was observed. Irradiation at temperatures between 538 and 704°C to a nominal fluence of 5 x 10^{21} n/cm^2 increased the strength at all test temperatures. The increase in yield strength of the Type 304 stainless steel over that of the unirradiated material ranged from 22% at room temperature to a high of 37% at a test temperature of 650°C. The highest increase in strength of the irradiated stainless steel over that of unirradiated material given a 30-day anneal at 550°C was 45%, occurring at a test temperature of 400°C. The ductility of the Type 304 stainless steel was reduced at all test temperatures by irradiation. The highest decrease in percent total elongation was 18% at 550°C when compared to the unirradiated stainless steel, and was 40% at 400°C when compared to the unirradiated material given a 30-day anneal at 550°C.

(ii) Hastelloy-X. Annealing the Hastelloy-X for 30 days at 550°C increased the strength and decreased the ductility at all test temperatures. The greatest increase in yield strength was 15%, occurring at room temperature. The largest loss in percent total elongation was 18%, occurring at 650°C. The smallest change in both yield strength and percent total elongation was observed at 550°C. Irradiation at temperatures between 538 and 704°C to a nominal fluence of 5 x 10^{21} n/cm^2 increased the strength of the Hastelloy-X at all test temperatures over that of both the unirradiated control materials. The maximum increase in yield strength of Hastelloy-X due to irradiation was 76% at 400°C and 64% at 550°C compared to unirradiated material and unirradiated material given a 30-day anneal at 550°C, respectively. The ductility of the Hastelloy-X was decreased at all test temperatures by irradiation when compared to unirradiated material; the largest decrease in percent total elongation was 29% at 550°C. The ductility of the irradiated Hastelloy-X was not significantly different from that of the unirradiated 30-day, 550°C annealed material except at 550°C where the change in total elongation was 24%.

The Type 304 stainless steel had a ductility minimum near 400°C and the Hastelloy-X had a ductility minimum at 550°C. The extent to which a ductility minimum exists in Type 304 stainless steel below 400°C will not be determined since tests are not planned in that temperature region. Comparison of the results of the Type 304 stainless steel and Hastelloy-X with that of V-20 w/o Ti and V-15 w/o Ti-15 w/o Cr irradiated under similar conditions is possible only at 550°C, since the vanadium-base alloys have not yet been tested over the entire temperature range. As reported in ANL-7342 (pp. 76-77), irradiation of V-20 w/o Ti to a fluence of 4.2 x 10^{21} n/cm^2 decreased the percent total elongation by 27%, and irradiation of V-15 w/o Ti-7.5 w/o Cr to a fluence of 3.4 x 10^{21} n/cm^2 decreased the percent total elongation by 20%.

6. Fuel Reprocessing

a. Processes for Fast Reactor Fuels. Studies are being made of a pyrochemical process for ceramic (e.g., oxide or carbide) fast breeder reactor fuels clad with stainless steel. The process applies salt-transport separations and liquid metal-molten salt extractions to the separation of fissile and fertile fuel constituents from the fission products. The conceptual flowsheet for the process has been described previously (see Progress Report for September 1966, ANL-7255, pp. 30-31).

An experiment is in progress to demonstrate the steps of the current pyrochemical flowsheet with the exception of fuel decladding and resynthesis. In the reduction step of the process, oxide fuel, suspended in a 47.5 m/o $MgCl_2$-47.5 m/o $CaCl_2$-5 m/o CaF_2 salt mixture, is reduced by a Cu-33 w/o Mg alloy. The reduction of 233 g of PuO_2, 458 g of UO_2, and 52 g of fission product oxides was carried out at 800°C in 4 hr with no difficulty. Two scrub steps were performed in which the metal alloy from the reduction step was contacted with additional reduction salt to complete the removal of the rare earths and other electropositive fission product elements. These two steps were also performed without difficulty. The next process step that was demonstrated was the salt transport of plutonium at 600°C from the Cu-33 w/o Mg donor alloy to a Zn-2 w/o Mg acceptor alloy, with 50 m/o $MgCl_2$-30 m/o NaCl-20 m/o KCl as the transport salt. Preliminary chemical analyses indicated that 93% of the plutonium had been transported in the first five cycles, which is slightly more than was expected (89%). The transport step was terminated after fourteen cycles. Based on the data obtained after five cycles, fourteen cycles should be sufficient to transport 99.9% of the plutonium. Analytical data on the actual amount of plutonium transported are not yet available.

Following the salt-transport step, an additional step was incorporated in this experiment to separate the plutonium from any copper which might have transferred to the Zn-2 w/o Mg acceptor alloy. The Zn-Mg-Pu acceptor alloy was contacted with $ZnCl_2$ to convert the plutonium to $PuCl_3$. Chemical analysis showed the oxidation to be 99.99% complete after 1.5 hr. The plutonium was then salt-transported to a Zn-4 w/o Mg alloy, reusing the salt from the previous salt-transport step. Seven cycles were performed to achieve transport of ~99.9% of the plutonium.

Four additional process steps will be required to complete the experiment: (1) recovery of a metallic plutonium product by solvent metal evaporation, (2) uranium wash with magnesium to remove copper and fission products, (3) recovery of uranium metal by solvent metal evaporation, and (4) two strip steps to remove plutonium from the waste reduction salt. Final results will be presented upon the completion of the experiment and the receipt of the complete analytical data.

A laboratory experiment has been performed to measure the solubility of neptunium in liquid cadmium. This information is needed for the development of methods for the recovery of neptunium from fast breeder reactor fuels by pyrochemical processes. The solubility was determined from samples taken after equilibrating 1.82 g of neptunium metal with 51 g of liquid cadmium in a tantalum crucible at several temperatures between 325 and 600°C. Preliminary data indicate that the solubility of neptunium in liquid cadmium is closer to that of uranium than that of plutonium. For example, at 393°C, the solubility of neptunium is ~0.3 a/o, whereas the solubilities of uranium and plutonium are 0.21 and 0.62 a/o, respectively.

Engineering studies are being carried out to develop the technology required for plant-scale application of pyrochemical processes. Corrosion testing of potential containment materials for pyrochemical processes would be improved if a method of testing could be developed which would yield data on mass-transport effects, in addition to the solubility, reaction, and penetration effects which are observable with current testing methods. In an effort to develop this type of test, a two-phase thermal convection loop was constructed and operated. The loop was designed to operate in an air atmosphere, and the principal objective of the first experiment was to test the design, control, and operation of one of these devices.

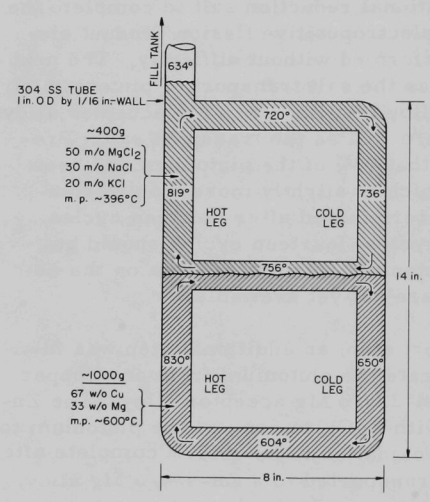

Fig. 11. Two-phase Thermal Convection Loop. Temperatures shown are operational temperatures, °C.

The general configuration of the loop is shown in Fig. 11. The loop was constructed of Type 304 stainless steel, and was charged with a Cu-33 w/o Mg metal phase and a 50 m/o $MgCl_2$-30 m/o NaCl-20 m/o KCl salt phase. The location of the metal-salt interface, which is critical to the operation of one of these devices, was determined by X-ray pictures of the operating loop. After seven days of successful operation, a change in the temperature profile indicated that a flow constriction had developed in the metal-phase portion of the loop. After sampling of both metal and salt phases, the loop was shut down and sectioned for metallographic examination.

Chemical and metallurgical analyses of the samples taken from the loop before and after shutdown indicate that iron and chromium (from the stainless steel) were transported to the cold leg of the metal phase and

deposited, forming a constriction. This transport is a phenomenon that had not been observed previously in Cu-Mg systems. The data indicate that mass transport of both iron and chromium can occur in Cu-Mg systems even though their solubilities are low. In mass transport the solubility of the transported species is often not as important as the temperature dependence of the solubility, and the solubilities of both iron and chromium in Cu-Mg systems appear to be strongly temperature-dependent.

Operation of this loop demonstrated both the feasibility and usefulness of this type of test. The design and operating experience derived from the test will be applied to subsequent thermal convection loops fabricated from tantalum or niobium.

The application of time-delay reflectometry to some pyrochemical instrumentation problems is being investigated. A time-delay reflectometer (TDR) determines the position of an impedance discontinuity in a conductor. This is accomplished by sending an electrical pulse along the conductor and measuring the time that is required for a pulse, reflected from an impedance discontinuity, to return to the instrument.

Initially the TDR unit will be used to measure levels of molten salts. This method of determining liquid levels appears to be superior to other methods such as resistance probes and bubblers. A mutual-inductance probe[4] developed for determining levels of liquid metals is quite insensitive to the presence of liquid salts. In preliminary tests, the TDR instrument was capable of detecting a change of salt level of less than 1 cm. It will be used to measure liquid levels in pilot-plant equipment for pyrochemical processing.

E. Fast Flux Test Reactor (FFTR)

1. Phase-A Analysis

The calculated worths of the boron control rods in the center of the Assembly-48 core of ZPR-3 were computed to be higher than the measured values by 13 to 32 percent. Since 22-group diffusion, 6-group diffusion, and 6-group (x, y) geometry S-2 transport calculations are found to be consistent to within a few percent of each other, it appears that group structure and group collapse is most adequate.

The deviation from experimental values has been pursued further without locating any major contributor to the discrepancy. Six-group (x, y) and (r, z) geometry in S-2 and S-4 transport calculations give results which agree within a few percent. This indicates that with the 6-group cross-section set 22612, the transport effect is small. The transport effect with

[4] Johnson, T. R., et al., An Induction Probe for Measuring Liquid Levels in Liquid Metals, ANL-7153 (Feb 1966).

the 22-group set 22001 is presently being checked with a one-dimensional SNARG calculation. Further, results obtained with the Argonne 224 set have been found to agree with 22001 set in a diffusion calculation.

A series of computations designed to study the effect of variations in axial buckling on rod worths showed that this is not a large enough effect. A similar conclusion may be stated of errors in cross section or concentration of rod and sodium channel materials other than natural boron and B^{10}. The B^{10} reaction rate at this rod surface is maximum in the 17th group, so that the addition of groups of lower energy would not change rod worths significantly. Preliminary studies of self-shielding effects again do not seem to account for the large discrepancies.

Further work to resolve this disagreement is planned to recheck and re-evaluate critical atomic concentrations and dimensions.

2. FFTR Design

A general outline for a second series of critical experiments has been submitted to PNL as Addendum I, Phase B experiments.

The FFTR split-core inverted conical design is too complex geometrically to apply the usual one- or two-dimensional neutronics analysis. The slightly oblong, hexagonally shaped core is designed with nonvertical fuel assemblies such that a 30 to 35% variation in cross-sectional area occurs over a core height of approximately 100 cm. This axial variation in composition when coupled with the sizable "gap" produced by the test region imposes a need for developing and exploring new analytical and experimental synthesis techniques.

Therefore, a primary objective of the next series of critical experiments (Phase B) for FFTR is to verify experimentally and establish the adequacy of the new synthesis methods to be used in the design and physics analysis of the reactor. In order to be able to apply the computational methods determined from the critical experiment program directly to the design of the FFTR, experiments and analyses are planned that will closely reflect the geometry and composition of the reactor. An important and integral phase of this critical experiment program is the extensive theoretical effort required to define those experiments which critically test the analytical methods.

A second objective is to plan those experiments which provide preliminary data on the nuclear parameters required to prepare a Preliminary Safeguards Report and for Title II design.

The geometrical and axial variation in composition of the core have introduced some interesting features to the usual reactivity feedbacks one considers in the preliminary assessment of safety problems. The two more

important reactivity coefficients, besides the axial expansion of fuel and mechanical movement of fuel subassemblies, are the prompt Doppler effect and the delayed sodium density and void effect. In order to better understand the analytical techniques derived for use on the complex FFTR concept, it has been proposed that four FFTR critical assemblies be studied. The first two critical experiments will be aimed at investigating the neutronic effects of introducing a "slotted" test region into a hexagonal-cylindrical core of uniform composition. The purpose of the third experiment is to study the split-core assembly having an axial variation in composition. The fourth core is included to study the combined effects of the conical geometry, and the nonuniform composition.

F. General Research and Development

1. Fast-reactor Core-parameter Study

Core compositions for carbide-fueled reactors have been determined for the same burnup and fuel-lifetime conditions used as the bases for the oxide-core scoping calculations. For realistic thermal-hydraulic conditions, the high density and high thermal conductivity of carbide fuels permit carbide cores to operate at higher power densities and/or longer fuel lifetimes than for oxide cores. Consequently, the core compositions of carbide-fueled reactors were also determined for carbide cores having essentially the same velocity-pressure drop characteristics as the oxide cores. For these conditions, the carbide cores contain sufficient fuel to operate ~40% longer than oxide cores.

Core compositions of metal-alloy-fuel reactors are being investigated. The alloy chosen for the metal-fueled reactor is U-Pu-10 w/o Zr.

The computer code used for the thermal-hydraulic analyses of the reactor cores is being revised. Planned revisions include the incorporation of two subroutines, VOID and HOTSPOT. The subroutine VOID will be used to estimate the diameter of the central-void formation along the longitudinal axis of oxide fuel elements and to determine the effect of void formation on temperature. Subroutine HOTSPOT will calculate hot-spot factors for the thermal analyses, based on input uncertainties on clad geometry, power peaking, thermal conductivities, etc., which will be treated in part as statistical phenomena and the remainder as multiplication factors.

Control requirements for the fast-reactor cores are also being studied. Gross core-volume requirements for poison-type control and midcycle to end-of-cycle reactivity changes are the major factors being investigated.

Results have been obtained in a study of the effects of thermal expansion of the core on reactivity. The calculations were performed with

the aid of the one-dimensional Mach-1 code by two methods: (1) a k-calculation incorporating a correction for the change in transverse leakage and (2) a perturbation calculation in which expansion is represented by a perturbation in the transverse leakage. In other words, for axial expansion a radial problem is run and the axial buckling is perturbed; for radial expansion an axial problem is run and the radial buckling is perturbed. The amount of the perturbation in the transverse buckling is obtained by assuming that the extrapolated height or radius changes by an amount equal to the core expansion in that direction. This is equivalent to assuming that the reflector savings remain the same. Since the reflector savings do in fact remain approximately the same, this is generally a good assumption. However, for low values of core height-to-diameter ratio (H/D), where the reflector savings represent a large percentage of the total extrapolated height, the change in reflector savings can have an appreciable effect. This causes the perturbation method to be somewhat in error for the case of axial expansion at low core H/D.

Radial expansions were taken as 1% and axial expansions were taken as 2%. This allowed the use of the same core compositions (reduced by 2% from the critical values derived through self-consistent diffusion theory) for both radial and axial expansions when using the k-calculation method. For the perturbation method, of course, full-density core compositions are input and the reduction in core density is achieved through perturbing the material in the core region. For a core power density of 400 kW/liter and core H/D ratios of 0.2 and 0.6, Δk results were:

For 1% radial expansion:

H/D	0.2	0.6
Perturbation	-0.00647	-0.00412
k-calculation	-0.00644	-0.00414

For 2% axial expansion:

H/D	0.2	0.6
Perturbation	-0.00187	-0.00290
k-calculation	-0.00136	-0.00289

It can be seen that excellent agreement exists between the k-calculation method and the perturbation method, except, as explained above, in the case of axial expansion at low core H/D.

As a check on the one-dimensional calculations, two core-expansion problems were run with the Candid 2-D code. The dimensions of the core region were increased by 1% in both radius and height, with the blanket and reflectors being unexpanded but their position coordinates moved outward due to the core expansion. The atom densities in the core region were

decreased by 3% from the values corresponding to full density. The reactors considered both had a core power density of 400 kW/liter. One had H/D = 0.2 and the other had H/D = 0.6. The values of expansion coefficient, Δk, were obtained by subtracting the k for the normal or unexpanded condition from the k for the expanded condition. Then the results can be compared with values obtained from the one-dimensional results. For the H/D of 0.2, where a difference exists between the k-calculation method and the perturbation method in the one-dimensional results, the k-calculation value was used, because it was judged to be more correct. The comparison then is as follows:

H/D	0.2	0.6
1-D Δk	-0.00715	-0.00557
2-D Δk	-0.00722	-0.00564

The results differ by only about 1%.

III. GENERAL REACTOR TECHNOLOGY

A. Applied and Reactor Physics Development

1. Fast-reactor Noise Analysis with an On-line Digital Computer

The on-line computer system (see Progress Report for January 1967, ANL-7302, pp. 56-57) is being used to make noise analysis of fast-reactor assemblies. A cross correlation between two detectors[5] makes tolerable the low order of detector efficiency possible in fast assemblies. The technique of polarity correlation[6] allows one-bit quantization of the signals, and so permits the highest possible sampling rate. Use of current detectors (rather than pulse counters) allows measurements at high power, which is important for plutonium assemblies.

Each detector is a plastic scintillator about 3.75 cm in diameter and 30 cm long. The noise goes to a Schmitt trigger that registers whether it is above or below its mean.

The computer can read a 24-bit data word every 6 μsec, so it can accept one bit of polarity information from each of the two Schmitt triggers every 0.5 μsec. The information is collected by a data terminal having four registers of twelve flip-flops each. At any one time, two registers are accepting data, each from one chamber. Within a register, the input to each flip-flop in turn is enabled at 0.5-μsec intervals by a clocked ring counter. The enabled flip-flop is set or left reset according as the noise from its detector is above or below the mean at the instant of sampling. After all flip-flops have been scanned, the contents of the registers are read into the computer while the other pair of registers are scanned. The first pair of registers are reset after readout is complete, and the cycle continues. After the desired number of data words have been received (typically, 70), the computer unpacks the data strings from the two chambers to one bit per word in memory. The polarity cross-correlation function is calculated and added to the results from previous calculations, and the cycle repeats.

It takes a greater amount of time to calculate the cross-correlation function than it does to collect the data. Therefore, a reduction in calculation time yields better data-collection efficiency. A significant reduction in calculation time came from reprogramming the standard calculation by using a particularization of the ideas of Simpson,[7] which eliminates the

---

[5]Nomura, T., Improvement in S/N Ratio of Reactor Noise Spectral Density, J. Nucl. Sci. Tech. 2, 76 (1965).

[6]Dragt, J. B., Analysis of Reactor Noise Measured in a Zero-power Reactor and Calculations on Its Accuracy, Proc. Symp. Neutron Noise, Waves and Pulse Propagation, Univ. Florida, Gainsville, Florida, USAEC Report CONF-660206, Paper 3-3 (1966).

[7]Simpson, S. M., Time-series Computations in FORTRAN AND FAP, Vol. I, "A Program Library," Program PROCOR (Addison-Wesley, Reading, Mass., 1966).

housekeeping instruction in the usual correlation loop. This process is faster by a factor of about 6 than the conventional algorithm using a loop.

The method was tested with Assembly No. 5 of the ZPR-6 fast critical assembly operating at a power level of about 5 W. The detectors were inserted near the center of the assembly. A 2-hr run gave a value of ℓ/β of 50.4 ± 0.2 μsec, which can be compared with a pulsed-neutron value of 52.1 μsec. A fast component was also observed which had a time constant of less than 1 μsec and an amplitude slightly larger than that of the slower component. The cross-correlation function as plotted by the computer is shown in Fig. 12.

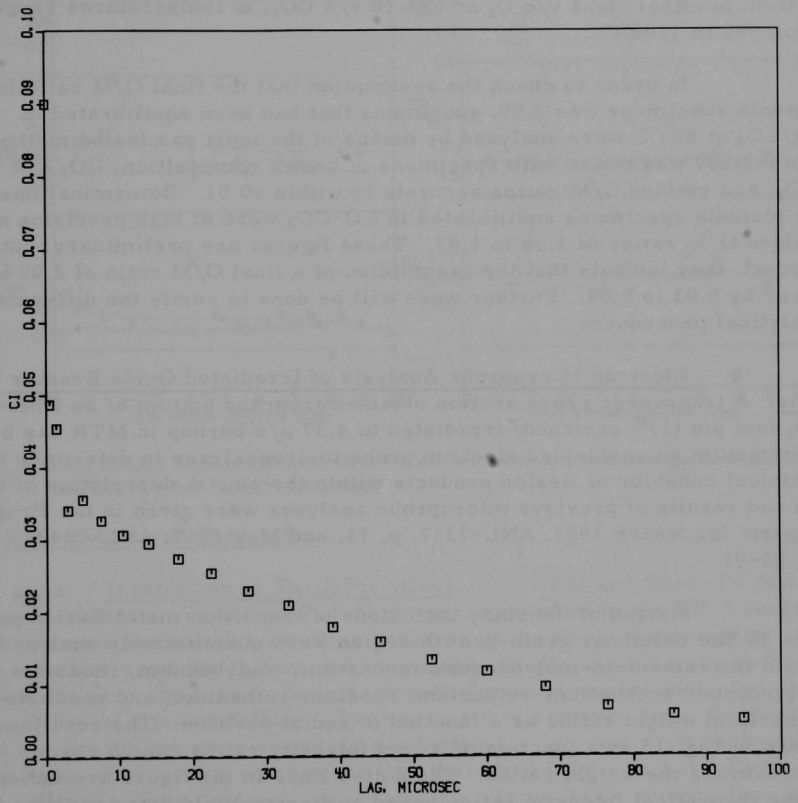

Fig. 12. The Cross Correlation of These Two Plastic Scintillation Detectors is Shown as a Function of Lag Time, in Microseconds.

B. Reactor Fuels and Materials Development

1. Chemistry of Fuel Materials

a. Thermal Stability of Plutonium Ceramics. Previous experiments[8a] on the determination of oxygen-to-metal (O/M) ratios of plutonia and urania-plutonia specimens were continued. These experiments are being made in support of an evaporation study[8b] of PuO_{2-x}. The O/M ratios are determined gravimetrically by measuring the weight change that occurs during equilibration of a specimen in an oxidizing atmosphere at 850°C. For plutonia specimens, the same final composition was obtained by equilibration in either He-1 v/o O_2 or CO-10 v/o CO_2, at temperatures ranging from 700 to 1100°C.

In order to check the assumption that the final O/M ratio in the plutonia specimens was 2.00, specimens that had been equilibrated in CO/CO_2 at 850°C were analyzed by means of the inert gas fusion method.[9] The method was tested with specimens of known composition, UO_2 and U_3O_8, and yielded O/M ratios accurate to within ±0.01. Determinations on the plutonia specimens equilibrated in $CO-CO_2$ were of high precision and yielded O/M ratios of 1.96 to 1.97. These figures are preliminary; but, if correct, they indicate that the assumption of a final O/M ratio of 2.00 is in error by 0.03 to 0.04. Further work will be done to verify the different analytical procedures.

b. Electron Microprobe Analysis of Irradiated Oxide Reactor Fuel Pins. A transverse cross section obtained from the bottom of an EBR-II UO_2 fuel pin (13% enriched) irradiated to 4.37 a/o burnup in MTR has been examined in an unshielded electron probe microanalyzer to determine the chemical behavior of fission products within the pin. A description of the pin and results of previous microprobe analyses were given in the Progress Reports for March 1967, ANL-7317, p. 73, and May 1967, ANL-7342, pp. 88-91.

Sixteen of the shiny inclusions of transition metal fission products in the columnar grain-growth region were quantitatively analyzed to obtain the ruthenium-molybdenum, technetium-molybdenum, rhodium-molybdenum, technetium-ruthenium, rhodium-ruthenium, and rhodium-technetium weight ratios as a function of radial position. The results are shown in Fig. 13 as a function of X-ray intensity ratios, which closely approximate the weight ratios. The dotted lines in the figure are indicative of the theoretical intensity ratios based on fission-yield data for U^{235}. Two types of inclusions were found. In one type (indicated by open points), the molybdenum content decreased as a function of radial position towards the outside of the pin, whereas in the other type (indicated by filled points),

[8] Reactor Development Program Progress Report: (a) February 1967, ANL-7308, pp. 55-56, (b) April 1967, ANL-7329, p. 66.

[9] Holt, B. D., and Stoessel, J. E., Anal. Chem. 36, 1320 (1964).

the molybdenum content increased. The results indicate a preferential migration of molybdenum in relation to the elements technetium, rhodium, and ruthenium. The Tc-Ru, Rh-Ru, and Tc-Rh ratios are in good agreement with the theoretical values, thereby indicating that technetium, ruthenium, and rhodium do not migrate preferentially. Further analyses are being made to determine the mechanism of migration of molybdenum, that is, whether molybdenum or a precursor is the mobile species.

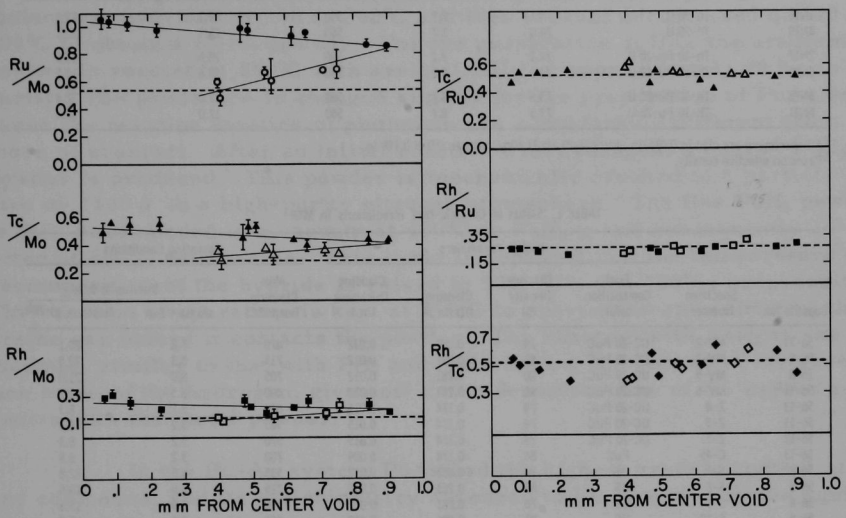

Fig. 13. X-ray Intensity Ratios of Transition Metal Fission Products in Columnar Grain-growth Region of Irradiated UO_2 Fuel Pin (4.37 a/o burnup)

2. Fabrication and Evaluation

a. Irradiation of Th-U-Pu Alloys. Six Th-U and Th-U-Pu fuel alloys jacketed in V-20 w/o Ti tubing were irradiated in the CP-5 reactor to determine the relative swelling behavior of the fuels, the restraint characteristics of the jacket, and the maximum attainable burnup before jacket failure. On June 5 the instrumenting thermocouples indicated the possibility of a jacket failure. The capsule was removed from the reactor and the specimens were examined nondestructively by neutron radiography. Since this examination established that there had been a jacket failure, the capsule will be destructively examined. Table XLIX summarizes design details and irradiation variables for these metal-fuel experiments.

b. Irradiation of High-temperature Materials. A series of irradiations is in progress on ceramic fuel materials being developed under the high-temperature materials programs. The materials under irradiation

include UC-20 w/o PuC, PuC, and US jacketed in Nb-1 w/o Zr. The irradiations are being made in instrumented capsules in the MTR. A summary of the irradiations is shown in Table L.

TABLE XLIX. Status of Metal-fuel Irradiations in CP-5

Specimen Number	Design Parameters[a]		Operating Conditions			
	Fuel Composition (w/o)	Effective Density (%)	Max kW/ft	Max Clad Temp (°C)	Burnup a/o (U + Pu)	Burnup fiss/cc x 10^{-20}[b]
1N16	Th-20 U	74.7	8.7	590	25.1	12.1
4N19	Th-20 U	74.0	8.7	560	25.1	12.1
2N17	Th-10 Pu-10 U	74.1	9.2	590	28.6	13.5
5N20	Th-10 Pu-10 U	73.0	9.2	590	28.6	13.5
3N18	Th-10 Pu-20 U	73.5	8.7	560	17.0	12.4
6N21	Th-10 Pu-20 U	73.5	8.7	560	17.0	12.4

[a]All specimens are clad in 0.015-in.-thick V-20 a/o Ti alloy, with an OD of 0.198 in.
[b]Based on effective density.

TABLE L. Status of Ceramic-fuel Irradiations in MTR

Capsule No.	Specimen Number	Design Parameters				Operating Conditions		
		Fuel Composition (w/o)	Effective Density (%)	Cladding OD (in.)[a]	Cladding Thickness (in.)	Max Cladding Temp (°C)	Burnup to Date a/o (U + Pu)	Burnup to Date fiss/cc x 10^{-20}[b]
56-11	MV-2	UC-20 PuC	79	0.281	0.012	470	7.8	20.1
56-8	MV-3	UC-20 PuC	81	0.281	0.012	715	8.3	22.0
56-8	MV-5	UC-20 PuC	80	0.281	0.012	705	8.0	21.0
56-11	MV-6	UC-20 PuC	80	0.281	0.012	480	8.3	21.7
56-13	Z-4	UC-20 PuC	79	0.174	0.015	665	3.2	8.3
56-13	Z-5	UC-20 PuC	79	0.174	0.015	585	3.2	8.3
56-13	Z-7	UC-20 PuC	79	0.174	0.015	570	3.2	8.3
56-13	C-45	PuC	84	0.174	0.009	700	3.2	8.8
56-8	S-7	US	80	0.281	0.012	535	6.6	12.8
56-8	S-8	US	89	0.281	0.012	725	8.6	18.6
56-8	S-9	US	76	0.281	0.012	750	8.6	15.8
56-8	S-10	US	91	0.281	0.012	690	8.6	19.0
56-11	S-15	US	82	0.281	0.012	380	5.7	11.3
56-11	S-16	US	90	0.281	0.012	510	7.6	16.6
56-11	S-17	US	88	0.281	0.012	500	6.3	13.4
56-11	S-18	US	77	0.281	0.012	610	8.1	15.1

[a]All cladding is Nb-1 w/o Zr alloy.
[b]Based on effective density.

c. Properties of (Th-U-Pu) Phosphide Bodies. The actinide elements Th, U and Pu react with the elements C (from Group IV), N, P, As, and Sb (from Group V), and S, Se, and Te (from Group VI) to form compounds having the NaCl-type structure. The electronic configurations of these compounds are extremely complex because of variations in the energy-state distribution of electrons and the changes in degree of mixed bonding (metallic, covalent, and ionic) that can occur. Because of interest in monocarbides, mononitrides, monophosphides, and monosulfides as fast reactor fuels, an appreciable effort has been made to determine their physical properties. Since little is known of the other compounds of uranium and of plutonium, a program was undertaken to prepare them.

Uranium and plutonium monophosphides and monosulfides have been synthesized by reaction of the decomposed hydride of uranium or plutonium with phosphine, arsine, or hydrogen sulfide gas. The phase

mixtures that result from these reactions were homogenized in the temperature range from 1000 to 1600°C to obtain the binary compounds. The details of this procedure have been described in the Metallurgy Division Annual Report for 1963 (pp. 139-143 in ANL-6868) for the phosphide and sulfides. The preparation of the monoarsenides is somewhat different and a technique for preparing them is reported here in detail.

High-purity metals of 99.99 w/o uranium or 99.97 w/o plutonium are hydrided at 100 to 200°C and then vacuum decomposed at 300 to 400°C to obtain a metal powder. For the preparation of UAs the uranium powder is reacted at 250°C with arsine (AsH_3) of approximately 99.9 v/o purity. The procedure is changed slightly for the preparation of PuAs because the reaction kinetics of plutonium are considerably different from those of uranium. After an initial reaction with hydrogen, a coarse PuH_3 powder is produced. This powder is mechanically crushed to a particle size of $<100\ \mu$ in a high-purity nitrogen atmosphere. The fine PuH_3 powder is then decomposed in a vacuum at 400°C to PuH_{2-x} and subsequently reacted at 250°C with arsine. This cycle is repeated, but the temperature of decomposition of the hydride is raised to 500, 600, and 700°C, progressively. The reaction temperature is kept at 250°C to prevent decomposition of the arsine gas before it contacts the powder. The reaction with AsH_3 is exothermic, similar to that with PH_3 and H_2S. During the course of the reaction some of the hydrogen, given off in the decomposition of the arsine gas, reacts with the metal powder.

In the Pu-As system PuAs had the highest arsenic content of any compound, and its stoichiometry appeared to be governed by the equilibrium of the overall reaction

$$2Pu + AsH_3 \rightarrow PuAs + PuH_{2-x} + \frac{1+x}{2} H_{2\uparrow}.$$

For this reason the reaction was carried as far as possible to completion by cycling to a decomposition temperature of 700°C several times. The uranium and plutonium arsenides were homogenized at 1000°C in a vacuum of 10^{-6} Torr. Weight losses of the monoarsenides during homogenization indicate that these compounds have vapor pressures considerably greater than those of the monophosphides and monosulfides.

The antimonides, selenides, and tellurides were prepared by arc fusion of the elements. High-purity uranium and plutonium and nonmetal elements with a minimum purity of 99.999 w/o were used in this work. Compositions of 50, 53, and 55 a/o nonmetal were prepared, so that the lattice constants of the binary phases in equilibrium with phases of higher nonmetal content could be reported.

Chemical analysis for oxygen and nitrogen showed that the antimony, selenium, or tellurium compounds have relatively low impurity contents when the compounds are made as described. The results of these analyses are listed in Table LI.

TABLE LI. Properties and Chemical Analysis of Uranium and Plutonium VA-VIA Compounds

Compound	Lattice Constant (Å)	Theoretical Density (g/cm^3)	Melting Point (°C)	Chemical Analysis	
				w/o O	w/o N
UP	5.5888 ± 0.0001	10.22	2610	0.04	0.06
PuP	5.6613 ± 0.0001	9.89	2600 (v)	0.05	0.02
UAs	5.7788 ± 0.0001	10.77	2540 (v)	0.07	0.005
PuAs	5.8586 ± 0.0001	10.34	2420 (v)	0.08	0.006
USb	6.2091 ± 0.0001	9.98	1850	0.06	0.03
PuSb	6.2411 ± 0.0004	9.86	1980	0.02	0.01
US	5.4847 ± 0.0001	10.87	2480	0.04	0.01
PuS	5.5412 ± 0.0001	10.59	2350	0.03	0.01
USe	5.7399 ± 0.0003	11.13	2080	0.09	0.03
PuSe	5.7934 ± 0.0001	10.86	2075	0.02	0.02
UTe	6.150 ± 0.001	10.55	1720	0.08	0.04
PuTe	6.183 ± 0.001	10.31	1870	0.02	0.02

(v) = Melting accompanied by vaporization.

Debye-Scherrer X-ray photograms were obtained with CuK_α NiK_α radiation and a 114.6-mm-dia camera. A computer program was used to obtain a least-squares fit of the X-ray diffraction data. The best precision lattice-constant values were selected from plots of the error factor determined for the different extrapolation techniques and weighting factors incorporated in this program.

Melting points of the compounds were measured in a V-shaped tungsten filament heated in flowing high-purity argon at a pressure of 3 atm. The pyrometer was calibrated by means of an NBS-certified tungsten lamp. Window and prism absorption corrections were also determined with this lamp. The error of the melting-point measurements is about ±30°C as estimated from the melting points of standards. The average of at least five determinations of the melting point for each compound are reported.

The lattice constants, theoretical densities, and melting points of the monophosphides, monoarsenides, monoantimonides, monosulfides, monoselenides, and monotellurides of uranium and plutonium are given

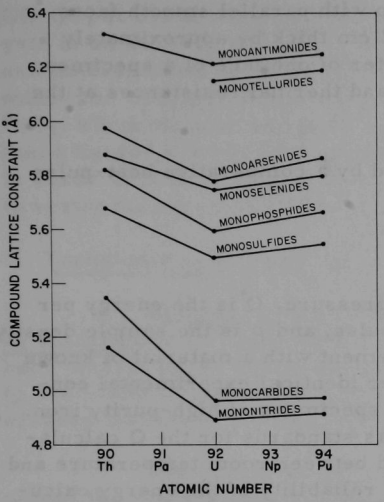

Fig. 14. Lattice Constants of the NaCl-type Actinide IVA-VIA Compounds Plotted as a Function of the Atomic Number of the Actinide Component

in Table LI. Although some of these compounds are known to have nonmetal defect structures and exist over a range of composition, only the maximum values of the lattice constants are reported.

The lattice constants of all the actinide-group IVA-VIA compounds (where "A" refers to groups of elements--in the Periodic Table--headed by nonmetallic elements) with the NaCl-type structure are plotted against the atomic number of the actinide component in Fig. 14. The interatomic distance generally expands with the number of electrons in the inner shell of the nonmetal element, but in the same period this spacing decreases as the number of electrons in the valence shell of the nonmetal increases. Data for this plot were taken from Table LI and various literature sources.[10]

Thorium monotelluride was reported to have the CsCl-type structure with a lattice constant of 3.827 Å and to decompose below 1000°C in a vacuum. In view of the unexpected structure reported, compositions of ThTe and $ThTe_{1.1}$ were prepared by arc fusion and examined. The CsCl-type structure was confirmed, and the lattice constant of the ThTe phase in equilibrium with a phase of higher tellurium content was 3.8319 ± 0.0001 Å. The melting point of ThTe was found to be 1680°C.

d. Development of Thermal Diffusivity Rig for Ceramic Materials. The potential usefulness of high-melting ceramic compounds of plutonium has prompted extensive investigation of their thermal properties. The heat capacities of the monosulfide and monophosphide of plutonium have now been measured between room temperature and 650°C.

Disk-shaped samples, 1.9 cm in diameter by approximately 0.5 cm in thickness, were electrical-discharge machined from cold-pressed and sintered cylinders of PuP and PuS. These disks were then

[10] Shalek, P. D., Preparation and Properties of Uranium and Thorium Monosulfides, J. Am. Ceram. Soc., 46(4), 155-161 (1963); Storms, E. K., Critical Review of Refractories, LA-2942 (1964); Ferro, R., The Crystal Structures of Thorium Arsenides, Acta Cryst. 8, 360 (1955); The Crystal Structures of Thorium Antimonides, Acta Cryst. 9, 817 (1956); D'Eye, R. W. M., Sellman, P. G., and Murry, J. R., The Thorium-Selenium System, J. Chem. Soc. (London) 2555 (1952); Argonne National Laboratory Annual Progress Report for 1964, Metallurgy Division, ANL-7000, p. 90; D'Eye, R. W. M., and Sellman, P. G., The Thorium-Tellurium System, J. Chem. Soc. (London) 3760 (1954).

lapped to a final thickness of 0.2 to 0.3 cm with parallel smooth faces. After lapping, a small platinum foil, 0.002 cm thick by approximately 0.32 cm in diameter, was fused to the center of one face of a specimen. This platinum foil lowered the electrical and thermal resistances at the thermocouple contact.

The heat capacity was obtained by a comparative heat-pulse method according to the expression

$$C_p = Q/\rho L T_m,$$

where C_p is the specific heat at constant pressure, Q is the energy per unit surface area absorbed from a laser pulse, and ρ is the sample density. The energy Q is obtained from a measurement with a material of known heat capacity and similar size, made under identical experimental conditions as the unknown. In this research, specimens of high-purity iron, platinum, and aluminum oxide were used as standards for the Q calculations. These materials were pulse-heated between room temperature and 900°C at varying energies to establish the reliability of the energy calculation. Measurements over this temperature range were necessary to make sure that there were neither excessive variations in energy absorption nor appreciable heat losses during the time of the experiment.

TABLE LII. Heat Capacities of Plutonium Monophosphide and Plutonium Monosulfide

Temp (°C)	C_p of PuP, (cal $g^{-1}°C^{-1}$)	C_p of PuS, (cal $g^{-1}°C^{-1}$)
25	0.0550	0.0538
100	0.0550	0.0545
200	0.0552	0.0553
300	0.0555	0.0560
400	0.0557	0.0568
500	0.0560	0.0575
600	0.0562	0.0580
650	0.0563	0.0584

Mean values are interpolated from the data at regular temperature intervals and are given in Table LII. Data points are now being put in a computer program to make a least-squares fit to the standard heat-capacity equation

$$C_p = a + bT + cT^{-2}.$$

e. Thermal Stability of Plutonium Ceramics. Experiments were continued on the determination of oxygen-to-metal (O/M) ratios of plutonium oxide and mixed uranium-plutonium oxide specimens. These experiments (see Progress Report for February 1967, ANL-7308, pp. 55-56) are being done concurrently with an evaporation study on PuO_{2-x}. The O/M ratios are determined gravimetrically by measuring the weight change that occurs during equilibration of a specimen in an oxidizing atmosphere at 850°C. The experimental results show that the same final composition was obtained by equilibration of PuO_2 specimens in either helium-1 v/o oxygen or CO-10 v/o CO_2 at temperatures ranging from 700 to 1100°C.

In order to check the assumption that the final O/M ratio in the PuO_2 specimens was 2.00, specimens that had been equilibrated in the

CO-CO_2 at 850°C were sent for analysis. The procedure used for the analysis is an absolute one that involves fusion of a specimen in liquid metal and measurement of the oxygen evolved. The O/M ratios that were determined for U_3O_8 and UO_2 were accurate to within ±0.01. Determinations for PuO_2, which were of high precision, yielded O/M ratios of 1.96 to 1.97. If these figures are correct, they indicate that work by Markin and Rand[11] is in error by 0.03 to 0.04 in the O/M ratio. Further analyses will be made to verify the accuracy of the analysis procedure.

3. Techniques of Fabrication and Testing

a. Determination of Elastic Moduli of High-temperature Materials by Ultrasonics. Transit times of shear and longitudinal velocities have been measured for specimens (of 3-in.-length) of cold-rolled carbon steel to 800°C and of stainless steel to 1000°C. Calculation of the elastic moduli of these materials was started in May.

The shortness of the specimens and the temperatures of use required the mechanical coupling of buffer rods to the specimens.

Calculations of the ultrasonic velocities and the elastic moduli to 1000°C of cold-rolled steel and Type 304 stainless steel have been completed. The resulting values are within 5% of the literature data. The measurements and calculations are going to be made several times to find any spread in the data.

A number of modifications were made in the furnace to simplify its operation. Buffer rod samples and thermocouples are now installed from the top without the removal of the yoke.

b. Ultrasonic Instrument and Transducer Development. The acoustic impedance of -325 mesh tungsten of 52 to 80% full density was reported to be 24 to 58 x 10^5 g $cm^{-2}sec^{-1}$ (see Progress Report for May 1967, ANL-7342, p. 94). Impedances in this range should match the "Z" values of ceramic transducer elements. The probe performance indicates that ultrasonic energy from the back face of the transducer elements has been penetrating the backing material and reinforcing the energy from the front face. Means of reducing this energy from the back face have been studied for some months.

Methods to reduce the amplitude of undesirable echoes from porous metal backings in ultrasonic transducer probes are still being investigated. Impregnation, making sawcuts, and the use of cones are methods that offer some promise.

[11] Markin, T. L., and Rand, M. H., "Thermodynamic Data for Plutonium Oxides," pp. 145-156 in Thermodynamics, Vol. I (IAEA, Vienna, 1966).

A porous tungsten sample, for example, was impregnated with Teflon and compared to an identical sample without Teflon. More ultrasonic energy was transmitted through the impregnated sample than through the porous one. Since increased attenuation is needed in a backing member to reduce the energy returning to the transducer element, Teflon-impregnated metal backings would be less efficient than porous metal backings.

Transducer probes with backing members having conical rear faces and sawcuts around the circumference are being fabricated.

c. Development of a Neutron-image Intensification System. Bench tests of a video amplifier developed by the Electronics Division indicated (see ANL-7342, pp. 94-95) that gain factors of about ten should be usable with the vidicon camera of a television system and that gain factors of 100 are obtainable. Actual television tests are required to determine whether the associated noise at that gain setting would be excessive.

Further tests with the contrast-expander amplifier, as used with the neutron television system, have been completed. The circuitry permits the operator to enhance the contrast of the television image near the white portion of the gray-scale image. This enhanced contrast comes at the expense of decreased latitude, in that the use of the contrast expander usually produces reduced contrast near the black end of the image.

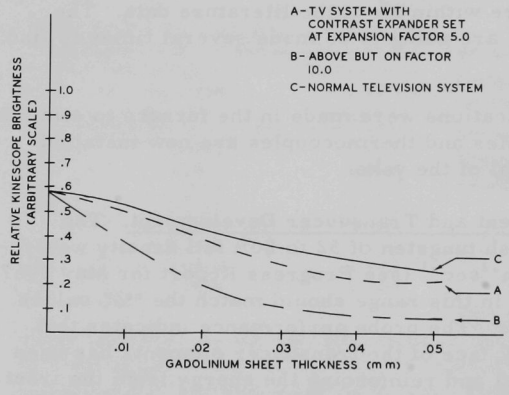

Fig. 15. The Relative Brightness of the Neutron Television Kinescope Presentation of a Gadolinium Stepped Wedge is Shown. The relative brightness values were obtained by a calibrated CdS photoconductive detector observing a small area (4 mm, dia) on the kinescope The television contrast settings were constant during this test, in which the expansion factor of the constant enhancement amplifier was varied. The expansion factor of 10.0 (curve B), yields much improved contrast of the image of the thinner steps.

As an example, we can examine the televised neutron image of a stepped gadolinium wedge in order to determine the relative contrast between the steps. Figure 15 shows the relative kinescope brightness of this type of image for several different situations. Television-system contrast was held constant; the expansion factor of the amplifier was varied. An expansion factor of 5.0 yields very little change in the slope of the curve for brightness versus object thickness. An expansion factor of ten yields a significant increase in slope

(and therefore in observed contrast) for the thinner object steps, at the expense of reduced contrast for the thicker steps. An expansion factor greater than ten yields increased contrast but also introduces a great deal of noise.

The amplifier appears to be useful for enhancing the television images of low-attenuation types of objects, but less useful for objects of higher attenuation, since these images would appear in the black region of the image where enhancement is normally not readily available.

C. Engineering Development

1. Development of Master-Slave Manipulator Systems

a. Electric Master-Slave Manipulator, Mark E4A. Brakes have been installed on all of the slave servo drive gear boxes. Tests of these can be made in July.

The Mark E4A is one of the manipulators being considered for the Hot Fuel Examination Facility to be constructed at the EBR-II site. This facility may use an argon atmosphere. Consequently, the Mark E4A slave arm is now being prepared for testing in argon to determine the load-time duty cycle.

A box is being designed to provide an argon atmosphere for tests of the entire slave arm. The sides will be easily removable to facilitate making different hook-ups.

Purging holes and tube connectors have been installed on all 28 slave motors as one step in preparing to test the slave arm in argon. Purging will be necessary because the motors are otherwise not vented, and air could remain inside the motors for hours or days after the arm was placed in an argon atmosphere.

b. Low-inertia Servo Motor for Manipulators. The special 2-pole, 2-phase low-inertia servo motor has been completed in mechanical fabrication and is out being wound. It is designed for possible use in a 100-lb master-slave manipulator. A gear drive for testing the motor has been designed and is now being manufactured. Some tests will be made on the motor during July.

Direct-current motors are being studied for possible use in future master-slave manipulators. Preliminary calculations show that dc motors can be designed to have a much higher torque-to-inertia ratio than ac motors. Also, the electrical time constant will probably be much lower. In addition, the calculations indicate that the efficiency could be high enough so that little or no forced cooling would be needed at the slave arm.

2. Heat Transfer and Fluid Flow

a. Niobium-1% Zirconium Loop. A facility has been built to investigate the heat transfer and two-phase flow characteristics of boiling sodium to a temperature of 2100°F and a pressure of approximately 8 atm. Among the variables to be investigated are boiling heat flux and temperature difference up to the critical flux occurrence, boiling and adiabatic two-phase pressure losses, vapor volume fraction, boiling stability parameters, and ultimately the transient behavior of these same quantities.

The thermal-radiation heater has been rebuilt and some additional instrumentation has been added to the system. Operation is underway; it is planned to extend the previously attained heat flux and temperature levels.

b. Heater Experiments

(i) Electron-bombardment Heater (EBH) Experiment. The initial tests have been terminated following satisfactory operation; further EBH tests will be carried out in the new EBH test facility that is under construction.

c. Heat Transfer in Double-pipe Heat Exchangers

(i) Countercurrent Turbulent Liquid-metal Flow. Experimentation with the third heat-exchanger test section continues. Experimentally determined heat-exchanger effectivenesses are in good agreement with the analytical predictions based on "fundamentals" rather than on the customary use of heat-transfer coefficients. Figure 16 shows the results of one series of runs during which the flow rate in the annulus was held constant (annulus-side Peclet number = 100) and the flow rate in the tube was varied. The figure compares experimental data with predictions of the analysis "from fundamentals," and with predictions of the customary engineering design relation based on fully developed uniform-heat-flux heat-transfer coefficients. Inaccuracies in the customary engineering relation are apparent. As related to actual heat-transfer coefficients, these inaccuracies can be attributed to two sources: (a) the heat transfer is not fully developed over a significant

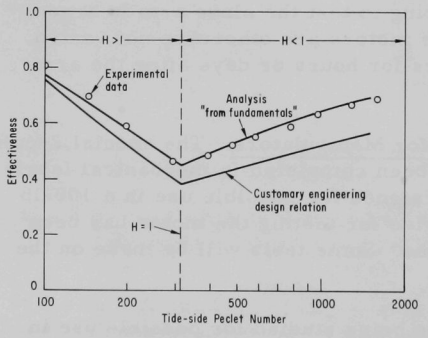

Fig. 16. Variation of Heat-exchanger Effectiveness with Tube-side Perclet Number for an Annulus-side Perclet Number of 100 (for mercury-to-mercury counterflow double-pipe exchanger. Test Section No. 3).

portion of the heat exchanger length (i.e., heat-transfer coefficients are not independent of axial position and are larger than fully developed values) and (b) fully developed heat-transfer coefficients (or, equivalently, the heat-flux distributions) depend on the operating conditions of the exchanger. In the region denoted $H > 1$ on Fig. 16, fully developed tube-side heat-transfer coefficients are less than those corresponding to uniform heat flux while annulus-side coefficients are larger; in the region $H < 1$, fully developed tube-side heat-transfer coefficients are larger than those corresponding to uniform heat flux while annulus side coefficients are less. When $H = 1$, the heat capacity-mass flow rate products on both sides of the exchanger are equal, and fully developed heat-transfer coefficients correspond to uniform heat flux. Inaccuracies for the case of $H = 1$ are solely a result of the higher local rates of heat transfer in the nonfully developed regions of the exchanger.

3. Engineering Mechanics

a. Core Structural Dynamics. Tests of single simulated fuel elements have continued (see Progress Reports for April 1967, ANL-7329, pp. 70-71; May 1967, ANL-7342, pp. 96-97). The data obtained from the earlier tests and from a similar test element were used to compute power spectral-density curves, that is, to obtain plots of $\hat{G}_y(f)$ versus frequency, where

$$\hat{G}_y(f) = \frac{1}{BT}\int_0^T Y_B^2(f,t)\,dt = \frac{\overline{Y_{B(f)}^2}}{B}.$$

where $\overline{Y_B^2}(f)$ is the mean-square value of displacement within a narrow frequency band with a center frequency of f kilocycles/sec, B is frequency bandwidth, and T is finite averaging time. The total area under the $\hat{G}_y(f)$ curves provides a value of mean-square displacement. Because the original data were taken with two mutually perpendicular transducers, the areas under the two curves may be summed. The square root of this summation yields a value for the maximum displacement of the rod (r_{rms}) in units of root-mean-square mills. The value of r_{rms} for the different test specimens at common flow rates have a variation of less than 5%.

The data (r_{rms}) were plotted versus the mean axial flow velocity (U in ft/sec) and found to be related by $r_{rms} = AU^n$, where for the present data $A(\chi) \simeq 0.14$ and $n \simeq 1.89$. These values of A and n are not exact. Further testing and a least-squares curve fit are required to verify them.

Another pump has been obtained from storage. The two pumps will be used in parallel in the present loop. When installation is complete, flow velocities of 30 ft/sec through the 2-in. test section should be possible.

4. Instrumentation and Control

The principal objective of this work is to develop in-core sensors to diagnose reactor performance and detect abnormalities (see Progress Report for January 1967, ANL-7302, p. 73). It concentrates on instrumentation important for reliable operation of large liquid-metal fast reactors. Methods of detecting local boiling in the coolant are being investigated. One such method, whose effectiveness is being evaluated for a high-temperature sodium environment, uses the acoustic-frequency spectrum, both audio and ultrasonic.

a. Acoustic Boiling Detection. This work aims to provide quantitative design information for acoustic boiling detection and to develop a high-temperature sound detector that can be immersed in sodium coolant.

The literature survey on boiling detection was completed. From the survey, it was concluded that the major technical problem in applying acoustic boiling detection is the presence of ambient noise, the most troublesome being mechanical pump noise. A possible solution involves using wideband sensors and electronics to detect ultrasonic emissions to 60 kc/sec. However, most of the sound is found in a band of 0.1-10 kc/sec, with frequency resonances caused by dynamics of bubble formation and by eigenfrequencies of the container geometry. Sound intensity depends on the heater surface, subcooling, and heat flux.

Tests to determine equipment specifications are continuing. Two types of low-temperature hydrophones and the associated equipment have been assembled and calibrated. The frequency response was obtained by using a white-noise sound source. One test hydrophone was checked on a vibration test facility for low-frequency cutoff. Another was also calibrated for static sensitivity by the pressure-step method.

The use of an instrumentation tape recorder will permit 100-kc/sec frequency spectra to be analyzed on the present vibration-test-facility spectrum analyzer. The accuracy of spectrum measurements is expected to be within 1% up to 80 kc/sec.

A quick feasibility test was performed to demonstrate that a hot-wire anemometer can be used to detect boiling sounds in water. The background spectrum of anemometer output contained a broad maximum at 55 kc/sec with no boiling in stagnant water. Lower-frequency container resonances in the boiling spectrum were detected by the anemometer and one of the standard hydrophones in symmetrical positions 8 in. from the heated wire. When receiving signals from a projector, the anemometer detected discrete sound frequencies to the 100-kc/sec limit of the instrumentation. Average signal-to-noise ratio for the anemometer was poorer than that of the hydrophone by a factor of ten (20 dB).

D. Chemistry and Chemical Separations

1. Fluoride Volatility Processes

a. Recovery of Uranium and Plutonium from Low-enrichment Fuels: Laboratory Support Work

(i) Chemistry of Ruthenium Fluorides. As part of the study of the kinetics of formation of ruthenium fluorides, two preliminary experiments were performed on the rate of reaction of BrF_5 with ruthenium metal. As in earlier fluorinations of ruthenium metal with BrF_3 (see Progress Report for May 1967, ANL-7342, pp. 98-99), ruthenium metal tagged with Ru^{106} was used, and the fluorination rates were monitored by measuring the change in activity of the metal sample (in a nickel boat) and of a 400°C NaF trap downstream from the metal sample. The volatile ruthenium fluoride formed was collected by the NaF trap. In both experiments the BrF_5 concentration was 34 v/o in nitrogen and the flow rate correspond to a room-temperature flow rate of about 125 ml/min.

In the first experiment, the reactor temperature was 395°C and the gas-phase temperature was 290°C. The reaction rate during the first 20 min of the experiment was high; about one-half of the metal was converted to RuF_5, and the estimated value for the observed rate constant was 0.0103 min^{-1}. During the next 40 min, the rate was much lower.

In the second experiment, no reaction was observed with the reactor temperature at 250°C, but with the reactor temperature increased to 300°C and the gas-phase temperature at 290°C, evidence of reaction was noted. The rate of reaction during the first 10 min gave a high rate constant of 0.0114 min^{-1}, followed by slower reaction (0.00116 min^{-1}) for 40 min. The count data indicated conversions of 75 and 50% of the ruthenium to RuF_5 in the two runs. The results suggest that reaction commences by ignition of the metal, and that the lower subsequent rate represents reaction of BrF_5 with an intermediate compound formed during the initial reaction period.

(ii) Fluorination of UO_2-PuO_2-Fission Product Pellets. A 2-in.-dia fluid-bed reactor is being used for development studies to establish optimum conditions for fluorinating UO_2-PuO_2 pellets containing nonradioactive fission product oxides. In the process, the pellets are first oxidized to U_3O_8-PuO_2 fines by reaction with oxygen. Next, the uranium oxides in uranium-plutonium mixtures are converted to volatile UF_6 by BrF_5, which converts plutonium dioxide to nonvolatile PuF_4. In a subsequent step, plutonium is recovered as volatile PuF_6 by the reaction of PuF_4 with fluorine.

An experiment on the reuse of alumina, runs Purse-20, -21, and -22, was carried out with added nonradioactive fission products to

simulate processing of fuel with a burnup of 30,000 MWd/ton. Previous experiments of this type had been done with fuel having a simulated burnup of only 10,000 MWd/ton. About 650 g of UO_2-PuO_2 pellets were charged in each run. Radioactive tracers, Np^{239} and Ru^{106}, were added to the reactor for runs Purse-20 and -22, respectively. A single batch of alumina (48-100 mesh) was used to process the three batches of fuel. Plutonium fluorination was postponed until the end of run Purse-22.

In each run, the pellets were oxidized with 20 v/o oxygen at 450°C for 4 hr, and the uranium was fluorinated with 10 v/o BrF_5 at 300°C for about 2 hr. An additional 2 hr of fluorination with BrF_5 was used in run Purse-22. Following the BrF_5 step of run Purse-22, plutonium was fluorinated with 90 v/o fluorine for 5 hr at 300°C, 5 hr from 300 to 550°C, and 3 hr at 550°C.

The preliminary results from run Purse-22 indicate that most of the Ru^{106} left the fluid bed during fluorination with BrF_5. Additionally, the plutonium content of a bed sample taken after 9 hr of recycle-fluorination indicates that about 96% of the 15 g of plutonium charged had been fluorinated at that point. Since an additional 4-hr-period of recycle-fluorination was carried out after the sample was taken, this result is considered very encouraging. The final plutonium content of the bed will be reported after analytical data are obtained.

(iii) Neptunium Fluoride Chemistry. The fluoride volatility flowsheet may include an operation in which a gaseous process stream flows through a fixed bed containing solid NaF to remove some of the volatile fluorides by formation of solid complexes with NaF. In order to obtain information for predicting the behavior of NpF_6 in this operation, experiments have been performed to study the reaction of NpF_6 gas with NaF.

A static system was used: a sample of NaF (contained in a shallow boat in a tube reactor) was exposed to NpF_6 (250-350 mm) at 150°C. A violet-colored solid complex was formed that was tentatively identified as $3NaF \cdot NpF_5$. An X-ray powder diffraction photograph of the complex can be indexed on the basis of a body-centered tetragonal unit cell with lattice constants $a = 5.449 \pm 0.001$ Å and $c = 10.853 \pm 0.003$ Å, and with a volume of 322 $Å^3$. Measurements of pressure and vapor density of the gas phase indicate that the reaction is probably

$$3NaF(s) + NpF_6(g) \rightarrow 3NaF \cdot NpF_5(s) + \tfrac{1}{2} F_2(g).$$

A valence-state analysis by first dissolving the complex in aqueous iodide solution and then determining the equivalents of iodine released per mole of neptunium showed that the neptunium had an average oxidation number of 4.6.

Additional experiments are planned to investigate the reaction of fluorine with the complex over a range of temperatures and pressures for the purpose of determining equilibrium constants for the reaction.

b. Recovery of Uranium and Plutonium from Low-enrichment Fuels: Engineering Work

(i) Engineering-scale Alpha Facility. The major objectives of experiments under way in the engineering-scale alpha facility are to demonstrate handling of PuF_6 in engineering-scale equipment and to determine the feasibility of fluoride volatility flowsheets. A BrF_5 feeding system and a BrF_5-Br_2-UF_6 off-gas system (see Progress Report for February 1967, ANL-7308, p. 75) have been installed recently in the engineering-scale alpha facility. Now the three steps of the current flowsheet--oxidation, fluorination with BrF_5, and fluorination with fluorine--can be performed in the facility.

In the current run (UBr-16), the newly installed equipment is being tested by processing a charge of 4.4 kg of UO_2 pellets. An 8-hr oxidation step has been performed at 450°C with 11-20 v/o oxygen. The oxidation went smoothly. Fluorination of the bed with BrF_5 is under way.

(ii) Process Development Studies for Uranium Dioxide Fuels. Engineering-scale studies are being performed in a 3-in.-dia fluid-bed reactor facility to determine the effects of important process variables on the fluorination of UO_2 fuels with BrF_5. The current program involves a series of eight statistically designed experiments to measure the effects of six independent variables on UF_6 production rate, BrF_5 utilization, off-gas composition, and uranium removal from the fluid bed.

The sixth and seventh experiments (runs BrF5-8 and -9) in this series have been successfully completed. In each run, 4.4 kg of fragmented UO_2 pellets were oxidized in a fluidized bed of 48 to 100 mesh alumina, using 19 v/o oxygen at 450°C. A difference was that run BrF5-8 had fission product compounds charged with the UO_2 whereas run BrF5-9 did not. In run BrF5-8, 12 v/o BrF_5 at 300°C was used in the uranium fluorination step, and in run BrF5-9, 20 v/o BrF_5 at 225°C was used. Both runs proceeded very smoothly.

The eighth run of this series is in progress. After its completion, one of the runs of the series will be repeated to obtain an estimate of experimental error. Quantitative effects of the independent variables will then be obtained.

IV. ADVANCED SYSTEMS RESEARCH AND DEVELOPMENT

A. Argonne Advanced Research Reactor (AARR)

1. General

The contract for Construction Package No. 1 has been awarded to Cowan Excavating Co. The groundbreaking ceremony was held on June 12, 1967. Removal of topsoil and digging of culverts has begun.

A contract for the rebound markers on the AARR site was awarded to Layne-Webster Co. The rebound markers were installed and all work completed by June 16, 1967.

Proposals for the primary heat exchangers and for fabrication of the permanent beryllium were received and are being reviewed. Drawings of the control-rod drive mechanism have been transmitted to ANL Central Shops for fabrication. A proposal on the primary pumps is awaiting AEC approval before contract award.

The architect-engineer is finishing the design and specifications for the foundation mat and containment liner.

2. Core Development

a. Temperatures of Reactor-vessel Internals. A thermal analysis has been completed of the reactor-vessel core-support ledge and portions of the aluminum reflector shroud and pedestal and the stainless-steel vessel adapter. This estimate of the temperature distributions in this region verifies the adequacy of the design. Although the calculations were made for an Inconel vessel, the similarity of their thermal conductivities make the temperatures also applicable for a stainless-steel vessel.

The downward flow of water exerts a large force on the core and reflector. The region encircled in Fig. 17 must support the reflector and the attendant load caused by the flow of water. The beryllium weight and the fluid force are transmitted through the reflector shroud and pedestal to the vessel adapter, which transmits the total load to the reactor-vessel core-support ledge.

The geometry chosen for study is between the bolts; the study does not provide information on the bolts or on sections containing gussets. The model used also does not include the thermal shield.

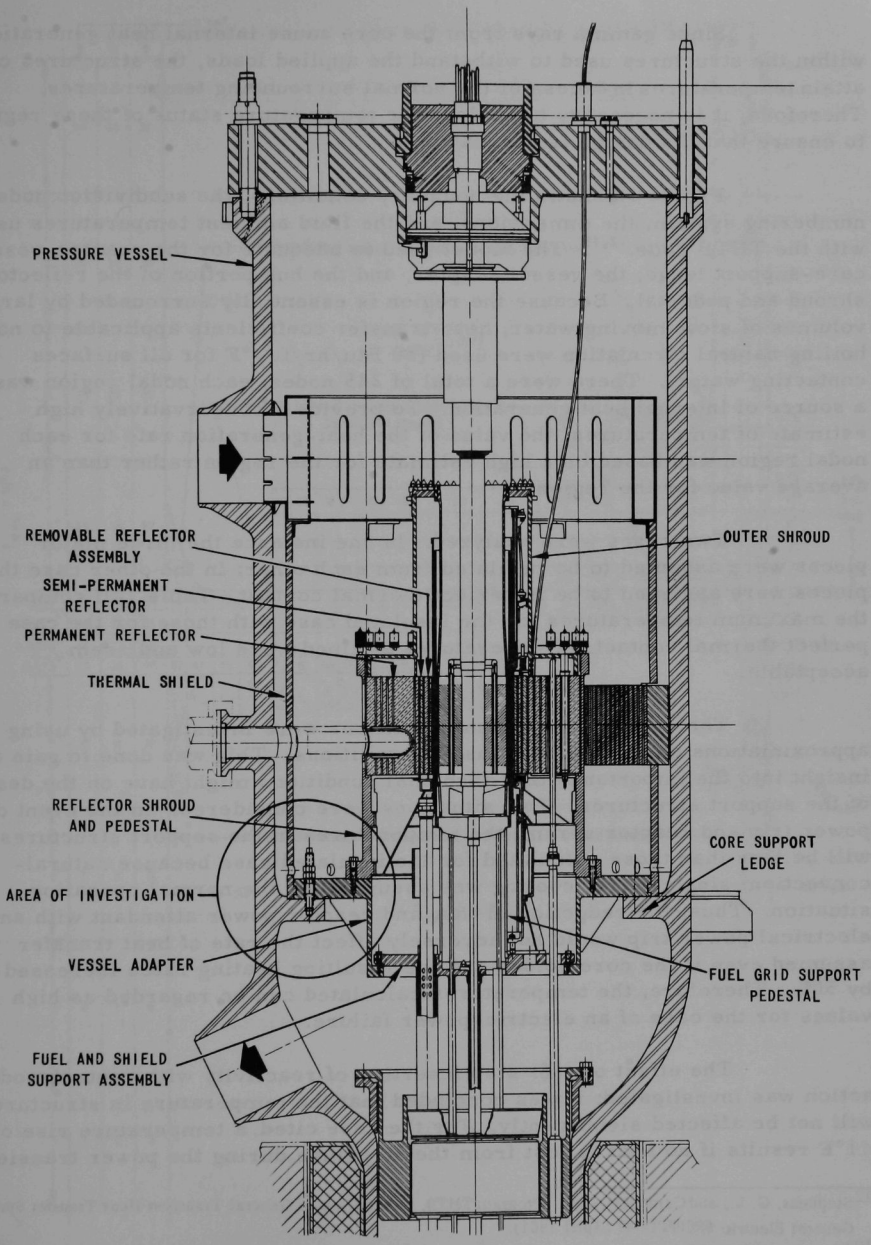

Fig. 17. Elevation View of AARR Pressure Vessel and Internal Structures

Since gamma rays from the core cause internal heat generation within the structures used to withstand the applied loads, the structures can attain temperatures in excess of the normal surrounding temperatures. Therefore, it is necessary to analyze the temperature status of these regions to ensure that the design is adequate.

Figure 18 shows the boundary conditions, the subdivision nodal numbering system, the dimensions, and the fluid ambient temperatures used with the THTB code.[12,13] The model used is adequate for the reactor-vessel core-support ledge, the vessel adapter, and the hub portion of the reflector shroud and pedestal. Because the region is essentially surrounded by large volumes of slow-moving water, heat-transfer coefficients applicable to non-boiling natural circulation were used (50 Btu/hr/ft^2/°F for all surfaces contacting water). There were a total of 245 nodes; each nodal region was a source of internal heat generation. To provide a conservatively high estimate of temperatures, the value of the heat-generation rate for each nodal region was based on a high estimate for the region rather than an average value for the region.

Two cases were analyzed. In one instance the three major pieces were assumed to be insulated from each other; in the other case the pieces were assumed to be in perfect thermal contact. Table LIII compares the maximum temperatures for the insulated case with those for the case of perfect thermal contact. Temperatures attained were low and seem acceptable.

The effects of transient conditions were investigated by using approximations of postulated transient conditions. This was done to gain an insight into the importance that abnormal conditions might have on the design of the support structures. Two situations were considered. In the event of a power trip and reactor scram, the temperatures in the support structures will be less than those calculated for the insulated case because natural-convection, single-phase cooling was assumed for the normal operating situation. Thus, the reduction in flow and reactor power attendant with an electrical power trip would not adversely affect the rate of heat transfer assumed even if the core voided and the resulting heating rates increased by 50%. Therefore, the temperatures calculated can be regarded as high values for the case of an electric-power failure.

The effect of a $1 step insertion of reactivity with control-rod action was investigated; it was concluded that the temperature in structures will not be affected significantly. For the case cited, a temperature rise of <1°F results if no heat is lost from the structure during the power transient.

---

[12] Stephens, G. L., and Campbell, D. J., "Program THTB, for Analysis of General Transient Heat Transfer Systems," General Electric #R60FPD647 (April 1961).

[13] Jesse, N. "THTB (GE)--Three Dimensional Transient Heat Transfer," Program Library 2209/RE 322, ANL, Revised August 21, 1966.

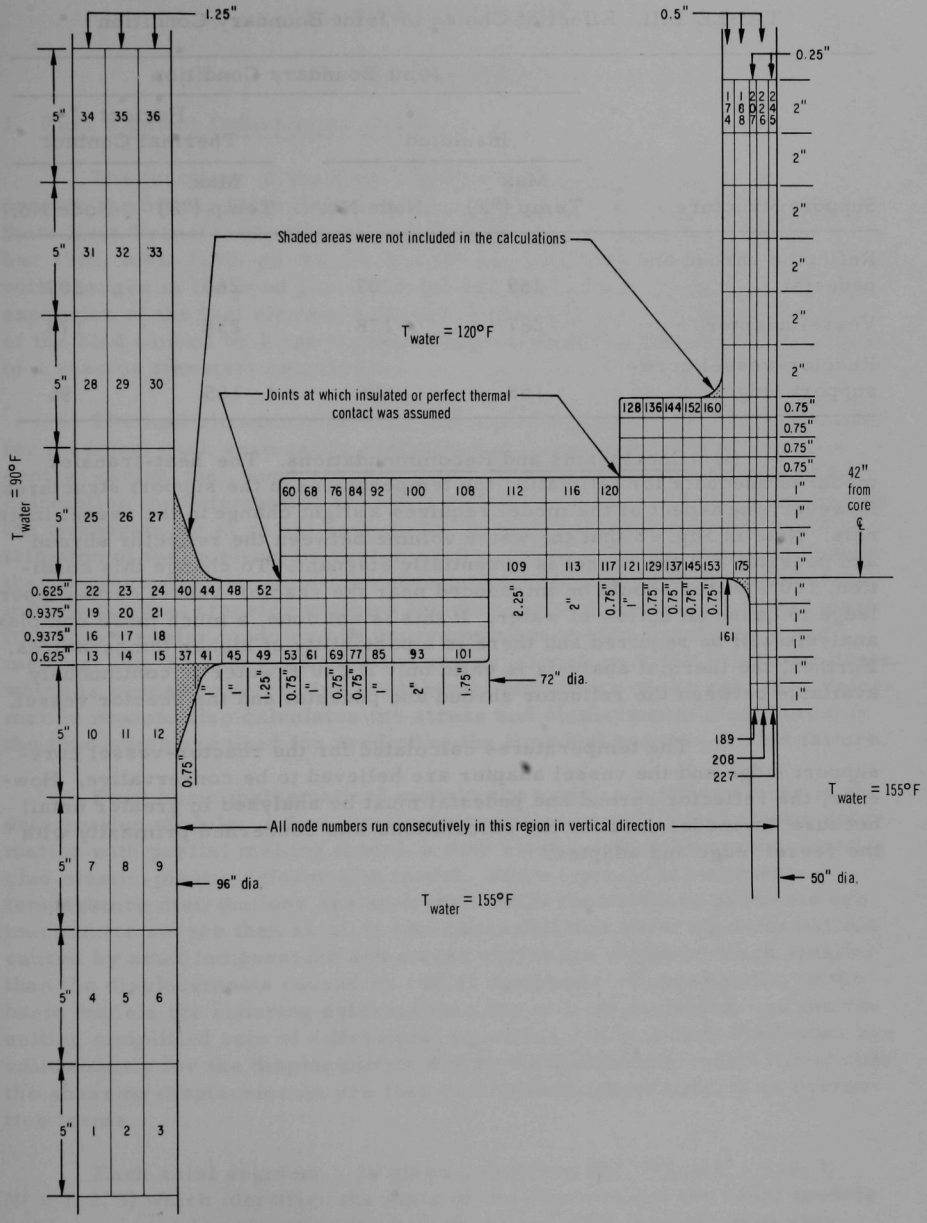

Fig. 18. Dimensions, Nodal Numbering System, Boundary Conditions, and Fluid Temperatures Used in Calculations.

TABLE LIII. Effect of Choice of Joint Boundary Condition

	Joint Boundary Condition			
	Insulated		Perfect Thermal Contact	
Support Structure	Max Temp (°F)	Node No.	Max Temp (°F)	Node No.
Reflector shroud and pedestal	259	207	260	207
Vessel adapter	287	178	238	178
Reactor-vessel core-support ledge	158	96	165	96

(i) Conclusions and Recommendations. The heat-transfer model is adequate for estimating the temperatures in the support structures. However, one aspect of the model requires a slight change in the vessel internals. Note in Fig. 18 that the water volume between the reflector shroud and pedestal and the vessel is essentially stagnant. To change this condition, 120°F water should be introduced near the reactor-vessel core-support ledge to cause an upflow of water. If this is not done, a much more complex analysis will be required and there is a possibility of higher temperatures. Further, the thermal analysis is valid only if 120°F water is continuously available between the reflector shroud and pedestal and the reactor vessel.

The temperatures calculated for the reactor-vessel core-support ledge and the vessel adapter are believed to be conservative. However, the reflector shroud and pedestal must be analyzed in greater detail because the model used for the calculations was concerned primarily with the vessel ledge and adapter.

V. NUCLEAR SAFETY

A. Accident Analysis

1. Fuel Element Deformation Module

The functions of the Fuel Element Deformation Module are (a) to provide the Steady State Heat Transfer Module (HTSS) and the Transient State Heat Transfer Module (HTTS) (see Progress Reports for November 1966, ANL-7279, pp. 46-47, and for January 1967, ANL-7302, pp. 84-86) with changes in the bond gap and axial and radial mesh caused by thermal expansion of the fuel element and (b) to predict plastic thinning and rupture of the clad caused by large thermal expansions of the fuel during the course of a reactor transient calculation.

The fuel element is divided into axial segments as in the heat transfer modules; each segment is comprised of concentric annular zones of central cavity, fuel, bond gap, and clad. At each time step in an accident calculation the deformation module receives from the heat transfer module the temperatures at radial node points in each axial segment and the distribution of fuel melting (if any) in each segment. The deformation module then permits calculation of the deformation of the fuel and clad, and transmits to the heat transfer modules the changes in the axial and radial mesh (the heat transfer modules are programmed to treat nonuniform space meshes) and the change in the bond gap as a function of the axial coordinate, which is needed to determine the thermal impedance of the gap. The deformation module also calculates the stress and displacement distribution in the clad which are used for predicting the time and position of clad failure.

Four basic mathematical models are used as building blocks in the deformation module: a fuel elastic deformation model, a fuel elastic deformation with partial melting model, a clad elastic deformation model, and a clad elastic-plastic deformation model. Since typical fuel-element-temperature distributions are such that radial temperature gradients are much more severe than axial, it was concluded that shearing deformations caused by axial temperature and stress variations would be much smaller than the displacements caused by radial variations. Consequently, in the basic models the shearing deformations are at first neglected, and the resulting simplified sets of differential equations and boundary conditions are valid exactly for the displacements due to the dominating radial variations; the shearing displacements are then determined approximately as correction terms.

Each axial segment j is given a case tag (M^j, N^j), $(M^j = 1, 2, 3;$ $N^j = 1, 2, 3)$ which identifies the state of the segment and the basic models to be combined in computing its deformations. The case tag may vary from one segment to another and for any given segment may vary with time.

If $M^j = 1$, segment j has no central cavity and no fuel melting has occurred; if $M^j = 2$, the segment has a central cavity and either no melting has occured or not enough to fill the cavity due to volumetric expansion on melting; if $M^j = 3$, enough fuel melting has occurred to fill any available central cavity in the axial segment and the liquid phase exerts pressure on the remaining solid fuel. If $N^j = 1$, a radial gap exists between the fuel and clad of segment j; if $N^j = 2$, the thermal expansion of the fuel has closed the gap the fuel is pressing on the clad, and the clad deformations are elastic (the clad stresses are below the yield point) and if $N^j = 3$, the gap is closed and the expanding fuel pressure on the clad is large enough to cause elastic-plastic clad deformations.

Cases (1, 1), (1, 2), (2, 1), and (2, 2) have been programmed along with the necessary branching to determine the appropriate case tag for each axial segment. For testing purposes the program has been run successfully with typical fuel-element radial and axial temperature profiles which are such that no melting occurs and the clad stresses remain below the yield point. In particular, the feasibility of adding correction terms into the primary deformations in order to account for the shearing deformations caused by axial variations has been demonstrated. Cases (1, 3) and (2, 3) are now being incorporated into the program, i.e., the possibility of plastic-clad deformations will be included next.

2. Densities in the Critical Region

The behavior of fluids in the thermodynamic critical region is an important facet of the equation of state. Recent studies by Essam and Fisher[14] of the lattice gas model of the critical point have given the relation

$$\frac{\rho_L - \rho_V}{2\rho_C} = D\left(1 - \frac{T}{T_C}\right)^{\beta}, \qquad (1)$$

where ρ is the density, T is the absolute temperature, and the subscripts L, V, and C correspond to the liquid, vapor, and critical conditions, respectively. The exponent β is called the critical index and has the value

$$\beta = 0.312 \pm 0.007 \cong 5/16$$

for the Ising model. The coefficient D was found to have the following values for various cubic lattices:

$$D = 1.570 \pm 0.001 \text{ simple cubic;}$$
$$= 1.491 \pm 0.001 \text{ body-centered cubic;}$$
$$= 1.488 \pm 0.001 \text{ face-centered cubic.}$$

[14] Essam, J. W., and Fisher, M. E., J. Chem. Phys. 38, 802 (1963).

This relation is expected to hold only in the region close to the critical point, since the Ising model assumes that the vapor and liquid coexistence curves are symmetrical about the critical point.

Real fluids, however, do not show this symmetrical behavior. Instead, the average of the vapor and liquid densities, although a straight line, has a slight negative slope.[15] This is most likely due to the creation of vacancy sites by thermal activation. This linear relation is called the "law of the rectilinear diameter" and has been found to be valid for a wide variety of fluids. In equation form this can be written as

$$(\rho_L+\rho_V)/2 = A - BT, \tag{2}$$

where A and B are constants and B is of the order of 10^{-4} (g/cc)/°K.

At the critical temperature T_C, $\rho_L = \rho_V = \rho_C$, and A can be eliminated to give

$$\frac{(\rho_L+\rho_V)}{2} = \rho_C - B(T - T_C)$$

or

$$\frac{\rho_L + \rho_V}{2\rho_C} = 1 + \frac{BT_C}{\rho_C}(1 - T_R), \tag{3}$$

where

$$T_R = T/T_C.$$

Adding Eqs. (1) and (3) gives

$$\frac{\rho_L}{\rho_C} = 1 + \frac{BT_C}{\rho_C}(1 - T_R) + D(1 - T_R)^{\beta}. \tag{4}$$

Subtraction gives

$$\frac{\rho_V}{\rho_C} = 1 + \frac{BT_C}{\rho_C}(1 - T_R) - D(1 - T_R), \tag{5}$$

which can be rewritten as

$$f_1(T_R) = \left(\frac{\rho_L}{\rho_C} - 1\right) + \frac{BT_C}{\rho_C}(1 - T_R) = D(1 - T_R)^{\beta}.$$

[15] Grosse, A. V., J. Inorg. Nucl. Chem. 21, 23 (1961).

From this equation it can be seen that low-temperature density values can establish the constants A and B in Eq. (2). At sufficiently low temperatures, where vapor densities are negligible, liquid density alone will determine these constants. For most metals the liquid density is linear with temperature over a wide range.

Similarly

$$f_2(T_R) = \left(1 - \frac{\rho_V}{\rho_C}\right) + \frac{BT_C}{\rho_C}(1 - T_R) = D(1 - T_R)^{\beta}.$$

If the logarithms of f_1 and f_2 are plotted versus the log of $(1 - T_R)$, the result should be a straight line of slope β and intercept of D when $T_R = 0$.

Since an estimate of T_C leads to an estimate of ρ_C from Eq. (2), liquid and vapor density data can be plotted and extrapolated. Hopefully, a proper choice of T_C will give identical values of D and β for liquid and vapor.

Equations (4) and (5) are reminiscent of the corresponding-states equations of Guggenheim[16] for many common gases, which give

$$\frac{\rho_L}{\rho_C} = 1 + 0.75(1 - T_R) + 1.75(1 - T_R)^{1/3}; \tag{6}$$

$$\frac{\rho_V}{\rho_C} = 1 + 0.75(1 - T_R) - 1.75(1 - T_R)^{1/3}. \tag{7}$$

Comparison of Eqs. (4) and (5) with (6) and (7) shows the reduced slope of the rectilinear diameter, BT_C/ρ_C, corresponds to 0.75, D corresponds to 1.75, and β corresponds to 1/3. Recent precision measurements[17] on common gases shows the exponent 1/3 to be valid as close to the critical temperature as $(1 - T_R) = 10^{-6}$. These data[17] were fit with $BT_C/\rho_C = 0.85$ and $D = 1.907$. It can be noticed that Guggenheim's equation predicts

$$D = \frac{BT_C}{\rho_C} + 1. \tag{8}$$

If this relation is general, measurement of the liquid density over a range of temperature would establish the rectilinear line, the assumption of T_C would give ρ_C and D, and vapor and liquid density data would lead to β and the equations of state given by Eqs. (4) and (5).

---

[16]Guggenheim, E. A., J. Chem. Phys. 13, 253 (1945).

[17]Straub, J. W., Chemie Ing. Technik 39, 291 (1967).

values for several substances are listed in Table LIV.

TABLE LIV. Test of Lattice Gas Model and Equation (8)

Substance	D	$\frac{BT_C}{\rho C}$	β	$D - \frac{BT_C}{\rho C}$
Rb	2.365	1.323	0.466	1.042
Cs	2.205	1.228	0.414	0.977
SO_2	2.300	-	0.398	-
H_2O	2.08	-	0.374	-
CO_2	2.075	0.962	0.337	1.113
N_2O	2.24	-	0.374	-
NH_3	2.00	-	0.336	-
Xe	1.835	-	0.354	-
Perfluoropropane	1.940	0.9044	0.341	1.036
Methyl chloride	1.865	1.033	0.334	0.832
Tertiary butyl alcohol	2.565	-	0.428	-
Ethane	1.875	0.796	0.310	1.079
n-heptane	1.740	1.006	0.310	0.734
$BiCl_3$	1.940	1.048	0.333	0.892
$BiBr_3$	1.896	0.999	0.333	0.897
$HgCl_2$	1.917	0.947	0.333	0.970
Straub[17] CO_2, N_2O, $CFCl_3$ and mixtures	1.907	0.850	0.333	1.057
Guggenheim[16] Ne, A, Kr, Xe, N_2, O_2, CO, CH_4	1.750	0.750	0.333	1.000
			Avg.	0.969

B. Coolant Dynamics

1. Sodium Expulsion

An experiment is being planned to investigate the mechanism of coolant expulsion in a simulated reactor environment, including measurement of the void distribution, expulsion velocities, pressure transients, and liquid superheats during coolant expulsion.

The programmed electron-bombardment heater has been received and is undergoing preliminary testing. Assembly of the sodium-expulsion experiment is continuing. Instrumentation is being assembled and checked.

2. Superheat

To determine the amount of liquid superheat required to initiate nucleate boiling in sodium under various conditions simulating a reactor environment, an experiment is being devised to measure the independent

and combined effects of pressure, dissolved gas, heat flux, surface characteristics, and the pressure-temperature history of the system.

The installation of the thermal-radiation heater is complete. Several leaks in the bell-jar housing of the test vessel have caused delays.

Data from previous test runs show significant effects of system pressure, heat flux, and the pressure-temperature history on the incipient boiling superheats in sodium.

3. Critical Flow

Calculations indicate that critical flow may occur in the core of a sodium-cooled reactor during an accidental power surge. Critical flow could lead progressively to detrimental effects such as voidage of the coolant channel, shock phenomena, and pressure buildup.

The experimental portion of the sodium study has been completed. Final reduction and analysis of the data are now being carried out. The results of these tests will determine the future of the sodium critical flow studies.

To investigate the basic processes controlling the two-phase critical flow of sodium, studies have been continuing using steam-water as the working media. Previous investigators[18-20] have found difficulties in determining the relationship between the exit and receiver pressures in two-phase critical flow. Single-phase critical flow produces a condition in which the exit pressure is independent of variations in the receiver pressure. However, those investigators noted a dependency between these two pressures for steam-water critical flow. To investigate the nature of the dependency, three test sections (see Fig. 19) were constructed. Test sections C7 and C120 are identical upstream of the exit plane but have different geometries downstream of

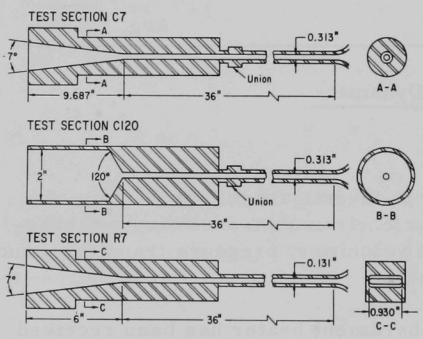

Fig. 19. Schematics of Test Sections

[18] Faletti, D. W., and Moulton, R. W., Two-phase Critical Flow of Steam Water Mixtures, AIChE J. 9, 247 (1963).

[19] Zaloudek, F. R., Low Pressure Critical Discharge of Steam-Water Mixtures from Pipes, HW-68936 (1961).

[20] Klingebiel, W. J., Critical Flow Slip Ratios of Steam-Water Mixtures, Ph.D. Thesis, University of Washington (1964).

the throat; Test section R7 has a rectangular cross section with a 7°-included-angle divergence downstream. According to the single-phase explanation of critical flow, the downstream geometry should exhibit no effect on the upstream conditions.

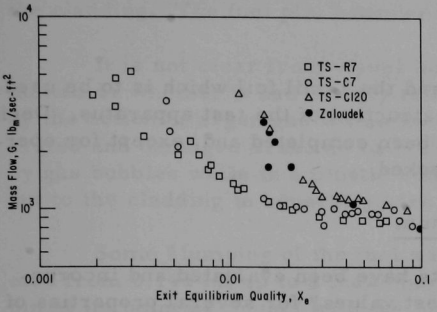

Fig. 20. How Exit Quality Varies with Mass Flow for Test Sections of Different Downstream Geometries (in all cases, exit pressure is 50 psia).

Figure 20 displays the experimental data obtained from each test section as well as the data of Zaloudek.[19] It is apparent that both 7°-divergent sections produced similar data and also that the data from C120 and the test section used by Zaloudek, which was similar to C120, are nearly the same. There is a definite discrepancy between the rapid-expansion test sections and the 7°-divergent ones. Since the downstream geometry is the only difference between C7 and C120, this must be the cause of the discrepancies in the data.

A possible explanation for the discrepancies is that the rapid-expansion test section produces a large radial-pressure profile immediately downstream of the exit plane; the subsonic layer next to the wall may adjust to this large gradient in a region near the throat so that a wall tap close to the exit plane may record a pressure which is not characteristic of the central core of the fluid. The 7°-divergent test sections reduce the magnitude of this effect by controlling the downstream expansion and thus making the pressure distribution more one-dimensional.

The relationship between the exit and downstream pressures was investigated for both C7 and C120. Section C120 exhibited dependence between the pressures similar to that found by other investigators; however, the exit pressure in C7 remained constant until the flow became subcritical. The behavior of C7 was more closely allied with the normal single-phase behavior; thus it was concluded that the data from C7 were more representative of the choking conditions than the data from C120.

4. Electron-bombardment Heater Tests

The operations of various electron-bombardment heaters (EBH), which will simulate in-pile experiments pertaining to reactor safety, are being examined in a large evacuated vessel. Both single-pin heaters and multipin heaters will be built and tested.

The fabrication of the first EBH test section is essentially complete; the three banks of powerstats have been connected into the high-voltage power supply. Further work on this experiment will continue after the evacuated test vessel and vacuum pumping station arrive.

5. Convective Instability

Welding the sheathed couples and the 1-mil foil which is to be used as a test-section wall has delayed construction of the test apparatus. Design of the electrical interlock system has been completed and, except for operating the lamps, it is installed and checked.

6. Thermophysical Properties of Sodium

Reviewers' ideas and comments have been evaluated and incorporated in a report that recommends "best values" for several properties of the liquid and vapor phases of sodium. The report is being modified to include liquid-phase compressibility and sonic-velocity data. In addition, estimates of the critical-point values of temperature, pressure, and specific volume are being included.

C. Fuel Meltdown Studies with TREAT

1. Unbonded EBR-II Pin in Flowing Sodium

The unbonded (i.e., argon-bonded) EBR-II Mark-I pin run in flowing sodium in the Mark-I integral TREAT loop (see Progress Report for April 1967, ANL-7329, p. 92) has been removed from the loop and examined. The 6% enriched test pin was surrounded by six empty dummy pins on an EBR-II subassembly pitch, and the fuel holder was wrapped in layers of tantalum sheet to shape the sample power in the axial direction. Sodium flow for the experiment was 4 m/sec, and the inlet coolant temperature was 380°C. The power transient was a "flattop," extending for approximately 7 sec with a nominal power level ~20% in excess of the goal of 168 W/g of fuel. The experiment was performed to provide information for use in evaluating possible consequences of loss of sodium bond in an EBR-II pin.

No flow or pressure anomalies were noted in the instrumentation record of the transient.

The clad pin showed no evidence of damage. Even the usual spirally warped condition was not present, nor was the cladding surface seriously discolored. Measurements taken at this time showed the diameter to be 0.173-0.1735 in., which does not indicate any expansion of the cladding tube.

The cladding had not stuck to the fuel surface at any point and was therefore easily peeled away. In only one area did the cladding inner surface appear to be attacked, leaving a scar. Preliminary microscopic examination of this cross section indicates that attack may not, in fact, have occurred here, but that the scar is instead a plaque of eutectic adhering to the cladding. The fuel pin, however, had sustained severe damage.

It is not clear from visual inspection whether the fuel had actually melted or whether it had merely reached the plastic state and been deformed by the action of argon gas within the cladding. However, some of the separated and damaged areas do have the appearance of having been squeezed by gas bubbles while in a plastic condition. Further, the fuel clearly flowed out to the cladding in several places.

Some slumping of the fuel was indicated by the growth in pin diameter from 0.144 in. up to a maximum of 0.155 in. The bottom tip of the fuel pin at its point of contact with the lower end fitting measures 0.145 in., and there is one area of reduced diameter near the upper end, but the diameter of the pin generally is 0.153-0.155 in.

There were no heavy deposits of fuel cladding, but some thin stripes were found on the surface of the bottom 3 cm of the fuel.

2. Mixed Oxide Dounreay Fast Reactor Test Pins

A shipment of 66 stainless steel-clad, gas-bonded, mixed-oxide (PuO_2-UO_2) fuel pins has been received from the United Kingdom. These pins, fabricated as Dounreay Fast Reactor test specimens, are to be used in a joint US-UK program of TREAT fast reactor safety experiments. This program will be the first systematic investigation undertaken in-pile of the failure, fuel motion, coolant motion, and pressure-pulse phenomena of this fuel type. Seven additional pins, irradiated unencapsulated in the Dounreay reactor to 5 a/o burnup, are to be phased into the program after enough experiments have been performed on unirradiated specimens to justify use of the small stock of irradiated samples.

The program of experiments is to investigate the lower end of the fuel-failure scale, and will be oriented toward pump failure and overpower exposures. Some cluster phenomena are scheduled to be studied during the experiments. Because of the need to develop models describing fuel behavior, some experiments are to be run using transparent capsules. The Mark-II integral TREAT loop (see Progress Report for March 1967, ANL-7317, pp. 106-107) is to be used for experiments which mockup potential accident conditions more closely. Present plans call for the experimental program on the mixed oxide to begin about January 1968.

3. Defected Elements

Nineteen $(U_{0.8}Pu_{0.2})O_2$ pellet-fueled elements were fabricated for irradiation in EBR-II followed by destructive testing in TREAT. The elements fit a standard B-37 irradiation assembly in EBR-II. Each element has an 18-in.-long fuel section that can be cut out and used in TREAT following irradiation in EBR-II. The elements will be used to introduce the variable of burnup into studies of failure thresholds and mechanisms. All jacket hardware was made from Type 304L stainless steel tubing or rod. The tubing was from stock previously inspected by personnel of the Special Materials Division and judged suitable for use in EBR-II. The $(U,Pu)O_2$ pellets were purchased from the Nuclear Materials and Equipment Corporation and were inspected by personnel of the Engineering Irradiations Group of the Metallurgy Division.

(i) Fabrication of Stainless Steel Components. Each fuel element consists of (a) a lower tip, (b) an upper end plug, and (c) an irradiation specimen or fuel section. The jacket tubes were made from short lengths of tubing cut with an abrasive cutoff saw. Both ends were faced in a lathe and one end spread open with a brass mandrel. The inside diameter was increased from 0.250 to 0.260 in. for a distance of 3/16 in. from one end. This provided necessary clearance between the pellets and the jacket tube, and allowed the use of a funnel to prevent the top of the tube from being contaminated during loading. Each tube was examined microscopically to ensure that no appreciable wall thinning occurred during this forming operation. Each section of tubing was measured for length with a vernier caliper, measured for outside diameter with a micrometer, measured for inside diameter with a wand-type air gauge, and inspected for brass or toolmarks with a microscope. Some brass that was found was removed with nitric acid. The acceptable tubes were cleaned in acetone and in alcohol, and were oven dried before the lower connector was attached.

The lower connectors were welded into the jacket tubes in the Building-350 glovebox system. The welds were made with a motor-driven TIG welder with copper chills to restrict the heat-affected zone. Dummy hardware was welded under various conditions and examined metallographically. As a final test, acceptable hardware was welded under the condition found most favorable and was examined metallographically.

Each jacket subassembly was fitted with a loading funnel and covered with shrinkable electrical insulation. This completely enclosed assembly was loaded inside the glovebox without any contamination to the outside portions of the jacket.

(ii) Assembly, Closure, and Inspection of the Fuel Section. The length, diameter, and weight of each pellet were measured. Then a protected jacket subassembly and the appropriate assortment of pellets were

placed in an inclined, contoured feeding trough. When the trough was vibrated, the pellets moved into the jacket tube. A tantalum disk was added and the distance between the disk and the top of the jacket was measured with a depth gauge. This measurement was used to ensure that the pellets were down and to determine the length of the restrainer spring to be used.

The restrainer springs were designed to support an 85-g load. The spring constant was 5.14×10^{-4} in./in./g and each spring was compressed a minimum of 0.25 in. This produced a force sufficient to support the pellets when the element is inverted. After the spring was loaded, the top of the jacket tube was reformed. This was done by squeezing the spread end in a collet using a brass sleeve as a protector. The upper connector was added and the element was checked for contamination. If clean, it was moved to the welding box where the upper connector was welded to the tube wall.

The upper connector was welded with the same equipment used in welding the lower connector and the same type of parameter study was run to optimize welding conditions. The upper-connector welds were also X rayed to detect wall thinning.

All fuel sections were checked for contamination. While in the glovebox, they were checked by counting the radioactivity on wipes. After being taken from the glovebox system, each fuel section was inspected directly with a gas-filled proportional counter. All material leaving Building 350 read less than 10 dpm of loose contamination and less than 500 dpm of fixed contamination.

All fuel sections were leak tested with a helium mass-spectrometer leak detector that was calibrated with a standard leak of 3.7×10^{-8} standard cm^3/sec. No element giving a leak indication greater than that of the standard leak was accepted.

Each completed fuel section was X rayed to show the overall position of the pellets within the fuel tube.

(iii) Assembly and Inspection of Elements. The fuel section was joined to the lower tip and the upper end plug by welding. The same motor-driven TIG welder was used and the welding parameters were established by metallography in the manner described for fuel-section welds. Each element was checked for straightness with a dial indicator and a surface plate. Most of the elements required straightening to meet a 0.010 in. TIR (total indicator reading) requirement.

D. TREAT Operations

The program of 100 transient tests of prototype fuel rods for the Power Burst Facility Reactor started last month was continued. Seventy of the scheduled 100 transients have been completed.

The out-of-pile portion of the large TREAT Sodium Loop was operated at a temperature of 500°C for a period of several hours. Leakage of sodium through the valve between the storage and dump tanks was about 2 gpm during this time. Since this amount of leakage can be tolerated during transient tests, it will not be necessary to remove and repair the dump valve prior to using the loop for fuel irradiations.

E. Chemical and Associated Energy Problems (Thermal)

1. In-pile Studies with Zircaloy-2-clad, UO_2-core Fuel Rods Simulating the Conditions of an Excursion Accident

The general objective of the in-pile studies of excursion accidents is to contribute to the development of experimental and theoretical information needed for the analysis of accidents in water-cooled thermal reactors. The experiments described below simulate an uncontrolled nuclear excursion which causes an immersed fuel element to overheat, with possible melting or vaporization and reaction with water. The energy release resulting from metal-water reactions may exceed that which would be expected from the nuclear energy release in an excursion. Molten fuel or cladding materials could be dispersed in water, resulting in a violent and destructive steam explosion. The hydrogen evolved from the chemical reaction with water can also react with the oxygen present in the containment building and release considerable energy.

The program to study the high-temperature behavior of Zircaloy-2-clad, UO_2-core (both vibrationally compacted and sintered-pellet) fuel rods during a reactor transient is a continuation of previous work. Three experiments using sintered-pellet fuel rods submerged in water within a transparent capsule in TREAT have now been completed in which high-speed motion pictures of the meltdown were taken.

The first of these photographic experiments (Run CEN-222T) was performed with a single $5\frac{5}{8}$-in.-long by 0.42-in.-dia fuel rod which was subjected to three consecutive neutron bursts (transients) of progressively higher energy. The conditions and results of the experiment are summarized in Table LV.

The first transient resulted in a fission-energy input of 165 cal/g UO_2, with a 238-msec reactor period. This corresponded to a maximum, or adiabatic, UO_2-core temperature of 2200°C. Since the UO_2 remained

solid, as would be expected, the transient was nondestructive in nature. The Zircaloy cladding attained a peak recorded temperature of 1165°C. Thus, both the core and the cladding were below their melting point.

TABLE LV. Results from In-pile (TREAT) Meltdown Experiment with a Zircaloy-2-clad, UO_2-core Fuel Rod Submerged in Water.

Rod dimensions, $5\frac{5}{8}$ in. long by 0.42 in. in diameter.
83 g (10 pellets) of sintered (92% theoretical density) UO_2, 10% enriched.
27 g of Zircaloy-2 (25-mil) cladding.
600 g of H_2O coolant, initially at 30°C.

	Run CEN-222T, Transient Number		
	I	II	III
Reactor Characteristics			
Integrated power, MW-sec	118	218	248
Peak power, MW	113	443	556
Period, msec	238	115	101
Results			
Peak cladding temperature, °C	1,165	1,700	2,200
Zircaloy-H_2O reaction, %	0	-[a]	7
Final appearance of fuel rod	Intact	Intact, but some local cladding failure may have occurred.	Some fragmentation but rod shape retained; partial meltdown and cladding distortion.
Energy Calculations			
Fission-energy input, cal/g UO_2	165	305	347
Total fission energy, cal	13,700	25,300	28,800
Chemical energy, cal	0	0[b]	2,950
Total energy, cal	13,700	25,300	31,750
Adiabatic UO_2 temperature, °C	2,200 (solid)	2,850 (melted)	3,200 (melted)
Calculated temperature rise of H_2O, °C	23	42	53
Observed temperature rise of H_2O, °C	25	43	52

[a]Not determined.
[b]Assumed.

The second transient resulted in a fission-energy input of 305 cal/g UO_2, with a 115-msec reactor period. This corresponded to an adiabatic UO_2-core temperature of 2850°C, with the UO_2 in a fully melted state. The Zircaloy-2 cladding reached a maximum temperature of 1700°C, as indicated by the cladding thermocouple. Thus, the cladding reached a temperature only slightly below its melting point of 1850°C. No definite sign of cladding failure was apparent from the motion-picture record of the second transient, although there is some indication that cladding rupture may have occurred at the top rear of the rod out of the field of view.

The third transient resulted in a fission-energy input of 347 cal/g UO_2, with a 101-msec reactor period. The corresponding adiabatic UO_2-core temperature was 3200°C (400°C above the UO_2 melting point). The measured peak cladding temperature was about 2200°C. From the motion-picture record of the third transient, the release of incandescent molten fuel was clearly visible.

Fig. 21. Fuel Rod after Run CEN-222T

The final appearance of the fuel rod after the third transient irradiation is shown in Fig. 21. The fuel rod retained its cylindrical form; however, extensive cladding damage did occur. There was an area of "crinkling" or inward deformation of the cladding which may have been caused by static or dynamic pressures acting to collapse the softened or melted Zircaloy. Globules of solidified UO_2 were found, after the transient, which had apparently escaped through cladding defects. At this energy level a more extensive fragmentation, as occurred in subsequent experiments described below, would have been expected. However, waterlogging of the fuel pin following cladding failure during the second transient above may have been responsible for the reduced fragmentation noted in this run. The inclusion of water in the void space of a fuel rod of this type would effectively lower the input energy to the UO_2 by acting as a heat sink. A cladding breach would vent the interior of the fuel rod, thereby reducing the internal pressure and consequently the strain on the cladding.

In the second photographic experiment (CEN-224T), a single fuel rod was subjected to a 450-cal/g UO_2 transient in TREAT on an 80-msec period. The results of the experiment are summarized in Table LVI. The fuel rod was completely fragmented in the test, as shown in Fig. 22. The motion pictures taken in the experiment showed the progressive heating of the rod during the transient power pulse. The first indication of severe heating was the appearance of a luminous band which encircled the rod, approximately 1/8 in. wide and 1/2 in. from the top of the rod. The total energy input at the time of the appearance of the luminous band was 217 cal/g UO_2. The appearance of the band was followed by fairly uniform heating of the entire rod. Then abruptly, within one frame of the film (~0.5 msec), a bright flash

occurred, i.e., the rod changed from a uniform red to a brightness that resulted in complete overexposure of the film, indicating extremely rapid heating. The flash occurred 1.39 sec after the initial incandescence, at a total energy input of 295 cal/g UO_2. Most of the water surrounding the rod was blown out of the inner container at this time. After a few milliseconds, the water fell back into the container surrounding the rod and quenched the glow. The autoclave window was clouded by residue of the fuel rod following the first flash. The bottom portion of the rod was obscured for the remainder of the film. However, large intact pieces of the rod were still discernible and the upper third of the rod was visible. A second bright flash and expulsion of water similar to the first occurred 0.51 sec later. Examination of the residue after the run showed complete fragmentation of the fuel rod, which indicates that at least the top portion was sundered during the second flash. An attached thermocouple recorded peak cladding temperatures in excess of 2200°C for both of the flashes.

TABLE LVI. Results from In-pile (TREAT) Meltdown Experiments with a Zircaloy-2-clad, UO_2-core Fuel Rod Submerged in Water.

Rod dimensions, $5\frac{5}{8}$ in. long by 0.42 in. in diameter.
83 g (10 pellets) of sintered (92% theoretical density) UO_2, 10% enriched.
27 g of Zircaloy-2 (25-mil) cladding.
600 g of H_2O coolant, initially at 30°C.

	Run Number	
	CEN-224T	CEN-225T
Reactor Characteristics		
Integrated power, MW-sec	321	235
Peak power, MW	865	465
Period, msec	80	107
Results		
Peak cladding temperature, °C	~2,300	730
Zircaloy-2-H_2O reaction, %	37	21
Final appearance of fuel rod	Complete destruction; fines and a few particles.	Fragmented into particles and a few fines
Energy Calculations		
Fission-energy input, cal/g UO_2	450	330
Total fission energy, cal	37,350	27,400
Chemical energy, cal	15,600	8,850
Total energy, cal	52,950	36,250
Adiabatic UO_2 temperature, °C	3,300 (partly vaporized)	3,000
Calculated temperature rise of H_2O, °C	88	60
Observed temperature rise of H_2O, °C	60	63

Photograph of Residue

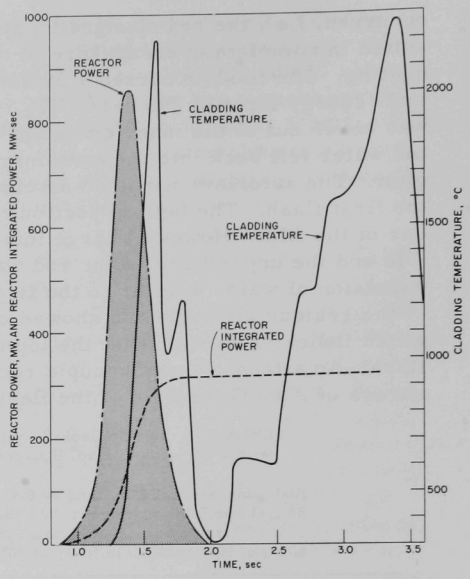

Oscillograph Record

Fig. 22. In-pile (TREAT) Meltdown Experiment CEN-224T

The third experiment, CEN-225T, was a transient with an energy input of 330 cal/g UO_2 on a 107-msec period. The results of this experiment are also summarized in Table LVI. The appearance of the fuel rod after the transient is shown in Fig. 23. The residue consisted of a few fairly large pieces and a small amount of fines, in contrast to the residue in CEN-224T which was almost entirely fines. The motion pictures taken in this experiment showed a fairly uniform heating of the fuel rod, starting as several incandescent patches that quickly grew and merged into an even redness. The length of time from first indication of boiling to the point at which the intensity of self-illumination caused overexposure of the film was approximately 0.35 sec, with the overexposure occurring at a total energy input of 330 cal/g UO_2. The total length of time in which the fuel appeared luminescent in the film was more than 5 sec. These observations compare well with the output of a thermocouple attached to the cladding. A 0.30-sec period was indicated between the start of heating and the thermocouple failure (which was assumed to be due to cladding failure) at an indicated temperature of 730°C.

The oscillograph records of the temperature and integrated power versus time for the latter two runs are also shown in Figs. 22 and 23. The temperature trace for CEN-224T, showing the double peak, cannot be compared with CEN-225T, due to the early failure of the thermocouple.

A comparison of the films of the two runs shows that CEN-224T exhibited a much more violent expulsion of water and rod fragments for both flashes than CEN-225T did in the single flash. The initial fuel-rod failure occurred at comparable energies for the two runs (295 and 330 cal/g UO_2), although the failure in CEN-225T was after completion of the transient power burst. Some of the fragmentation of the rod from CEN-225T appeared to happen during the cooling period, since approximately 3/4 of the rod could be seen in its original position at the end of the film.

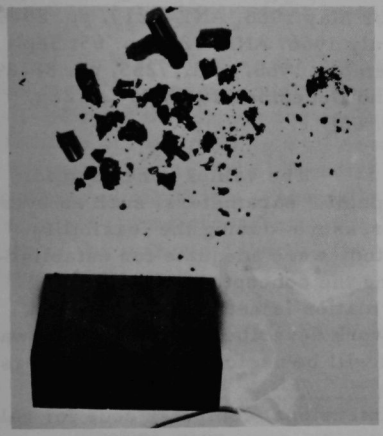

Photograph of Residue

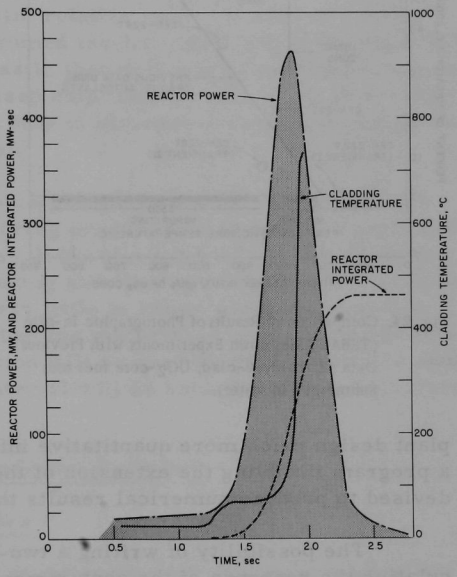

Oscillograph Record

Fig. 23. In-pile (TREAT) Meltdown Experiment CEN-225T

Figure 24 compares the Zr-H_2O reaction data from the three photographic experiments with those of previous runs using scale-up and high-pressure type autoclaves (see Progress Report for April 1966, ANL-7204, p. 80). Good agreement is evident.

Further experiments of this type using both vibrationally compacted and sintered-pellet fuel, in conjunction with development and extension of the TREAT calculational studies, may provide a mechanistic explanation of excursion failure of fuel rods. In particular, the photographic technique has proven to be a most useful tool in deducing the sequence of events which occur during the meltdown.

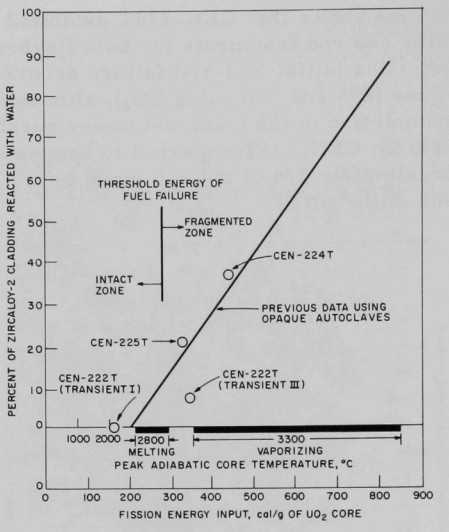

Fig. 24. Comparison of Results of Photographic In-pile (TREAT) Meltdown Experiments with Previous Data (Zircaloy-2-clad, UO_2-core fuel rods Submerged in water).

F. Containment

1. Containment by Energy Absorption

A re-evaluation of the work done during the past year on the feasibility of the energy-absorption concept as applied to water reactors and LMFBRs showed that the results, conclusions, and recommendations were correct, thereby affirming its applicability to these reactor types (see Progress Reports for May 1966, ANL-7219, pp. 80-81; July 1966, ANL-7245, p. 65; September 1966, ANL-7255, pp. 88-89; and December 1966, ANL-7286, p. 82).

The values generated for specific parameters, such as overpressure, during the feasibility study were adequate for establishing the concept, but for detailed plant design much more quantitative information is needed. To this end, a program involving the extension of the work described in ANL-7214[21] was devised to produce numerical results that will be useful to plant designers.

The possibility of writing a two-dimensional computer code for calculating the response of the containment structures resulting from a core excursion has been investigated. Two theories often used in the analysis of the behavior of structures subjected to intense impulsive loads are hydrodynamic theory of shock propagation and elastic-plastic wave propagation.

In the hydrodynamic theory, the medium under consideration is treated as a compressible fluid without shear resistance and viscosity. Because of this simplified assumption, the governing differential equations become more manageable. This is, indeed, the type of theory used in almost all existing codes. This theory yields very good results in media in the immediate vicinity of the core, where the explosion is very violent and where the amplitudes of stress waves are very large. The medium, solid or fluid, behaves like a compressible fluid. However, at regions remote from the core, the amplitudes of stress waves are considerably below the

[21] Sorenson, H. C., and Fistedis, S. H., Hydrodynamics of a New Concept of Primary Containment by Energy Absorption, ANL-7214 (Dec 1966).

modulus of elasticity of the material; also, the effect of shear resistance, if the medium is a solid, can no longer be ignored in the analysis. That is, the stresses are no longer isotropic. Therefore, the results obtained from the hydrodynamic theory in regions remote from the core become quite inaccurate.

In the elastic-plastic theory of wave propagation, the material is considered to possess a finite shear modulus and the behavior of the material is described by an elastic-plastic relation involving stress, strain, and strain rate. Because of the assumed incompressibility of the material in the plastic region, the elastic-plastic theory of wave propagation becomes increasingly inaccurate with increased amplitude of the stress pulse. Consequently, this theory is applicable only to stresses considerably below the modulus of elasticity of the material.

In view of these factors, the code is being written to include both theories. The basic equations are being prepared. Lagrangian coordinates will be used throughout the analysis. If the computer capacity allows, the fracture of material, as well as opening and closing of cracks, will also be considered in the code. Because very little is known about the dynamic strength of materials, especially when the material is under a biaxial stress, the quasi-static stress-strain relation will be used as the constitutive equation of the material, that is, the material will be considered as strain-rate independent.

G. Plutonium Volatility Safety

1. Chemistry of Tellurium Fluorides

Studies have been continued to determine the efficiency with which sorbents can remove low concentrations of TeF_6 from air streams. A tellurium decontamination factor (DF) of >1350 is the objective. In these studies, an isotopic dilution technique employing Te^{125m} tracer was used that allows direct measurement of the decontamination factor obtained across the bed of sorbent.

A series of experiments was completed in which the effect of selected variables on the adsorption of TeF_6 on BPL-type 12 to 30 mesh activated charcoal was determined. The experiments were a half-replicate, factorially designed set using the variables of bed height (1 or 2 in.), gas velocity (20 or 40 ft/min), and TeF_6 concentration (190 or 380 ppm). The results showed that of the several variables studied, only bed height had a significant effect on the DF obtained. TeF_6 loadings in these experiments ranged from 2 to 5 percent. The results also indicated that for the optimum conditions used, a DF greater than 10,000 could be attained with a packed bed of BPL activated charcoal. Earlier observations (see Progress Report, May 1967, ANL-7342, p. 126) that TeF_6 is desorbed from activated charcoal during air purging were in error, the result of a malfunction of the scaler which has since been corrected.

VI. PUBLICATIONS

Papers

Tables for the Calculation of Operating Parameters for Compound Solvent-Extraction Columns
T. R. Johnson
AIChE Journal 13(3), 607 (May 1967) Letter

Radiography with Reactor Neutron Beams
Harold Berger
Symposium on Research Reactor Applications, General Atomic Division of General Dynamics, San Diego, June 16, 1967, Abstract No. 4.

The Lattice Parameter of High-Purity Thorium with Reference to Impurity Content and Heat Treatment
Bernhard Blumenthal and J. E. Sanecki
J. Nucl. Mater. 22, 100-102 (April 1967)

Compatibility of Two Ni-Ti Alloys with Mercury
J. Y. N. Wang
Corrosion 23, 149-150 (May 1967) Note

Thermal Design of EBR-II Primary Tank Components
T. R. Bump and H. O. Monson
Mech. Eng. 89, 71 (March 1967) Abstract

Analysis of Temperature and Pressure within the Containment Structure of the Fast Reactor Test Facility (FARET)
Ira Charak
Mech. Eng. 89, 71 (March 1967) Abstract

Axisymmetric Bending of a Coupled Plate Structure
Henry Halle
Mech. Eng. 89, 71 (March 1967) Abstract

Spontaneous Fission Half-Lives of Cm^{242} and Cm^{244} by Absolute Alpha and Neutron Counting
R. J. Armani and Raymond Gold
IAEA Symp. on Standardization of Radionuclides, Vienna, October 10-14, 1966. Intern. Atomic Energy Agency, Vienna, 1967, p. 621.

Absolute Determination of Fission Rates in U^{235} and U^{238} and Capture Rates in U^{238} by Radiochemical Techniques
R. J. Armani
IAEA Symp. on Standardization of Radionuclides, Vienna, October 10-14, 1966. Intern. Atomic Energy Agency, Vienna, 1967, p. 613

Extension of the Range of Determination of Manganese Sulphate Content for Neutron Source Measurements
Alexander Devolpi, R. J. Armani, and K. G. Porges
J. Nucl. Energy 21, 521 (June 1967) Letter

Absolute Calibrations of Fission Neutron Source Strength Relying upon an Improved Manganese Bath Technique and Absolute Beta-Gamma Coincidence Counting
Alexander Devolpi, K. G. Porges, and R. J. Armani
IAEA Symp. on Standardization of Radionuclides, Vienna, October 10-14, 1966. Intern. Atomic Energy Agency, Vienna, 1967, p. 717

Cf^{252} Fission Neutron Spectrum from 0.003 to 15.0 MeV
J. W. Meadows
Phys. Rev. 157, 1076-1082 (May 20, 1967)

Absolute Determination of Fission Fragment Emission Rates with a Prompt Neutron-Fission Coincidence Method
K. G. Porges and Alexander Devolpi
IAEA Symp. on Standardization of Radionuclides, Vienna, October 10-14, 1966. Intern. Atomic Energy Agency, Vienna, 1967, p. 693

Fast Neutron Scattering from Elemental Mo, Sn, Sb, and Te
A. B. Smith and R. R. Hayes
Nucl. Phys. A93(3), 609-630 (1967)

Multi-Angle Fast Neutron Time-of-Flight System
A. B. Smith, P. T. Guenther, R. N. Larsen, C. H. Nelson, P. L. Walker, and J. F. Whalen
Nucl. Instr. Methods 50(2), 277-291 (1967)

Converting AEC to a TEC: "Technological Excellence Commission"
B. I. Spinrad
Nucleonics 25(6), 52-53 (June 1967)

The Complex Relaxation Length of Neutron Waves in Multi-Group Transport Theory
Armando Travelli
Neutron Noise, Waves, and Pulse Propagation, Proc. Symp., University of Florida, Gainesville, February 14-16, 1966. USAEC Symp. Ser. 9, CONF-660206 (May 1967), pp. 55-68

The following appeared as abstracts in Trans. Am. Nucl. Soc. 10(1) (June 1967)

A Track-Etch Plastic-Film Technique for Neutron Imaging
Harold Berger and I. R. Kraska
p. 72

Performance of Vibratorily Compacted Mixed-Oxide Fuel Rods under Fast-Reactor Conditions
F. L. Brown, L. A. Neimark, B. J. Koprowski, J. E. Ayer, and J. H. Kittel
p. 101

Performance of Advanced U-Pu-Zr Alloy Fuel Elements under Fast-Reactor Conditions
W. N. Beck, F. L. Brown, B. J. Koprowski, and J. H. Kittel
p. 106

Potential of Advanced Fuels for a Fast Test Reactor
W. J. Bailey, P. D. Cohn, D. T. Aase, F. G. Foote, F. M. Heck, J. H. Kittel, G. A. Last, W. E. McHugh, A. A. Strasser, and C. W. Wheelock
p. 108

Compatibility of Stabilized Hypostoichiometric Uranium-Plutonium-Monocarbide Fuels with Stainless Steel
W. R. Jacoby, R. G. Palm, and T. W. Latimer
p. 108

Photographic Studies of UO_2 Pellet Fuel Rods in Water Subjected to Nuclear Transients in TREAT
L. J. Harrison, R. C. Liimatainen, and F. J. Testa
p. 127

Fast-Neutron Spectra and Radiation Damage Rates in EBR-II
A. D. Rossin, F. S. Kirn, R. J. Armani, and D. M. Smith
p. 129

ANL Reports

ANL-7203 HIGH CONVERSION CRITICAL EXPERIMENTS
A. R. Boynton, Q. L. Baird, K. E. Plumlee, W. C. Redman, W. R. Robinson, and G. S. Stanford

ANL-7207 PHYSICS MEASUREMENTS WITH MODIFIED DILUENT COMPOSITIONS IN TUNGSTEN-BASED, ALUMINUM-REFLECTED FAST REACTORS
W. G. Knapp and R. C. Doerner

ANL-7296 HEAT TRANSFER FROM A SPHERE TO LIQUID SODIUM DURING FORCED CONVECTION
Larry C. Witte

ANL-7320 PROCEEDINGS OF THE INTERNATIONAL CONFERENCE ON FAST CRITICAL EXPERIMENTS AND THEIR ANALYSIS, October 10-13, 1966

ANL-7350 CHEMICAL ENGINEERING DIVISION RESEARCH HIGHLIGHTS, May 1966-April 1967